THESIS

ESTIMATING LIQUEFACTION POTENTIAL OF SANDS USING THE PIEZOVANE

Submitted by

Clinton E. Scott

Department of Civil Engineering

In partial fulfillment of the requirements

for the Degree of Master of Science

Colorado State University

Fort Collins, Colorado

Summer 1989

COLORADO STATE UNIVERSITY

July 10, 1989

WE HEREBY RECOMMEND THAT THE THESIS PREPARED UNDER OUR SUPERVISION BY CLINTON E. SCOTT ENTITLED ESTIMATING LIQUEFACTION POTENTIAL OF SANDS USING THE PIEZOVANE BE ACCEPTED AS FULFILLING IN PART REQUIREMENTS FOR THE DEGREE OF MASTER OF SCIENCE.

Committee on Graduate Work

Co-Advisor

Advisor

Department Head

ABSTRACT OF THESIS

ESTIMATING LIQUEFACTION POTENTIAL OF SANDS USING THE PIEZOVANE

Laboratory test results are presented indicating feasibility of estimating liquefaction potential of saturated cohesionless soil using the piezovane, a shear vane incorporating pore pressure measurement. Utilizing a calibration chamber, piezovane shear tests are conducted on medium-fine subrounded quartz sand. Partially drained tests show small negative pore pressure peaks in dense samples and small positive peaks in relatively loose samples, indicating a reasonable trend of volumetric strain tendencies during shear. The piezovane induces positive pore pressure at denser initial states than steady states (zero contraction) determined by CU triaxial tests, but peak shear strength trends and direct shear test results indicate that observed pore pressure response adequately reflects actual contractive and dilative tendencies during piezovane shear.

Clinton E. Scott
Civil Engineering Department
Colorado State University
Fort Collins, CO 80523
Summer, 1989

ACKNOWLEDGEMENTS

I gratefully acknowledge my primary advisor, Dr. Wayne A. Charlie for his suggestion of this research and enthusiastic direction throughout its progress. Special thanks are deserved by my co-advisor, Dr. Thomas J. Siller, for his technical guidance and general support, Dr. Donald O. Doehring for his advice and service on my graduate committee, and Mr. J. W. France for his suggestions and helpful discussion of this research. The Air Force Office of Scientific Research supplied the research apparatus. Mr. Bill Butler advised the triaxial testing and familiarized me with the calibration chamber. Mr. Wayne Lewis performed the relative density determinations. Dr. Deanna Durnford, Mr. Randy Rosane, Mr. Chris Johnson, Mr. Steven Pierce and Mr. Bob Kiesel provided technical assistance. Mr. David Devitt ably provided much of the graphics in this thesis. Ms. Carol Smoot assisted in the final preparation of this manuscript. Above all, I wish to thank my wife, Kay, for her patience and loving support throughout this research effort.

TABLE OF CONTENTS

LIST OF TABLES

LIST OF FIGURES

LIST OF SYMBOLS

Symbol	
a	spherical radius of influence, cm
C	pore pressure parameter
cc	cubic centimeter
cm	centimeter
CD	consolidated, drained
CU	consolidated, undrained, with pore pressure measurement
C_u	coefficient of uniformity
C_v	coefficient of consolidation, m^2/s
D	vane diameter, cm
D_r	relative density, %
D_{50}	diameter of 50% passing, mm
e	void ratio
e_c	void ratio at end of consolidation
g	gravitational constant, 9.81 m/s^2
H	vane height, cm
K	coefficient of lateral stress
K_o	coefficient of lateral stress at rest
k	coefficient of permeability, cm/s
kPa	kilopascal
M	torque, N-m
m	meter
m_v	coefficient of compressibility, 1/kPa
ms	millisecond
mv	millivolt
N	newton
p'	$(\sigma_1' + \sigma_2')/2$, kPa
p_s'	$(\sigma_1' + \sigma_2')/2$, at steady state, kPa
pwp	pore water pressure, kPa
q	$(\sigma_1 - \sigma_2)/2$, kPa
q_s	$(\sigma_1 - \sigma_2)/2$, at steady state, kPa

R^2	correlation coefficient
S	shear strength, kPa
S_p	peak shear strength, kPa
S_{ref}	reference shear strength, kPa
S_s	steady state shear strength, kPa
S_{su}	undrained steady state shear strength, kPa
S_{us}	undrained steady state shear strength, kPa
S_{uv}	undrained vane shear strength, kPa
S_{vs}	vane shear strength at steady state, kPa
S_{vp}	peak vane shear strength, kPa
s	standard deviation
T	dimensionless time factor
t_f	time to failure from start of shear, s
U	pore pressure dissipation (%)
u	pore pressure, kPa
ϵ_s	strain at steady state, %
γ_d	dry unit weight, kN/m^3
ρ_d	dry density, Kg/m^3
ϕ'	effective angle of internal friction, degrees
ϕ'_s	effective angle of internal friction at steady state, degrees
σ	stress, kPa
σ'	effective stress, kPa
σ'_f	effective stress normal to failure plane, kPa
σ'_{fs}	effective stress normal to failure plane, at steady state, kPa
σ'_1	effective major principal stress, kPa
σ'_3	effective minor principal stress, kPa
σ'_{3c}	effective isotropic consolidation stress, kPa
σ'_{3s}	effective minor principal stress at steady state, kPa
σ'_v	effective vertical stress, kPa
σ'_{vc}	effective vertical consolidation stress, kPa
σ'_h	effective horizontal stress, kPa
τ_f	shear strength, kPa
τ_d	driving shear stress, kPa

I. INTRODUCTION

A. Statement of Problem

The need to improve and develop in situ methods for evaluating liquefaction potential of sands has been expressed by Peck (1979) and Poulos (1988) among others. Current techniques do not provide a fundamental determination of liquefaction potential. Methods utilizing the Standard Penetration Test and Cone Penetration Test are restricted to correlative approaches due to the highly empirical nature of test data correction and interpretation. Soil properties associated with liquefaction, such as dilative/contractive tendencies and shear strength, cannot be determined directly by common penetration test methods (Marcuson et al., 1980).

Addition of pore pressure measurement to in situ techniques is thought to assist in direct determination of liquefaction potential since porewater pressure response is fundamental to liquefaction. The piezocone, or cone penetrometer with pore pressure measurement, has been utilized in a limited number of field studies to directly evaluate liquefaction susceptibility (Schmertmann, 1978, Campanella et al., 1983, and East et al., 1988). Interpretations from such studies are limited due to complex failure modes, volumetric strains caused by cavity expansion, and uncertainty in the effect of pore pressure measurement location.

B. Objective

Absence of a reliable in situ device for direct, quantitative evaluation of liquefaction potential has prompted recent development of the piezovane. The piezovane is a vane shear device with pore pressure measurement. The instrument has several advantages over other in situ devices; vane shear induces large, unidirectional strains which closely represent those thought to occur in natural liquefaction failure. In addition, cavity expansion is minimized. This study is an initial step in researching the feasibility of the piezovane to estimate liquefaction potential of saturated cohesionless soils.

The objective of this study is to determine if piezovane testing, under laboratory conditions, can 1) identify contractive and dilative volumetric strain tendencies during shear, and 2) measure undrained shear strength at large deformations (steady state shear strength). The ability of the piezovane to reliably estimate the above parameters indicates its usefulness for direct evaluation of liquefaction potential.

II. LITERATURE REVIEW

A. Liquefaction Occurrence

Liquefaction is responsible for numerous landslides, failures of earth structures, and extensive structural and foundation damage. Liquefaction can be triggered by earthquakes, blasting, and static loading. Catastrophic failures from earthquake induced liquefaction occurred in San Francisco in 1906 (Youd and Hoose, 1976), Niigata, Japan in 1964, (Seed and Idriss, 1967), and elsewhere. Blast induced liquefaction has been studied by Charlie et al. (1980, 1985a, 1985b) and Long et al. (1981) among others. The most notable case of liquefaction triggered by static loading is Fort Peck Dam, where failure occurred during construction (Poulos, 1988). Numerous other occurrences of liquefaction are summarized by Seed (1968) and Gilbert (1976).

B. Definition of Liquefaction

Liquefaction is generally associated with large deformations as a result of decreased shear strength in loose, saturated cohesionless soils. A general definition is provided by Castro and Poulos (1977) as:

> ...a phenomenon wherein a saturated sand loses a large percentage of its shear resistance when subjected to undrained monotonic, cyclic or shock loading, and flows in a manner resembling a liquid until shear stress acting on the mass are as low as the reduced shear resistance.

A similar definition is also given by the Committee on Earthquake Engineering (1985) as, "..all phenomena involving excessive deformations or movements as a result of transient or repeated disturbance of saturated cohesionless soils."

Other definitions have been developed based on 100% pore pressure buildup (zero shearing resistance) in cyclic triaxial and simple shear tests (Seed and Lee, 1966, Peacock and Seed, 1968, and Finn et al., 1971).

This research utilizes the steady state concept of liquefaction where shearing resistance is decreased, but not necessarily zero, at large deformations. Thus, the definition by Castro and Poulos (1977) is appropriate for this study.

C. Pore Pressure Response and Liquefaction Potential

Terzaghi's (1946) principle of effective stress shows that

$$\sigma' = \sigma - u \tag{2.1}$$

where σ' is effective stress, σ is total stress, and u is pore pressure. The shear strength, τ_f of a cohesionless soil is

$$\tau_f = \sigma_f' \tan \phi' \tag{2.2}$$

where σ_f' is the effective stress normal to the shear plane and ϕ' is the effective angle of internal friction. To be consistent with current literature on vane shear, subsequent referral to shear strength will use S instead of τ_f.

For saturated cohesionless soils during undrained shear, equations 2.1 and 2.2 show that a reduction in shearing resistance will result from increased pore pressure. Increased pore pressure indicates contractive volumetric strain during shear. Figure 2.1 shows typical stress-strain curves for a contractive soil. Liquefaction requires this condition of decreased shearing resistance in loose sands due to increased pore pressures (Castro, 1975 and Casagrande, 1976).

Figure 2.2 illustrates that a dense, or dilative, soil cannot liquefy because there is no permanent loss in shear strength. With undrained conditions, shear strength increases due to decreased pore pressure. Deformations are restricted to those caused only by the triggering mechanism and will cease when triggering is stopped.

In summary, soils exhibiting contractive tendencies have the potential for pore pressure buildup and are liquefiable. Soils exhibiting dilative tendencies are non-liquefiable.

D. Steady State of Deformation

1. Definition

According to Castro and Poulos (1977), during liquefaction flow, a soil will tend toward a "steady state" of deformation. Originally termed critical state by Casagrande (1940), the steady state of deformation is described by Poulos (1981) as

> ...that state in which the mass is continuously deforming at a constant volume, constant normal effective stress, constant shear stress, and constant velocity....is achieved only after all particle orientation has reached a statistically steady state condition and after all particle breakage, if any, is complete, so that the shear stress needed to continue deformation and the velocity of deformation remain constant.

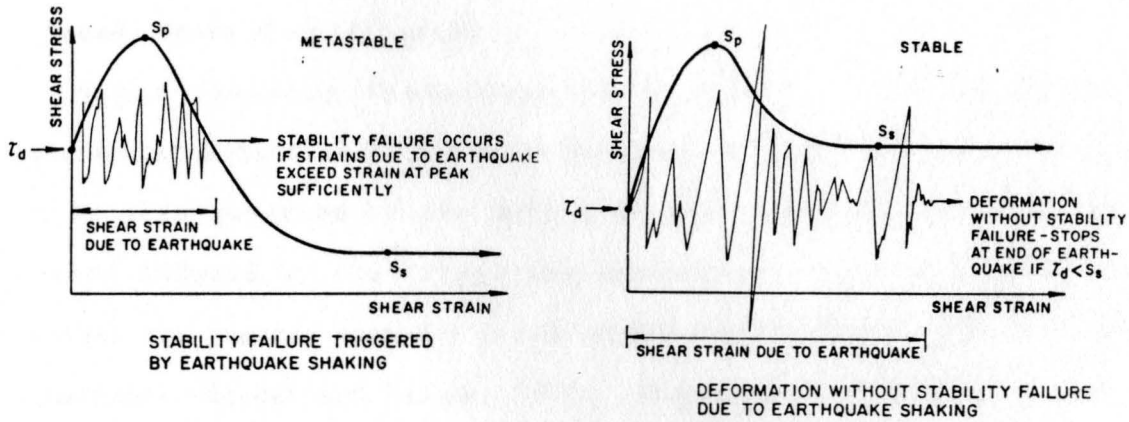

Figure 2.1 Deformation With and Without Failure.
(Poulos, 1988)

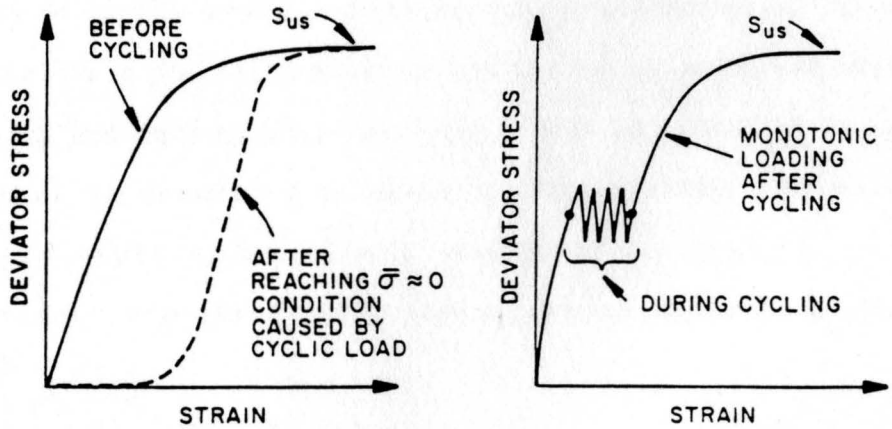

Figure 2.2 Undrained Stress Strain Curves for Dense Sand
(Committee on Earthquake Engineering, 1985)

The term steady state was chosen since it is analogous to the condition of the same name in conventional fluid mechanics. Poulos further states that the steady state flow structure and corresponding shear strength is not dependent on initial structure, but only on effective normal stress and velocity during deformation.

2. Steady State Shear Strength

Since shearing resistance can be nonzero at steady state, liquefaction potential is not only dependent on contractive behavior, but is also governed by the soil's steady state shear strength and strains induced by the triggering mechanism. If initial shear stresses are greater than the steady state shear strength, the soil is liquefiable (Castro and Poulos, 1977). Where initial shear stresses are less than the steady state strength, liquefaction will not occur. This relationship is shown in Figure 2.1. In the case of static loading as a triggering mechanism (Figure 2.3), the initial or driving shear would simply be at or very near the peak stress. Liquefaction would occur from loss in strength with small additional strains.

Based on the above relationships, evaluation of liquefaction potential is a stability analysis problem using undrained steady state strengths and driving shear stresses. This approach to liquefaction potential is described in detail by Poulos (1988) and Poulos et al. (1985). Application of the steady state concept is gaining acceptance, especially for sloping ground conditions (Robertson, 1986).

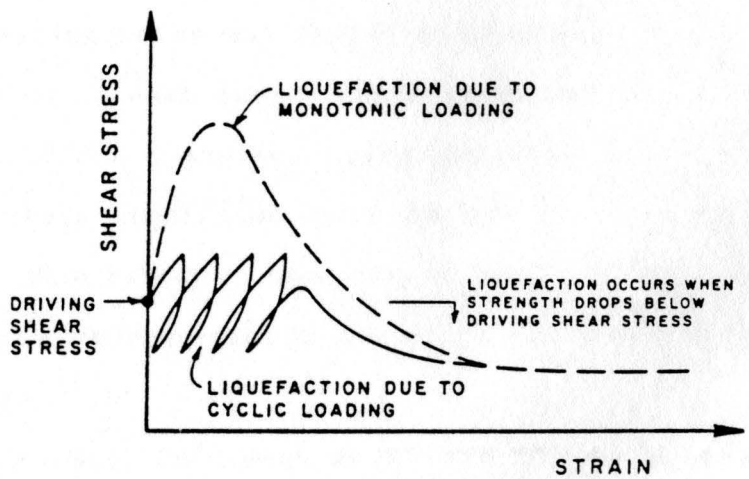

Figure 2.3 Liquefaction Due to Different types of Loading (Poulos et al., 1985)

3. The Steady State Line

The steady state density or void ratio, e, is not constant for a given soil, but varies with effective stress, commonly expressed by minor principal, σ_3', or normal, σ_f', stress components. It follows from Equation 2.2 that undrained steady state shear strength, S_{su}, can be expressed as a function of void ratio. Roscoe et al. (1958) observed that all loading paths in stress-void ratio space converge to one unique line at sufficiently large deformations. This stress-density relationship is called the steady state line (SSL). It is usually plotted as void ratio on a linear scale and σ_{3s}, σ'_{fs} or S_{su} on a linear or logarithmic scale. Figure 2.4 illustrates such a line and the paths taken during shear of elements in dilative (point A) and contractive (point B) initial states. The steady state line is a boundary between states of positive and negative volumetric strain tendencies during shear.

Loading paths may temporarily cross the line but eventually return to it when steady state structure is attained (Castro and Poulos, 1977). Likewise, a point initially on the steady state line may deviate significantly to the left or right during the non-steady state. This behavior, according to Poulos (1981), is the result of particle rearrangement prior to reaching a steady state flow structure.

According to Castro et al. (1982a), the steady state line is unique for a given cohesionless soil and is independent of stress history or loading path. Factors affecting the position and shape of the steady state line include angularity and particle size distribution. In general, curves are steeper and less linear with increasing angularity. Broader gradation (higher C_u) shifts the

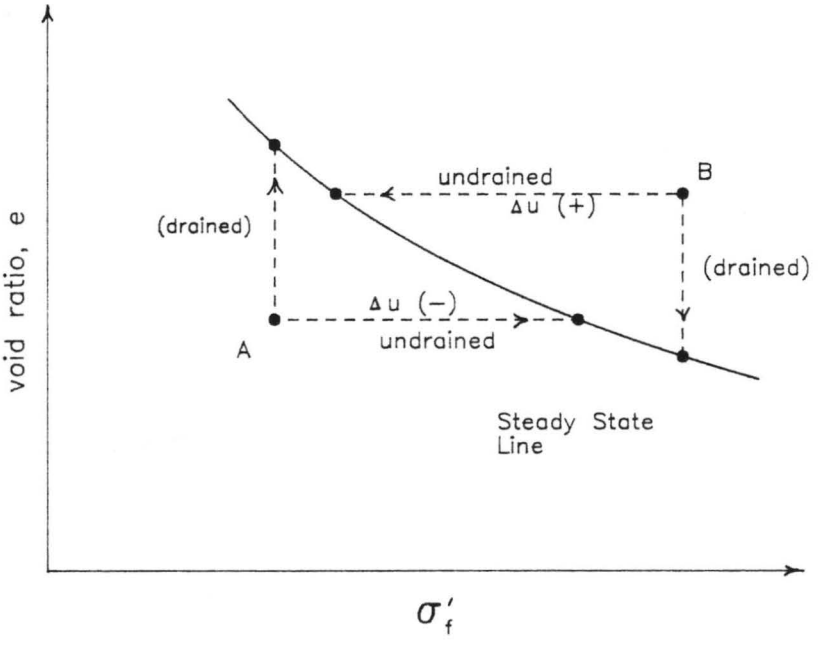

Figure 2.4 The Steady State Line (After Poulos et al., 1985)

curves downward toward lower void ratios (Castro and Poulos, 1977, and Castro et al., 1982a). Numerous steady state lines for soils of differing grain size, angularity, and size distribution are given by Poulos et al. (1985).

In practice, however, steady state lines seem to be dependent on test methods. Casagrande (1971) observed that strain controlled and stress controlled CU triaxial tests produce different steady state lines for the same sand. A study by Taylor (1939) indicated differing critical void ratios between consolidated drained (CD) direct shear tests and CD triaxial tests.

E. Laboratory Methods for Liquefaction Evaluation

This study uses the steady state approach in evaluating liquefaction potential and is concerned only with laboratory tests which determine steady state behavior. Cyclic triaxial and cyclic simple shear tests run for the purpose of 100% pore pressure buildup (Seed and Lee, 1966) are not applicable to this research.

1. Triaxial testing

Castro et al. (1982a) assesses the application of triaxial testing to the steady state approach in determining liquefaction susceptibility. Conclusions relevant to this research are listed below.

- The steady state line is independent of stress history.
- Isotropically consolidated, monotonically loaded, undrained triaxial compression (CU) tests on contractive samples provide the best method for establishing the steady state line.

- Variation of results from the steady state line are due to different gradations between samples, measurement errors and strain limitations.

A method utilizing CU tests in field evaluation of liquefaction potential is given by Poulos et al. (1985). The major drawback of this approach is the requirement of "undisturbed" sampling to approximate in situ conditions of void ratio and stress. "Undisturbed" sampling is expensive, and actual sample disturbance is unavoidable (Peck, 1979).

2. Direct shear tests

Direct shear tests have been used in the past to establish steady state lines (Casagrande, 1940, and Taylor, 1939). France (1987, personal communication) recommends that the direct shear test be discarded and replaced by CU triaxial tests. In the direct shear test, redistribution of void ratios is significant and stresses imposed at the boundaries are not fully understood.

3. Calibration chambers

Laboratory investigation of in situ tools such as piezocones, pressuremeters, and dilatometers require the use of testing chambers to provide controlled stress and strain conditions. Such devices are usually large, steel cylindrical cells accommodating samples of 1 to 2 cubic meters, and are referred to as calibration chambers. Elaborate chambers have been developed by Schmertmann (1978), Woods and Henke (1981), Bellotti et al. (1982), Al-Mukhtar et al. (1988), and others. These chambers are equipped with circumferential membranes and can

impose boundary conditions of vertical and horizontal constant total stress.

Bellotti et al. (1982) introduced the practice of preflushing with carbon dioxide gas before saturation as an alternative to vacuum saturation. Methods using CO_2 have the advantage over vacuum methods because no tensional stress history is introduced. Recent work by Bellotti et al. (1988) discusses saturation methods in detail and mentions that degree of saturation does not significantly affect cone penetration resistance.

An evaluation of the use of calibration chambers with the cone penetration test is given by Been et al. (1988). Possible sources of error include density determination, nonuniformity of stresses due to arching, chamber size and boundary effects.

F. In Situ Methods for Liquefaction Evaluation

The need for development and increased application of in situ testing has been expressed by Casagrande (1976), Peck (1979), and Poulos (1988) among others. Advantages of in situ testing include 1) cost effectiveness, 2) a larger tested volume, and 3) avoidance of difficulties in laboratory testing such as sample disturbance and improper simulation of stresses.

1. Field Correlation Methods

The most common field correlation methods utilize the Standard Penetration Test and Cone Penetration Test. The widely used Standard Penetration Test (SPT) provides a large amount of data for correlation in areas where earthquake induced liquefaction has occurred. Recently, considerable effort has been made to correct SPT N values

(blowcounts) for depth, energy, grain size, and equipment. Empirically corrected data has been used by Seed (1985) to produce correlations with liquefaction. This method is qualitative due to inherent limitations of the SPT. These limitations include lack of repeatability, insensitivity to layering, and unknown dynamic mechanisms (Peck, 1979 and Tokimatsu, 1988).

The Cone Penetration Test (CPT) has advantages over the SPT that include better repeatability, standardization, and more thorough interpretation of soil profiles. However, the limited number of case histories necessitate correlating CPT tip resistance to SPT N values and then using the SPT correlations as indices (Robertson and Campanella, 1985, Seed and DeAlba, 1986, and Ishihara, 1985). In addition to sharing some of the uncertainties of SPT correlations, use of the CPT is limited by 1) absence of sampling, 2) depth limitations, and 3) unreliability in coarse grained soils (Tokimatsu, 1988).

A less common field correlation tool is the flat plate dilatometer. Marchetti (1982) and Robertson and Campanella (1986) have studied its value in evaluating liquefaction potential, but their interpretations have not been field proven and apply only to clean sands.

Geophysical methods are also used. The shear wave velocity of a soil has been correlated with the potential for pore pressure buildup under cyclic loading (Dobry et al., 1981). This method is conservative since 100% pore pressure buildup in cyclic tests does not necessarily induce liquefaction in dense sands (Castro and Poulos, 1977).

2. Piezocone

The piezocone (sometimes called piezometer probe) is essentially a standard or electric cone penetrometer equipped for measuring pore pressure. A direct approach at using the piezocone for liquefaction evaluation has been attempted in a field studies by Schmertmann (1978), Campanella et al. (1983), and East et al. (1988). Current work by Canou et al. (1988) utilizes a miniature piezocone in the laboratory. Observed positive and negative excess porewater pressures in appropriate loose and dense sands offers promise as a field index. However, pore pressure responses in the field appear to be less than predicted. Sands had to be in a very dense state (DR > 80%, σ < 100 kPa) for minor development of negative excess pore pressure. This is explained by an overriding contractive behavior due to cavity expansion and normal stresses at the tip (Castro et al. 1982b). Other factors influencing pore pressure response are location of pore pressure measurement (Robertson, 1986), penetration rate (Canou et al., 1988) and permeability (Castro et al., 1982b). At this time, quantitative interpretation of piezocone data is restricted to estimates of drainage, equilibrium groundwater conditions, and soil profiling (Campanella and Robertson, 1988). Evaluation of liquefaction potential by the piezocone is qualitative.

G. Vane Shear Test

1. Background

The modern field vane is commonly a four bladed downhole device with a height to diameter ratio (H/D) of 2. It was introduced to widespread use by Cadling and Odenstad (1950) as a tool for determining the undrained shear strength of clays. Figure 2.5

illustrates the vane shear principal. Operation of the vane involves advancing it to the zone of interest and applying torque to induce failure. Typically, the undrained shear strength, S_{uv}, is calculated from the maximum applied torque using Cadling's equation,

$$S_{uv} = \frac{2M}{\pi D^2 (H+D/3)} \qquad (2.3a)$$

or, if H/D = 2 (ASTM D2573),

$$S_{uv} = \frac{6M}{7\pi D^3} \qquad (2.3b)$$

where M is the applied torque (corrected for shaft and bushing friction), H is the vane blade height, and D is the diameter circumscribed by the vane blades. The equation is derived by a simple integration over the failure surface area assuming a right cylindrical failure surface, uniform shear stress and isotropic soil properties. Other equations allowing for strength anisotropy and various surface shapes on the cylinder ends are summarized by Donald et al. (1977).

2. Pore Pressure Response

Pore pressure response during vane shear increases with increasing rotation rates. Measurement of induced pore pressure was first attempted in laboratory tests by Wilson (1963). An analytical model by Blight (1968) gives excess porewater dissipation, U, as:

$$U = 1 - \frac{1}{T}\left\{\frac{4}{\pi^3}\sum_{n=1}^{\infty}\frac{(-1)^n}{n^3}\sin\frac{n\pi}{2}\exp\left(-\pi^2 n^2 T\right)\right\} \qquad (2.4)$$

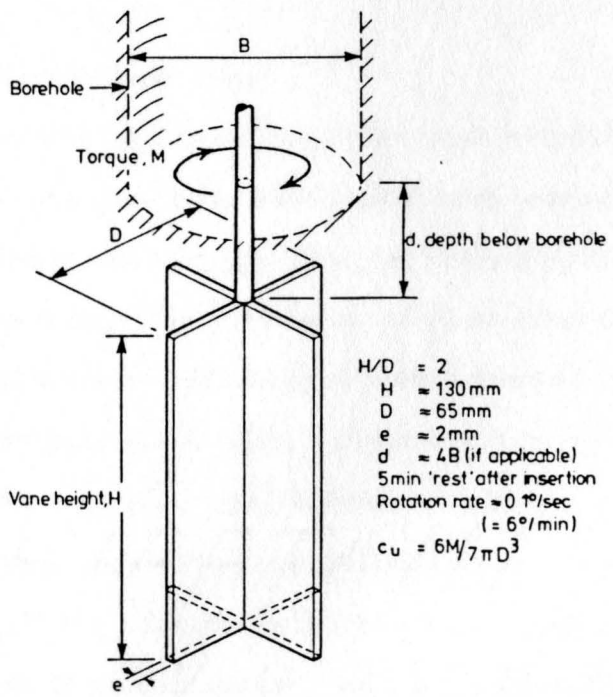

Figure 2.5 The Vane Shear Principal (Chandler, 1988)

where $T = C_v t_f / a^2$ = dimensionless time factor, C_v is the soil's coefficient of consolidation, t_f is the time to failure, and a is the spherical radius of influence or constant pressure outer boundary. Blight indirectly confirmed the model in a field test on silt size mine tailings. Since time to failure is a function of strain rate, the above model appears useful in selecting vane rotation rates.

In addition to contractive/dilative pore pressure response on the shear plane, pore pressure is induced by stresses normal to the vane blade faces. Laboratory studies and finite element modelling by Matsui and Abe (1981) and Kimura and Saitor (1983) show that excess pore pressure is positive on the face of the vane blades toward the direction of rotation and negative on the blade face opposite the direction of rotation.

3. Factors Affecting Vane Shear

The mechanisms during vane insertion and rotation are quite complex. Numerous studies have been done both analytically and empirically to increase the understanding of actual stress conditions during shear and determine the effects of vane dimensions, soil anisotropy, strain rate, drainage, vane insertion and test interpretation on determined strength. Comprehensive reviews of these studies by Mahmoud (1988), and Chandler (1988) indicate the simplifying assumptions implied by equation 2.3 are valid for most applications. That is, the shear zone is cylindrical in shape, strength is mobilized in direct shear, and radial stresses control strength.

4. The GEI Vane

The study by Castro et al. (1982b) involved a small (D = 4.1 cm), eight bladed vane tested in a small calibration chamber. The vane was equipped for pore pressure measurement on the vane shaft, but only drained tests were successfully accomplished.

Drained test results indicated dilation and contraction caused changes in effective stresses normal to the vane shear surface. Unexpected low strengths in some tests suggested the presence of arching due to inelastic compression.

H. Summary of Literature

Liquefaction is responsible for numerous landslides, failures of earth structures and foundation damage. The most common triggering mechanism causing liquefaction is earthquake loading. Other mechanisms include blasting and static loading.

The definition of liquefaction, using the steady state concept, is a loss of shearing resistance to the point where the driving shear mechanisms cause the soil mass to flow in a manner resembling a liquid. Liquefaction has the potential of occurring when the driving shear stresses exceed the undrained steady state shear strength in a contractive, saturated, cohesionless soil. The steady state shear strength is the shearing resistance at large deformations, or steady state, where stresses and volume remain constant.

The conditions of stress and void ratio at steady state are represented by the steady state line. The steady state line is thought to be unique for a given soil. However, type and rate of loading may also influence the position of the steady state line. The recommended laboratory method for evaluating liquefaction

potential is the CU triaxial test for establishing the soil's steady state line and subsequent testing of "undisturbed" samples.

In situ methods for evaluating liquefaction potential include the use of SPT and CPT data correlated with the occurrence or non-occurrence of liquefaction. These indirect determinations involve numerous empirical corrections which limit their reliability. The piezocone shows promise for a more direct determination of liquefaction potential. Experience is limited, and effects of cavity expansion and unknown stress states at the cone tip are thought to be significant. Other in situ methods include the dilatometer and geophysical methods.

Shear strength from the vane test is calculated from measured torque using Cadling's equation (equation 2.4), or a variation of the equation depending on anisotropy. Study of pore pressure response during vane shear of clays shows that pore pressure buildup is proportional to rotation rate and of opposite sign on opposing blade faces. An analytical spherical model of pore pressure dissipation appears to be useful in selecting vane rotation rates. Numerous studies of the complex mechanisms affecting vane shear have been done and attempts to correct for these influences have been made.

III. SOIL PROPERTIES

The soil chosen for this study, Lytle Sand, is a fine grained, subrounded to sub-angular quartz sand. It has characteristics that are sufficiently different from a medium grained angular sand used in another piezovane testing study. Other factors influencing this selection include availability and the need for detailed testing of this soil for other ongoing studies.

A. Source

The sand is derived from selected sandstones of the lower Cretaceous Lytle formation in northern Colorado. These sandstone units are fluvial in origin, having a depositional environment associated primarily with braided stream systems (Dolson, 1981). The in place composition varies but is approximately 85% quartz, 10% chert and silica cement, and 5% clays for the units of interest.

The sandstones of Lytle formation are selectively quarried, processed and sold as glass sand by Colorado Lien Company of Fort Collins, Colorado. The processing includes a minimum of three dry screening cycles to remove the coarse fraction. Fines are removed in a wet system using a spiral classifier, scrubber, hydrospec and cyclone separators respectively (Monell, 1989). The resulting product is a fine grained, narrowly graded sand consisting almost entirely of quartz and silica. Design specifications restrict 95 percent to lie between the number 40 and 140 sieve sizes.

B. Index Properties

A summary of index properties is given in Table 3.1. Figure 3.1 shows a scanning electron microphotograph of the sand. Sieve analyses (ASTM D422) used number 20, 40, 60, 80, 100, and 200 sieves. Resulting gradation curves are shown in Figure 3.2. Minimum and maximum dry densities were determined using ASTM D2049.

Permeability was determined for dense (e = .67) and loose (e = .78) samples using ASTM 2434. Twelve individual readings gave a mean permeability of 0.01 cm/s (standard deviation of .0018 cm/s) with no appreciable difference between the dense and loose samples.

Grain shape is subrounded to subangular using the Powers classification system (Blatt et al., 1972). The distribution of roundness appears to be bimodal, possibly as a result of the crushing and screening process.

Table 3.1. Index properties for Lytle Sand.

Classification (USCS)		SP
Coefficient of uniformity, Cu		1.7
D50		.26 mm
Minimum density:	e_{max}	.80
	γ_{dmin}	14.5 kN/m^3
	ρ_{dmin}	1480 kg/m^3
Maximum density:	e_{min}	.58
	γ_{dmax}	16.4 kN/m^3
	ρ_{dmax}	1672 kg/m^3
Permeability, k		1 x 10^{-2} cm/s
Shape		Subrounded to Subangular

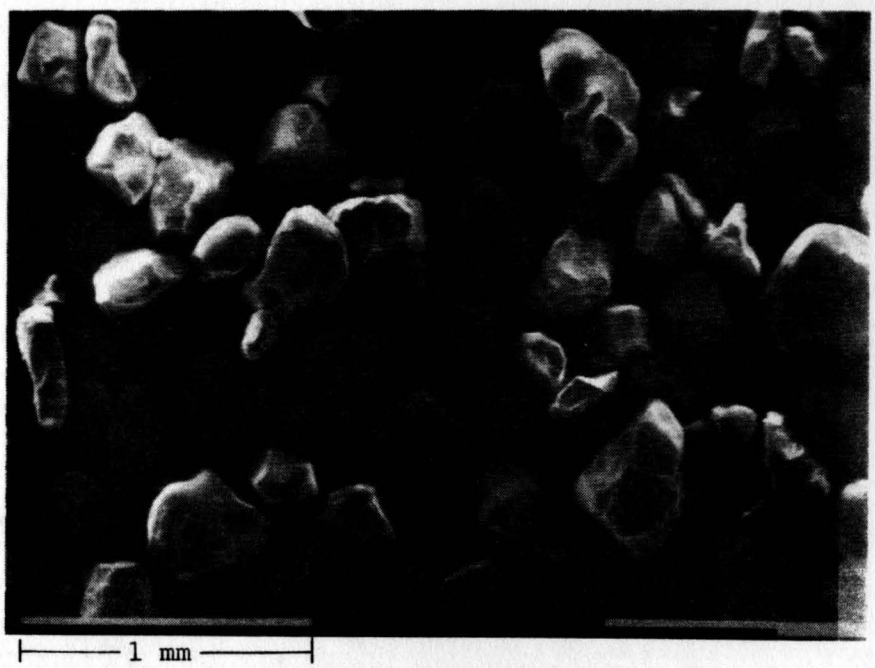

Figure 3.1. Scanning Electron Microscopy of Lytle Sand (taken at 39X).

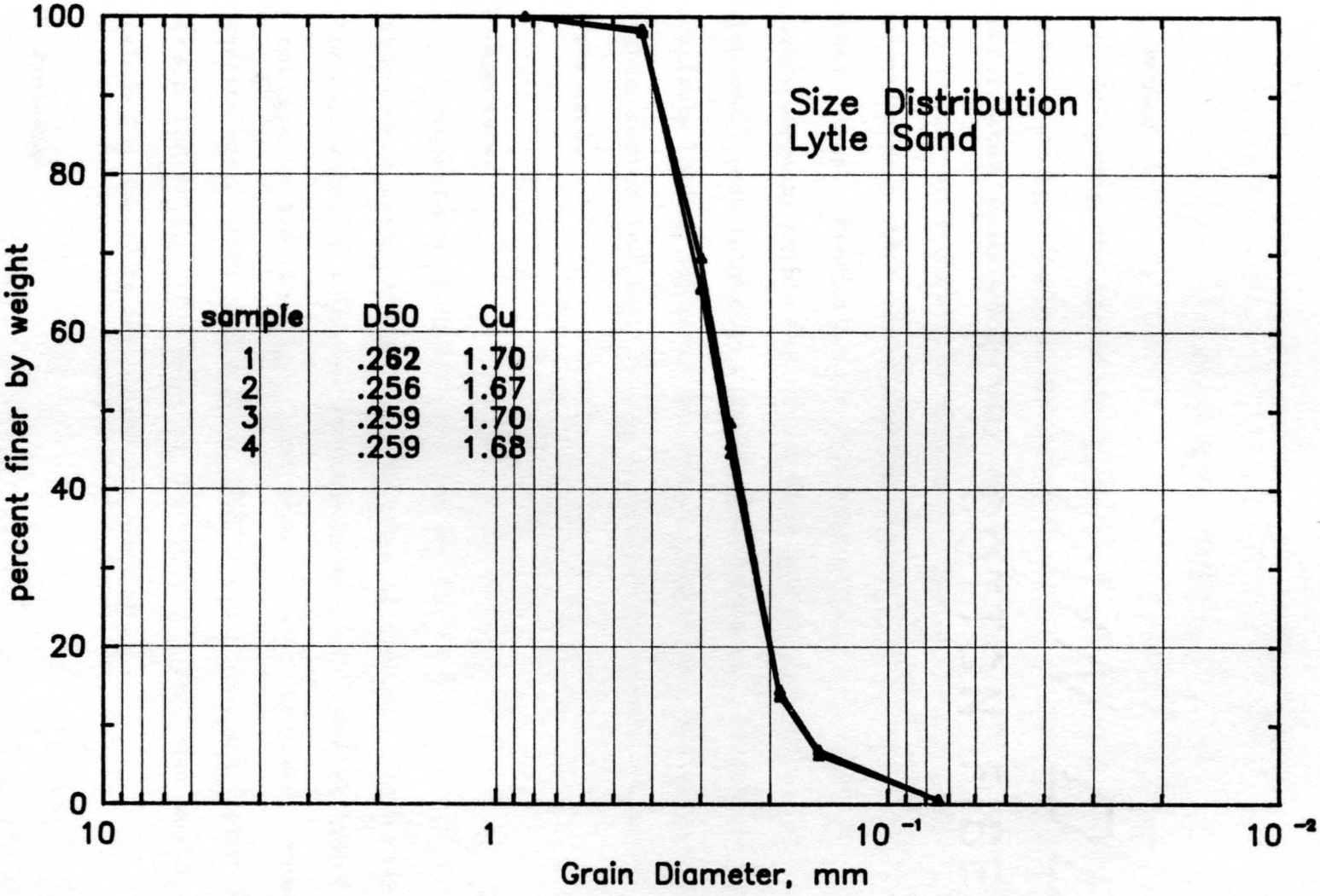

Figure 3.2 Grain Size Distribution Curves for Lytle Sand

IV. TRIAXIAL TESTING

A. Method

Following the recommendation by Castro et al (1982a) for establishing steady state relationships, this study utilized consolidated, undrained triaxial tests with pore pressure measurement (CU tests) on contractive specimens. Undrained contractive tests achieve steady state of deformation at much lower strains (<20%) than other tests. Previous work involved stress controlled tests, but Castro suggests strain controlled tests may be appropriate for sands with small peak to steady state changes in stress. In this study, the available loading apparatus was strain controlled. Resulting stress-strain curves indicate strain controlled tests were compatible with Lytle sand.

B. Apparatus

A conventional triaxial cell and an ELE Ltd Tritest 50 loading device were used for applying stresses to samples. Fluid pressures were controlled by a Wykeham Farrance model 13530 panel equipped with a calibrated Bourdon gage, hand pump and oil dashpots. Porewater pressure measurement used a Druck PDCR510 transducer and Vishay P30-A Strain Indicator. The base of the triaxial cell was modified to include CO_2 access to the sample for preflushing.

C. Procedure

Experimental procedure followed that outlined by Butler (1988, personal communication) for sands. The procedure uses guidelines

established by Silver (1977) and the Subcommittee on Soil Testing (1987).

Specimens were constructed in a split mold 3.6 cm in diameter by 7.3 cm in height. Samples consisted of 10 equal dry mass lifts placed by moist tamping. Although sample placement method was not critical in this type of test, it was important to maintain uniform densities. Lift height was controlled using the undercompaction method prescribed by Ladd (1978). The recommended undercompaction value of 5% (bottom lift) was used with no evidence of resulting nonuniform void ratios (forced failure planes, nonrepeatability, etc.). After placement, the sample diameter was measured in 3 places with a pi tape. Sample height was determined with a stand caliper. Both measuring devices are accurate to within .001 inches. Care was taken to minimize any unmeasured volume changes during subsequent saturation, consolidation, and shearing.

D. Test Results

A total of 15 tests were completed. Test R7 was terminated due to a membrane leak. Plots of the data are shown in Appendix A. Figure 4.1 shows four distinctive stress-strain type curves observed in the study by Castro et al. (1982a). Referring to Castro's figure, most of the tests in this study could be classified as either type A or B which are entirely contractive as desired. However, tests R1, R3, R5, R9, and R12 exhibited dilative tendencies during the latter part of shear. This stress-strain character is similar to the type D curves but to a lesser degree since induced pore pressures remained positive. These tests will subsequently be referred to as type BD.

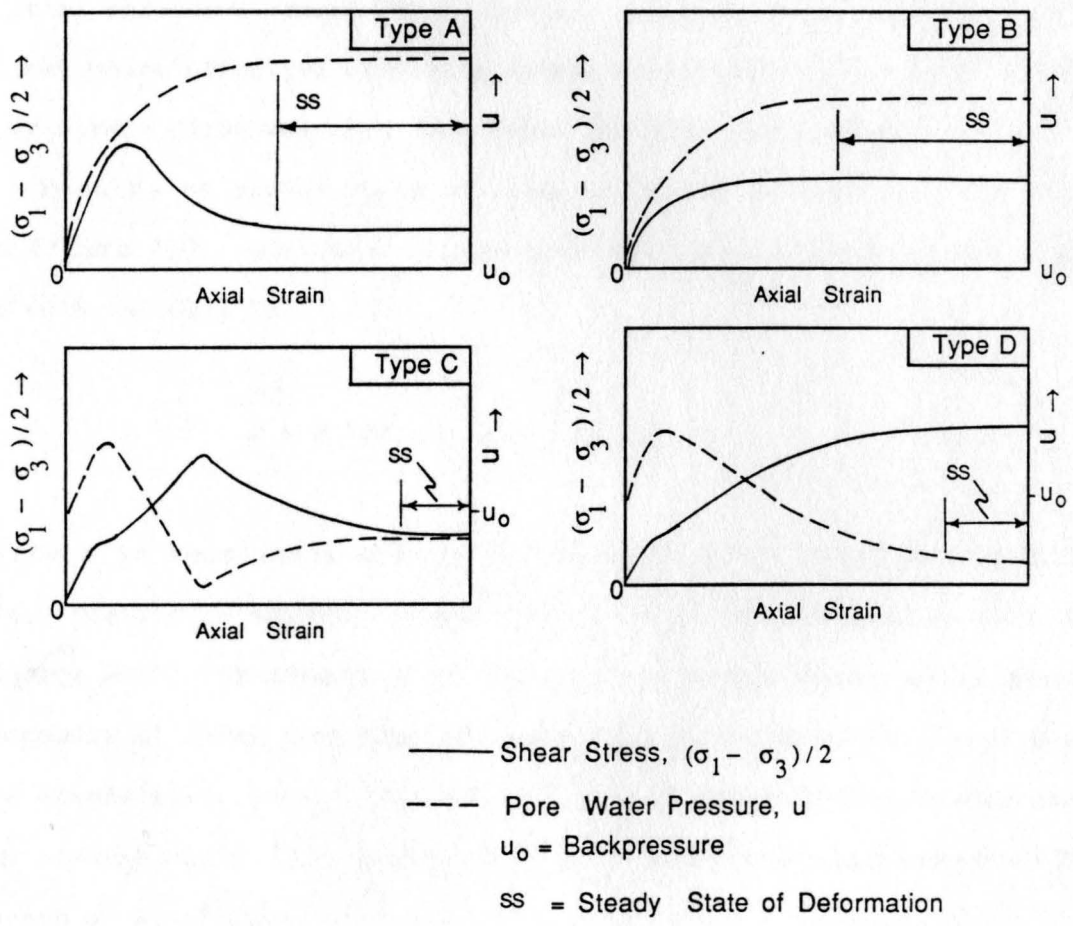

Figure 4.1 Typical Stress Strain Curves for CU Tests (After Castro et al., 1982a)

E. Interpretation of Data

Steady state exists at strains where shear stress and effective confining stress stabilize with continued deformation. Ideally, this is observed where slopes approach zero on the σ_3' versus strain and q versus strain curves. Peak and steady state are easily identified in the contractive (type A and B) tests. Difficulties arise in determining steady state of shear in dilative tests. Stresses stabilize at large strains where boundary effects and redistribution of void ratios become significant. Although some dilation occurs in the type BD tests, effective confining stress is still lower than initial effective stress in all tests. Steady states were selected either where effective confining stress stabilized or the slope of the q vs strain curve was zero, whichever behavior was present.

Results of steady state stresses are given it Table 4.1 and shown in Figure 4.2. A linear regression best fit steady state line (R^2=0.9, s=.017) is

$$e = 0.987 - 0.0872 \log \sigma'_{3s} \qquad (4.1)$$

where e is void ratio and σ'_{3s} is effective minor principal stress in kPa. Scatter is somewhat greater for the type BD samples as seen in Figure 4.2. Examination of the consolidation-shear state plots (Appendix A) shows that type BD tests were consolidated to states near the steady state line. This relationship of consolidation states near the steady state line and resulting scatter was also observed by Castro et al. (1982a).

Table 4.1. Summary of CU triaxial test results.

test	e_c	σ'_{3c} (kPa)	p'_s (kPa)	q_s (kPa)	ϵ_s (%)	σ'_{3s} (kPa)	ϕ'_s (deg)	S_{su} (kPa)	σ'_{fs} (kPa)
R1	0.734	487	803	404	8.2	399	30	349	600
R2	0.802	616	510	261	5.4	249	31	224	376
R3	0.721	772	1342	687	12.7	655	31	590	990
R4	0.787	723	569	293	6.0	276	31	251	418
R5	0.770	344	531	264	14.0	267	30	229	400
R6	0.794	550	465	240	7.0	225	31	206	342
R8	0.752	676	643	318	9.2	325	30	276	485
R9	0.731	751	1286	629	13.4	657	29	549	978
R10	0.780	618	565	280	5.3	285	30	243	426
R11	0.799	688	559	295	8.1	264	32	251	403
R12	0.781	619	824	409	12.0	414	30	355	620
R13	0.913	274	22	14	7.9	8	29	12	22
R14	0.868	445	53	31	10.8	22	30	27	45
R15	0.836	308	90	49	11.0	41	30	42	72
R16	0.826	376	101	56	11.2	45	31	48	81

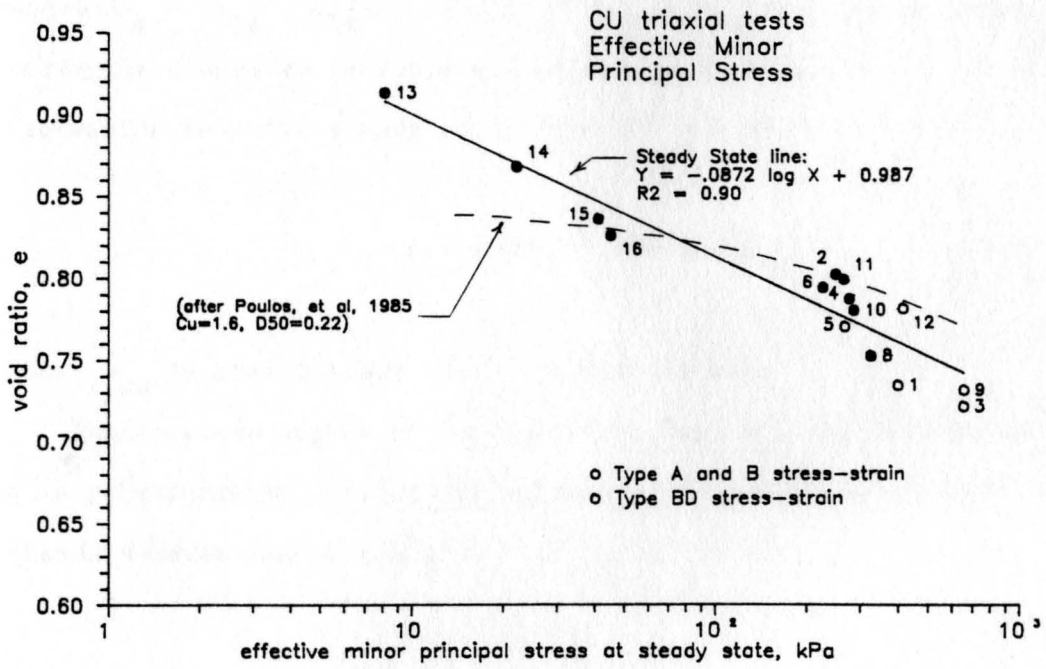

Figure 4.2 Effective Minor Principal Stress at Steady State

Shown in Figure 4.2 is the approximate location of a curve for a similar sand tested by Poulos et al. (1985). The SSL from this research is in the same general range of states, but exhibits more linearity. This difference in shape could be attributed to slight differences in angularity (Castro et al., 1982a).

Steady state shear strength is determined from stress paths. The q versus p' relationships (Lambe and Whitman, 1969) during shear are reasonably well behaved, so stress conditions at steady state are easily identified. To calculate steady state shear strength, S_{su}, the following equation was used.

$$S_{su} = q_s \cos [\sin^{-1} (q_s/p'_s)] \qquad (4.2)$$

where $q_s = (\sigma_{1s} - \sigma_{3s})/2$, and $p'_s = (\sigma'_{1s} + \sigma'_{3s})/2$. Steady state shear strengths are given in Table 4.1 and shown in Figure 4.3. The linear regression best fit steady state line ($R^2 = 0.89$, $s = 0.018$) is

$$e = 1.009 - .098 \log S_{su} \qquad (4.3)$$

where S_{su} is steady state shear strength in kPa.

Steady state angles of internal friction, ϕ'_s, are determined from p'-q relationships. Friction angles have a mean value of 29.9^o with a standard deviation of 1.8^o.

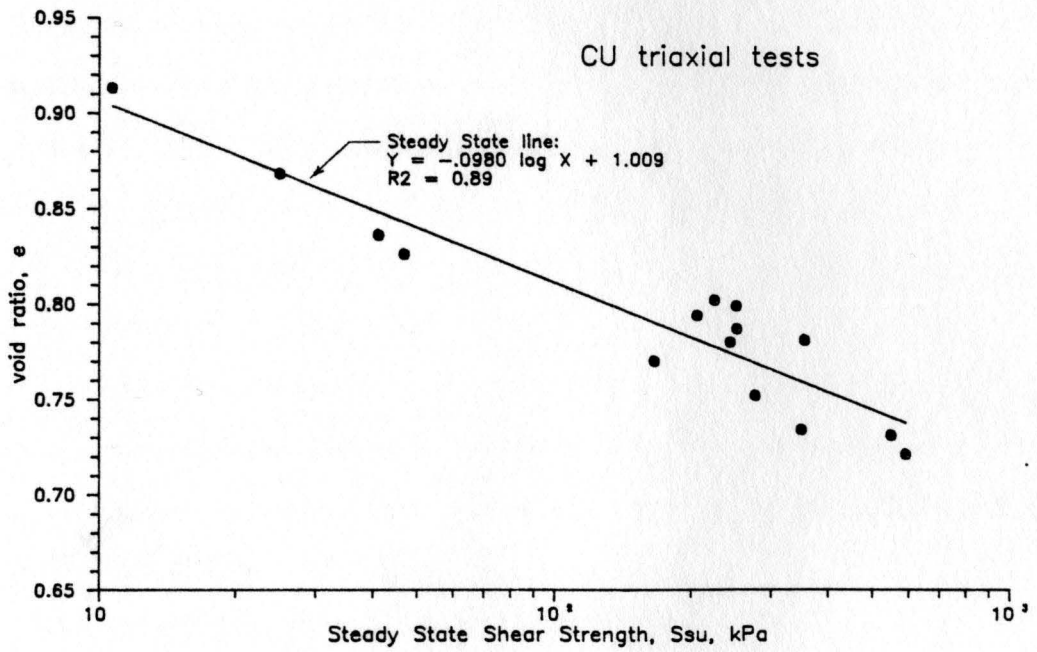

Figure 4.3 Shear Strength Steady State Line

Steady state effective stresses normal to the plane of shear, σ'_{fs} are calculated from equation 2.2 using the above values of ϕ'_s. The linear regression best fit steady state line ($R^2 = 0.9$, $s = 0.017$) is

$$e = 1.034 - .099 \log \sigma'_{fs} \qquad (4.4)$$

where σ'_{fs} is in kPa. Values of σ'_{fs} and ϕ'_s are listed in Table 4.1.

V. PIEZOVANE INVESTIGATION

A. Approach

Laboratory testing of the piezovane requires simulating field conditions while controlling stresses and sample densities. The soil mass should be infinite acting in terms of total stress, strain and transient porewater pressure response during shear. For high permeability soils, a large sample volume and high strain rates are necessary to approach undrained conditions on the shear plane while maintaining a constant pressure outer boundary. The calibration chamber designed by Dr. W.A. Charlie and W.T. Butler meet these conditions within practical reason and was chosen for this research (Butler, 1988, personal communication). The following guidelines were considered in designing this investigation.

- Samples should be placed moist using the undercompaction method.
- Samples should be consolidated to states that show both contractive and dilative tendencies during shear.
- High, uniform vane rotation rates are desirable for undrained conditions and repeatable results.

Ideally, strain rates should allow effectively undrained ($U < 10\%$) conditions on the shear plane. However, the selection of a high rotation rate was moderated by factors such as physical limitations in turning the vane and inertial effects.

B. Apparatus

1. Piezovane

The piezovane is 63.5mm in diameter by 127mm in height and has a blade thickness of 3.2mm. These dimensions satisfy ASTM D2573 recommendations for a conventional NX casing size vane. The vane shaft is 19mm in outside diameter as opposed to the ASTM recommended 12.7mm. Four 1.5mm ports provide continuous fluid from the vane blade edges to a pressure transducer mounted in the male connection at the top of the piezovane. A detailed drawing of the piezovane is given in Figure 5.1.

2. Calibration Chamber

The chamber used in this study is a K_o (zero lateral strain) cell with vertical stress applied across a membrane in the bottom. More elaborate cone testing chambers are equipped with side membranes to provide constant lateral total stress (Been et al., 1988, and Bellotti et al., 1982, 1988). Since there is zero net volume displacement by the vane and shaft during rotation, the less expensive, more reliable K_o design was chosen for this investigation.

A diagram of the calibration chamber is shown in Figure 5.2. It accommodates a .214 m^3 sample that is .78 m in height and .59 m ($\simeq$10 vane widths) in diameter. Shaft friction is minimized by a Thompson linear bearing. Vertical motion of the bearing allows advancement of the piezovane so each sample can be tested twice. The cap, bearing and shaft are removed as a unit for sample placement. A diffuser provides fluid access to the sample. It consists of 3/8" Polyflo^{TM} tubing in concentric rings 45 and 28 cm in diameter. The tubing is

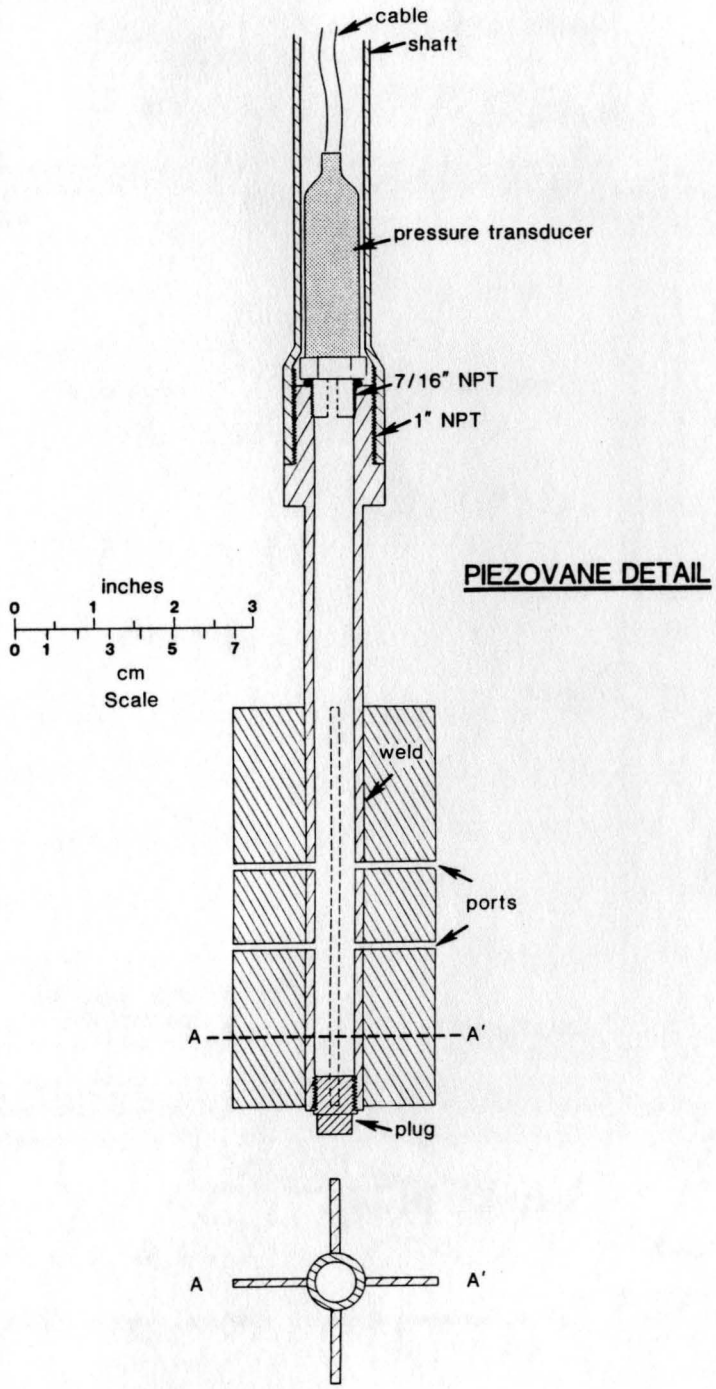

Figure 5.1 Diagram of Piezovane

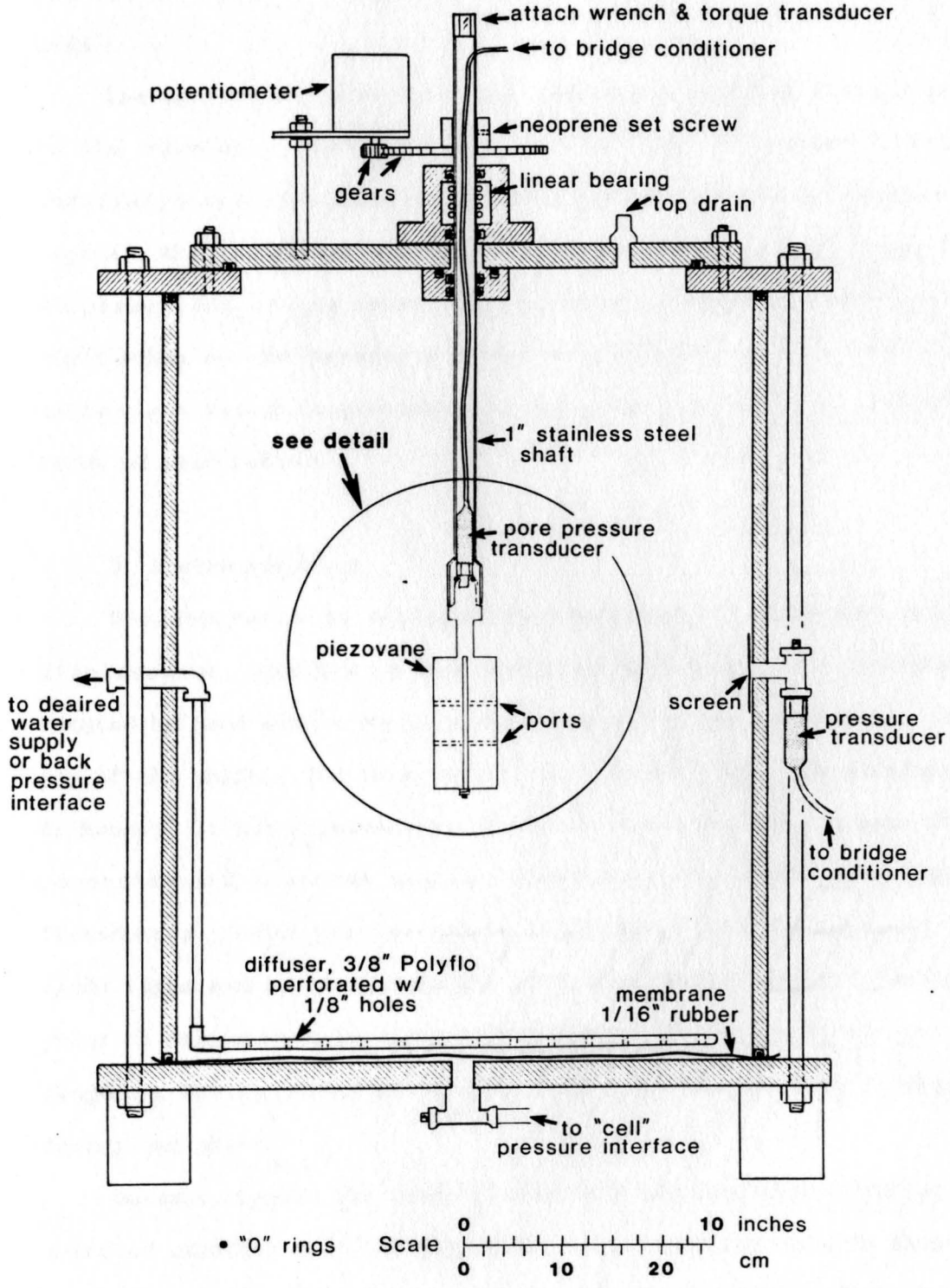

Figure 5.2 Diagram of Calibration Chamber

perforated with 48 holes 3.2 mm in diameter and screened with 200 mesh.

The system for saturating the sample and applying fluid pressure to the chamber is shown in Figure 5.3. The air-water pressure interfaces contain paraffin diaphragms surrounded by kerosene to separate the two phases and minimize gas solution. Due to large fluid displacements during consolidation, volume changes are measured from sight tubes on the pressure interfaces instead of burettes. This method was found to provide more than adequate precision (±.00035 in terms of void ratio).

3. Instrumentation

The apparatus is equipped to electronically measure angular displacement, applied torque and pore pressure. The piezovane is rotated by hand with a torque wrench placed in the torsion cell at the top of the shaft. The torsion cell is a strain gage type manufactured in-house. It has a resolution of 4mv or about one N-m. A gear driven potentiometer measures angular displacement to within ±0.4 degrees. Transducers provide pore pressure measurement at two opposing vane blade edges and at the mid-height perimeter of the sample. The second point of measurement provides determination of the transient nature of response during shear along with a check on the piezovane transducer during non-shear.

Output signals are read by transient data recorders (TDR's) at a selected sampling rate and digitized. The digitized data is then read into a personal computer for graphics display and floppy disk storage. Real-time graphics and data are provided by an oscilloscope. A

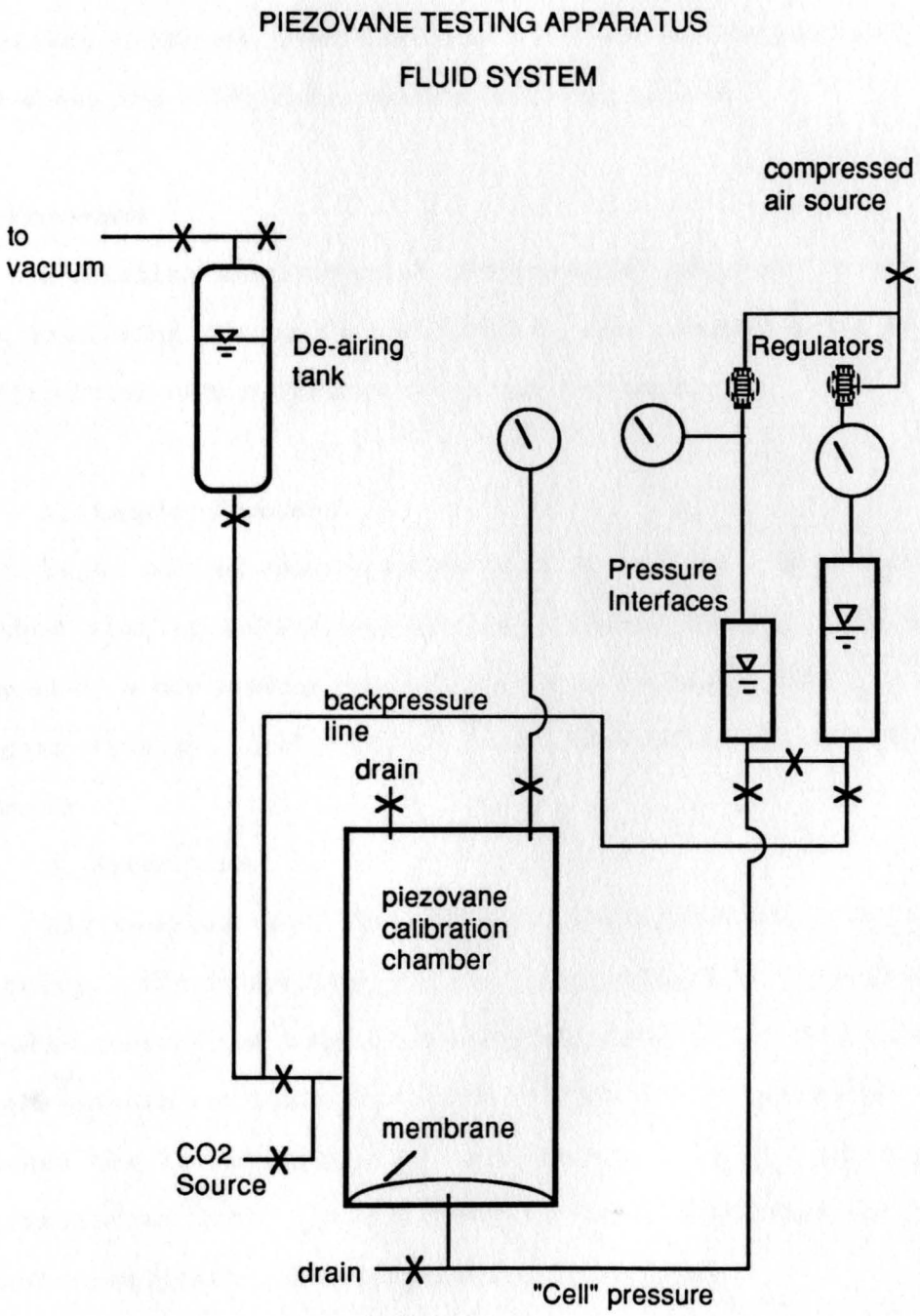

Figure 5.3 Diagram of Fluid Pressure System

diagram of the instrumentation and data recording system is shown in Figure 5.4.

Photographs of the piezovane, data acquisition system and fluid pressure panel are given in Figures 5.5 and 5.6 respectively. Figure 5.7 shows the calibration chamber with cap removed.

C. Procedure

A detailed description of the procedure is given in Appendix C. The following discussion highlights the procedure and encountered difficulties with reference to particular tests.

1. Sample placement

Eight out of nine samples were placed by a moist compaction method similar to the one used in triaxial testing. Sample PV7 was placed by a dry pluviation method (Rad and Tumay, 1987) to obtain a higher density. All samples were recycled except for minor makeup amounts.

2. Saturation

All samples were flushed from the bottom with CO_2 prior to wetting. After wetting, 1.5 to 3 pore volumes of deaired water were flushed through the sample. Saturation data is given in Table 5.1. Backpressure was limited to about 140 kPa by the apparatus. Test PV4 showed the lowest degree of saturation, with a C pore pressure parameter of 0.81. Several samples were rechecked for "C" values after consolidation with no appreciable decrease.

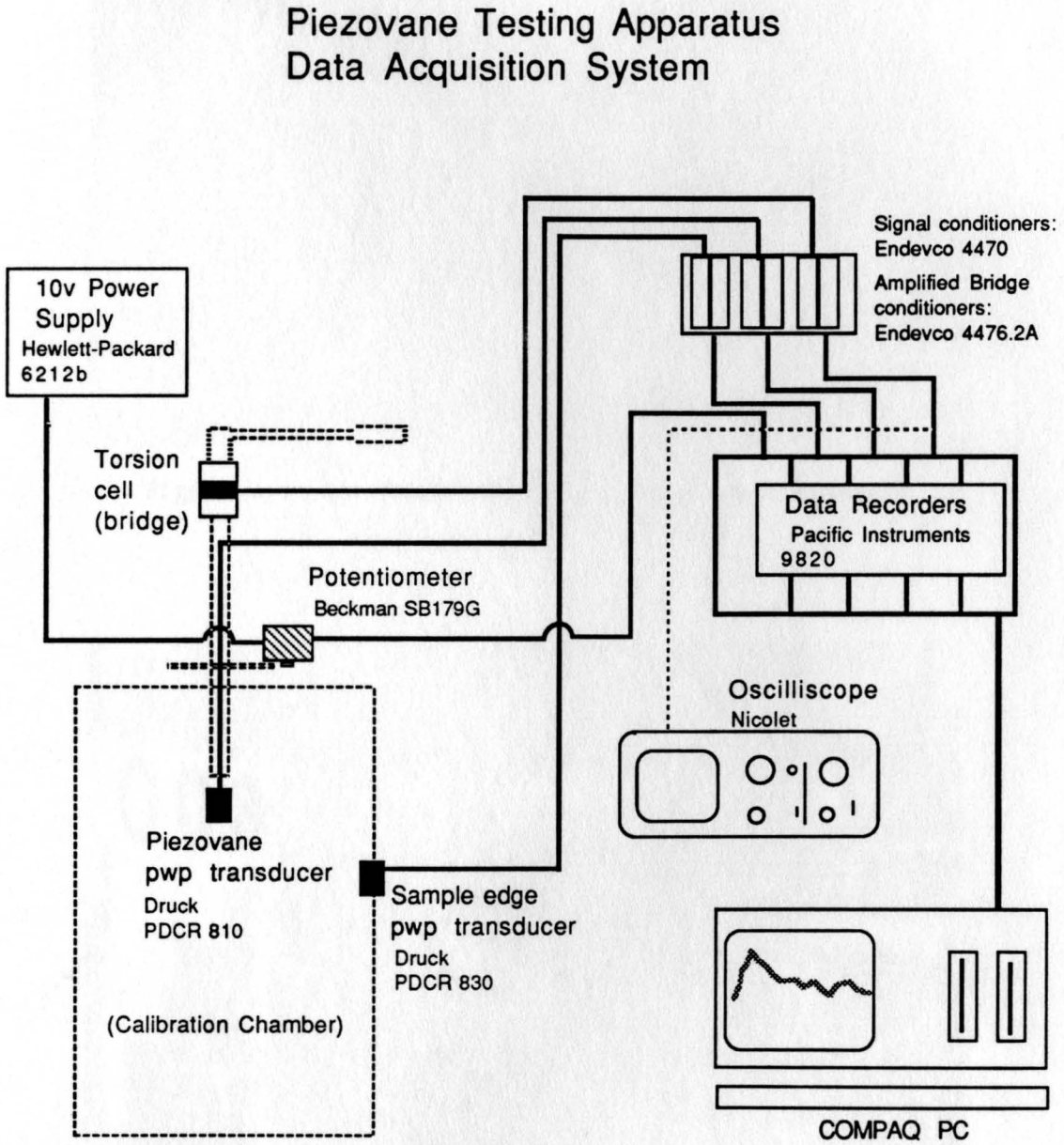

Figure 5.4 Diagram of Instrumentation and Data Recording System

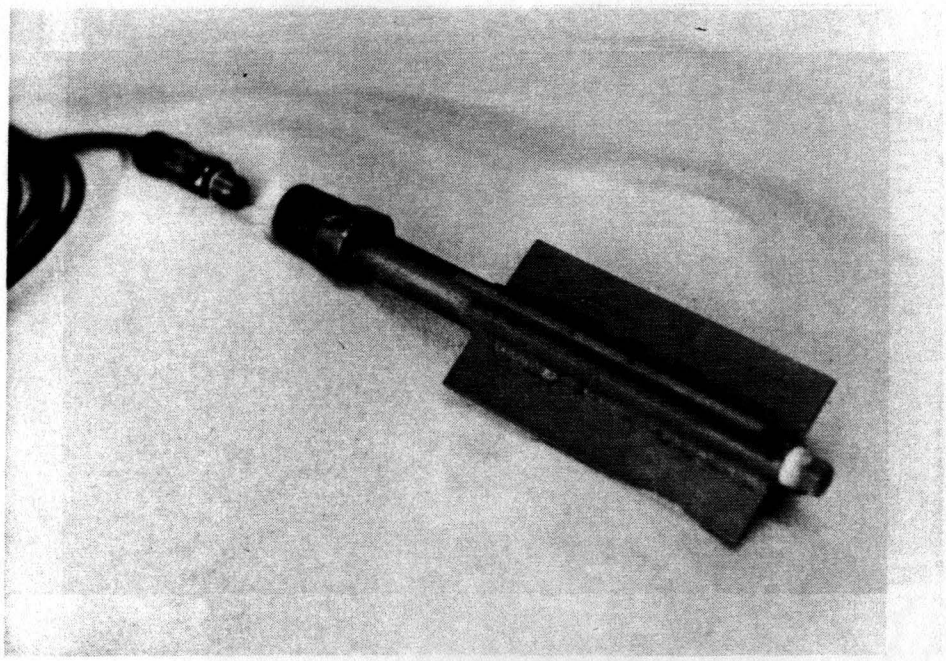

Figure 5.5 Piezovane and Druck Pressure Transducer

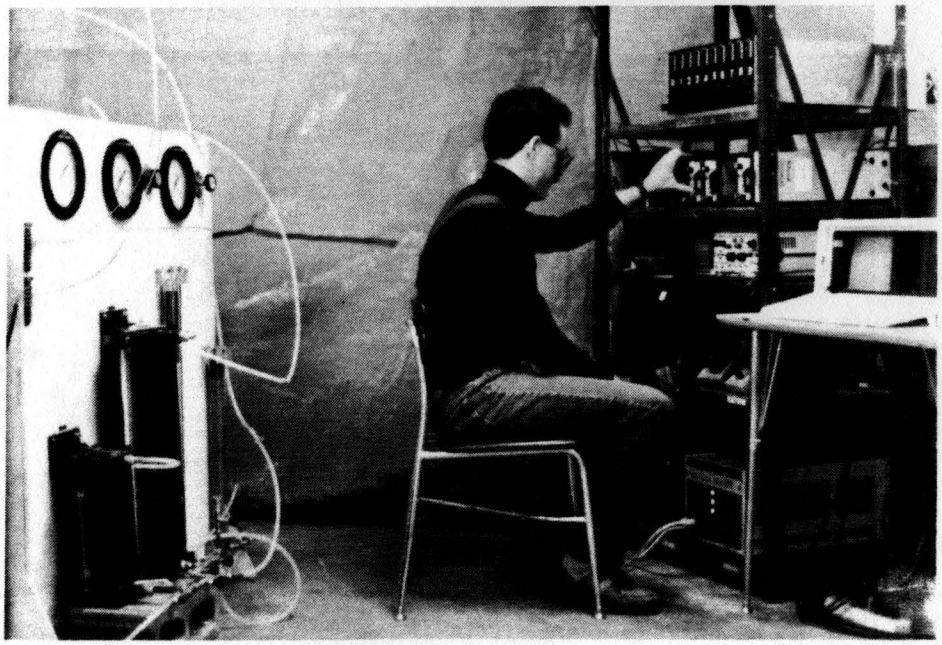

Figure 5.6 Pressure Interfaces and Data Acquisition System

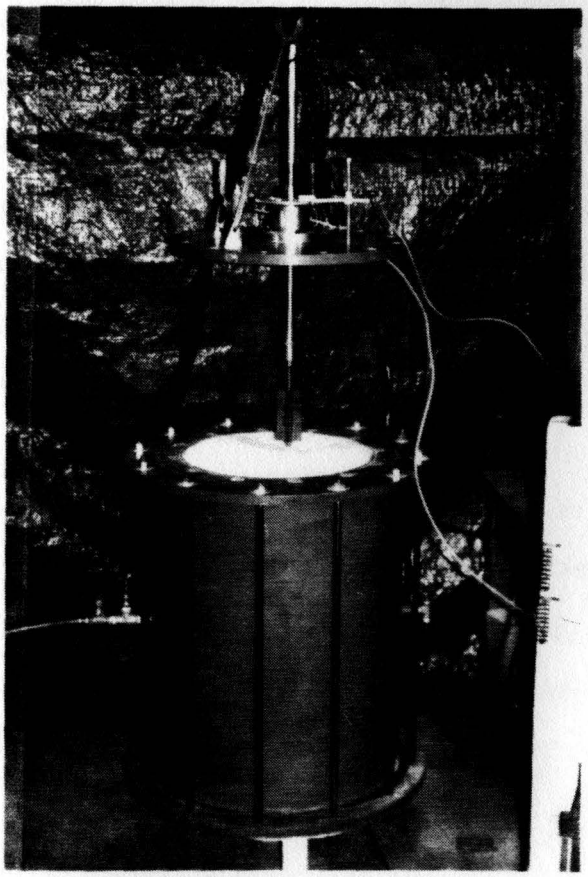

Figure 5.7 Calibration Chamber before Piezovane Insertion

Table 5.1. Saturation data for piezovane tests.

test	Backpressure (kPa)	"C" Parameter Before Consolidation	"C" Parameter After Consolidation
PV1	138	.88	.86
PV2	103	.86	(membrane leak)
PV3	69	.89	
PV4	138	.81	.84
PV5	103	.82	
PV6	103	.94	
PV7	103	.82	
PV8	103	.95	.94
PV9	103	.92	.90

3. Consolidation

Samples were consolidated using 17 or 34.5 kPa increments. A period of 10-12 hours was allowed after the last increment and before shearing. Total consolidation time averaged 20 hours. Consolidation data from nine tests are presented in Figure 5.8. Collapse is significant in samples placed loose. I was unable to consolidate any samples to a state above the triaxial steady state line.

4. Shearing

The first test, PV1a, was rotated at a rate of 11 seconds per revolution (33^{o}/sec) and gave minimal transient pore pressure response. The target rate was then set at 4 to 5 seconds per revolution ($72\text{-}90^{o}$/sec) for the remainder of this investigation. Since shearing was done by hand, target rates were not always maintained.

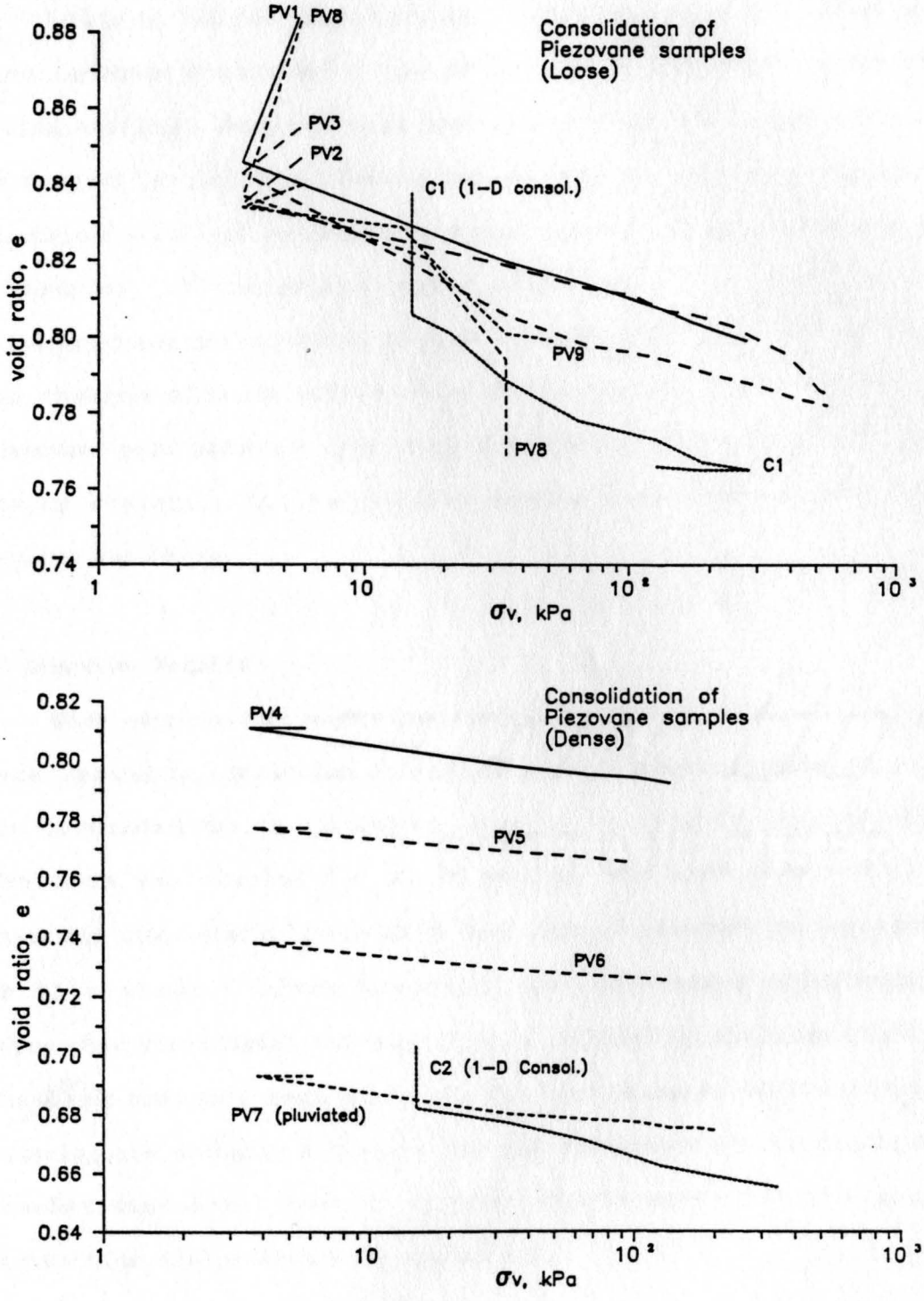

Figure 5.8 Consolidation of Loose and Dense Piezovane Samples

5. Data Processing

Voltage values for torque, pressure, and rotation were simultaneously recorded in 16 ms intervals and stored by the TDR's during testing. Data was then loaded onto floppy disks and converted to respective units of Newton-meters, kPa, and degrees. Significant electrical noise of unknown origin was experienced in the sample edge transducer. These spikes were filtered out by an algorithm which eliminated any points which created a slope greater than 0.5 kPa/ms and changed sign on either side of the point. Both the side and piezovane pore pressure data were smoothed with a 64 ms triangular moving average. The torque and angular displacement data did not require smoothing.

D. Shearing Results

Nine samples were placed and consolidated. A total of 8 samples were tested to completion, giving 16 sets of shearing data. Test PV2 was terminated due to a membrane leak at the end of consolidation. The data was sampled out to 95 seconds for each test. Only the shearing time intervals (usually less than 10 seconds) are considered in this study. After shearing, pore pressures asymptotically approached the initial value or a value allowed by the sensitivity of the back pressure regulator. Excess pore pressure dissipation after shearing was probably a function of the efficiency of the calibration chamber diffuser. Torque, angular displacement and pore pressure versus time are presented in Appendix C.

1. Torque and pressure versus displacement

Torque and pressure are plotted versus displacement to examine stress-strain relationships. All tests show low pore pressure response, indicating drainage. Most tests, however, exhibit a definite positive or negative peak in pore pressure, indicating contractive and dilative tendencies. Seven tests show contractive peaks and nine tests show dilative peaks.

Figure 5.9 shows a contractive test. Induced pore pressure at the piezovane exhibits a definite positive peak. Less response is observed at the sample edge, indicating transient conditions during shear. After peaking, torque tends to oppose the piezovane pore pressure. This relationship may reflect effective stress changes normal to the shear plane. The vertical spikes represent pauses in rotation from physical difficulty in rotating the vane.

A dilative response is shown in Figure 5.10. The opposing tendency of the torque and piezovane pore pressure is very pronounced. Response of the sample edge is minimal, indicating little boundary influence.

The above examples represent extremes of observed pore pressure response. All other test results indicate intermediate response. Plots of torque and pore pressure versus displacement for all tests are given in Appendix B.

2. Drainage

The low magnitudes of pore pressure response prompted further investigation into drainage. Using time rate of displacement data, Blight's equation (equation 2.5) and measured soil properties,

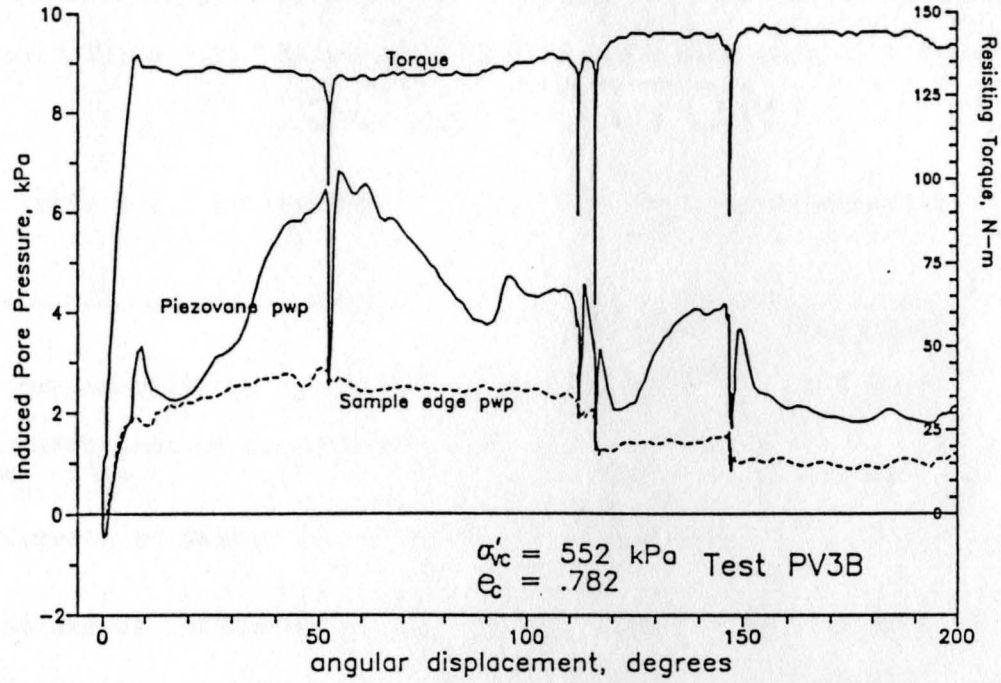

Figure 5.9 Piezovane Test Results showing Contractive Behavior

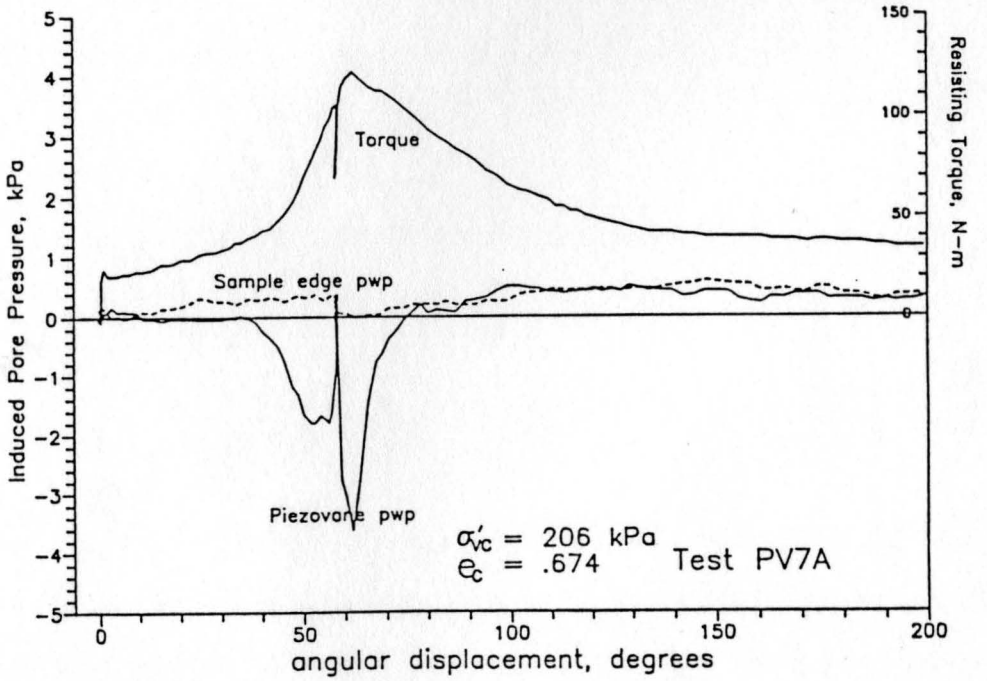

Figure 5.10 Piezovane Test Results showing Dilative Behavior

estimates of excess pore pressure dissipation were determined and are shown in Table 5.2. Estimates indicate tests were partially drained.

Table 5.2. Estimation of Excess Pore Pressure Dissipation.

	Best Case	Worst case
Compressibility, m_v, m^2/kN	5.5×10^{-4}	1.5×10^{-5}
Coefficient of Consolidation, C_v, m^2/s	185	6793
degrees to failure	5	20
sphere of influence, a, cm	9.35	6.35
dimensionless time factor, T	0.15	70.19
Excess Pore Pressure Dissipation, U (%)	36	99.7

Calculations used a permeability of 0.01 cm/s and an average rotation rate of rate of 72^{o}/s.

VI. ANALYSIS OF RESULTS

From the piezovane data, two dependent steady state variables common to the triaxial tests can be determined with a relative degree of confidence. These are effective stress normal to the shear plane, σ'_f, and shear strength, S. Calculation of these variables from vane tests requires the standard assumption of a uniform, cylindrical failure surface where radial effective stresses, σ'_h, control shear strength (Mahmoud, 1988).

A. Comparison of results

Piezovane steady state variables σ'_{fs} and S_s are presented in Table 6.1 and compared with steady state lines of the CU tests in Figures 6.1 and 6.2. The following discusses the calculation of these variables and how they compare with the CU triaxial tests.

1. Effective normal stress

During vane shear, effective stress normal to the vertical shear plane, σ'_f, can be estimated from effective vertical stress, σ'_v, by

$$\sigma'_f = K_o \, \sigma'_{vc} - \Delta u \qquad (6.1)$$

where Δu is induced pore pressure during shear. The coefficient of lateral stress, K_o, is assumed to be $(1 - \sin\phi')$, where ϕ_s' is the effective angle of internal friction. Calculations use an angle of 30^o which is the average value determined by the CU triaxial tests.

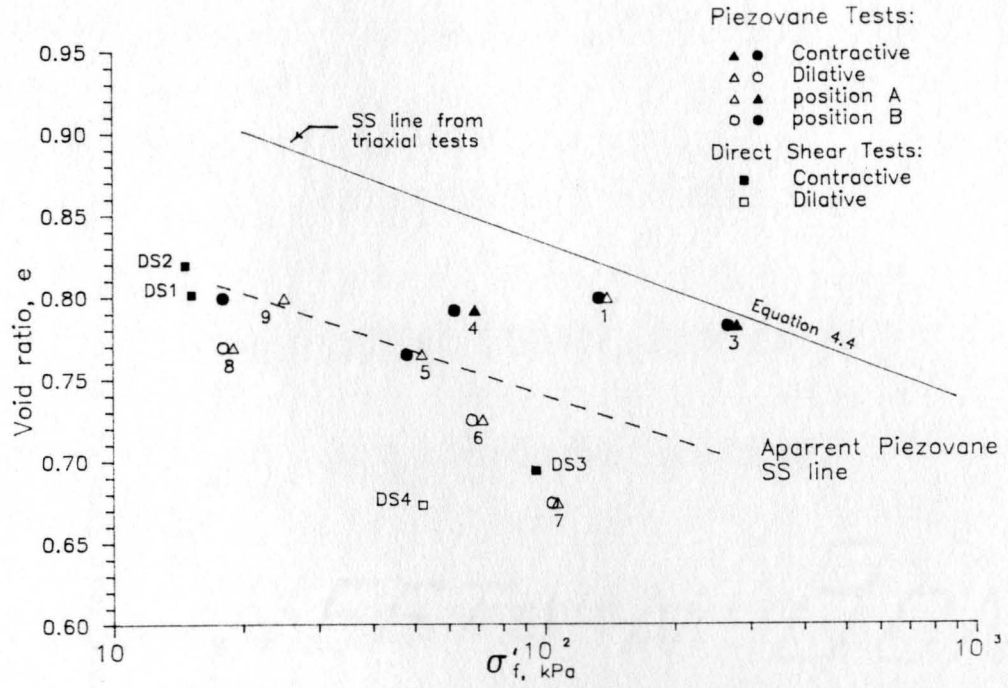

Figure 6.1 Comparison of Effective Normal Stress

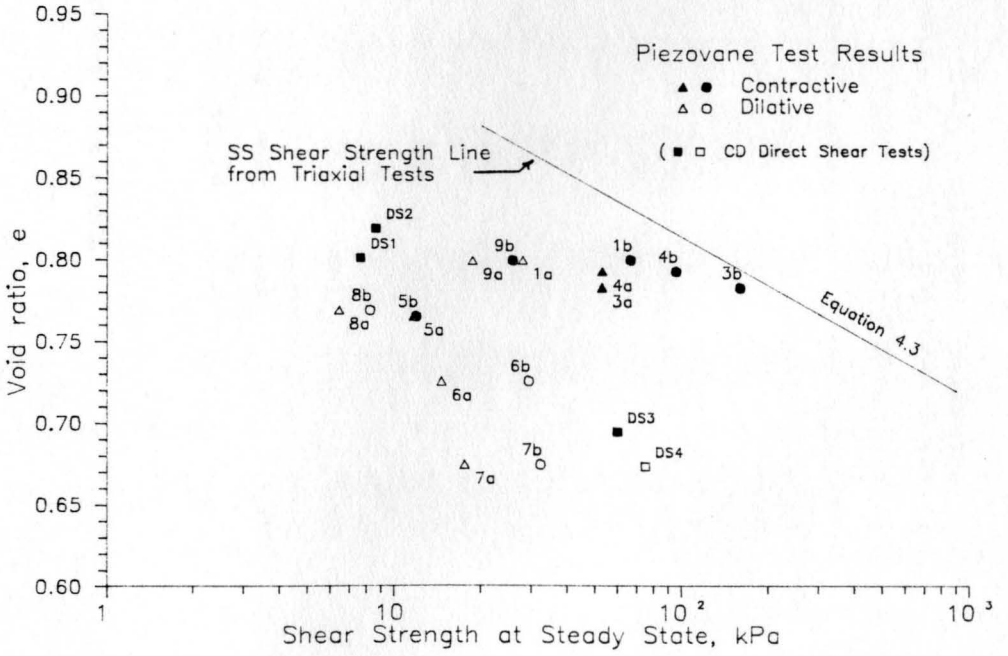

Figure 6.2 Comparison of Steady State Shear Strength

Table 6.1 Summary of Piezovane Test Results

test	e_c	σ'_{vc} kPa	σ'_h(1) kPa	Δu, kPa Peak	Δu, kPa SS	σ'_f, kPa Peak	σ'_f, kPa SS	S_V, kPa (2) Peak	S_V, kPa (2) SS	S_{ref}(3) kPa
PV1A	.799	276	138	0	1	138	137	64	23	80
PV1B	.799	276	138	1	2	137	136	109	54	79
PV3A	.782	552	276	1	5	275	271	102	43	159
PV3B	.782	552	276	7	4	269	272	133	130	155
PV4A	.792	138	69	0	-0.5	69	68	100	43	40
PV4B	.792	138	69	4	7	65	62	140	78	38
PV5A	.765	104	52	-0.5	0	52	52	21	10	30
PV5B	.765	104	52	2	4	50	48	37	10	29
PV6A	.725	138	69	-2	0	71	69	38	12	41
PV6B	.725	138	69	1	0	68	69	98	24	39
PV7A	.674	206	103	-4	0	107	103	113	14	62
PV7B	.674	206	103	-0.5	-0.5	104	104	102	26	60
PV8A	.769	34	17	-2	0.5	19	17	10	5	11
PV8B	.769	34	17	-1	3.5	18	14	13	7	11
PV9A	.799	52	26	-1	1	27	25	28	15	16
PV9B	.799	52	26	2.5	8	23	18	41	20	14

1. estimated as $K_o \sigma'_v$, where $K_o = 1 - \sin \phi'$
2. using modified Cadling's equation (eq. 6.2)
3. estimated, assuming $S = \sigma'_h \tan \phi'$

Equation 6.1 requires the additional assumption that total horizontal stresses remain constant and no volume change occurs. Effective normal stresses calculated in this manner are compared with the triaxial steady state line in Figure 6.1. Tests are labelled as contractive or dilative based on observed peak pore pressures. An apparent steady state line is implied by the piezovane that is parallel to, and below, the CU triaxial steady state line. This comparison is made with the initial void ratios since soil volume changes in the shear zone surrounding the piezovane are unknown.

2. Shear strength

Piezovane steady state shear strengths are calculated from

$$S_{vs} = \frac{3M}{4\pi D^3} \qquad (6.2)$$

which is Cadling's equation modified for stress anisotropy (Appendix D). The torque, M, is selected where values remained relatively constant with strain and time after the peak. Compared with the triaxial steady state shear strength line in Figure 6.2, piezovane results are much lower and exhibit a great deal of scatter.

B. Interpretations

The following interpretations are made to determine if observed pore pressure response adequately reflects volumetric strains during shear. Possible reasons for the difference between piezovane and CU triaxial test results are suggested.

1. Effect of volume change

Observed pore pressure response and estimates of dissipation in Table 5.2 indicate nearly drained conditions existed during piezovane shear, and volume changes occurred along the shear plane. Because a zero strain outer boundary was imposed, volume changes caused changes in normal stress. Due to limited pore pressure response, changes in effective stress were approximately equal to changes in total stress.

Volume change effects can be investigated by comparing observed behavior with a hypothetical case where no volume or total stress changes occur. Assuming no volume or total stress changes occurred during shear, an estimated, or reference (Castro et al., 1982b), shear strength on a vertical plane is calculated. Using the normal stresses calculated from equation 6.1 along with equation 2.1 gives

$$S_{ref} = \sigma_f' \tan \phi_s' \qquad (6.3)$$

Values of S_{ref} are compared with measured shear strengths in Figure 6.3. The position B tests are slightly less than the reference values, and the position A tests are significantly less. Assuming a reasonably constant friction angle, this indicates normal stresses decrease during shear.

When peak shear strength, S_{vp}, is plotted against the S_{ref} values in Figure 6.4, measured strengths are generally greater than the reference values, implying that effective stresses normal to the shear plane increase during shear. This same relationship was observed by Castro et al. (1982b) for drained vane shear in dilative sands well

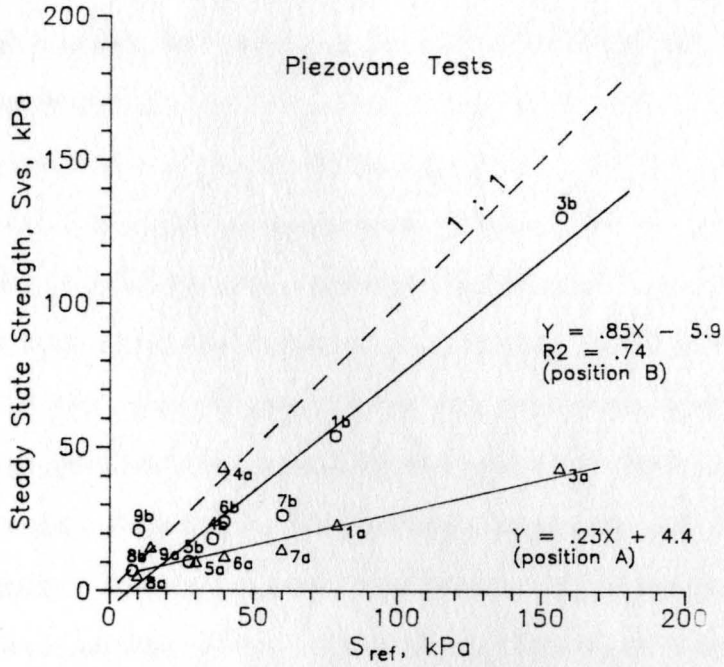

Figure 6.3 Measured Steady State Shear Strength Versus Reference Shear Strength

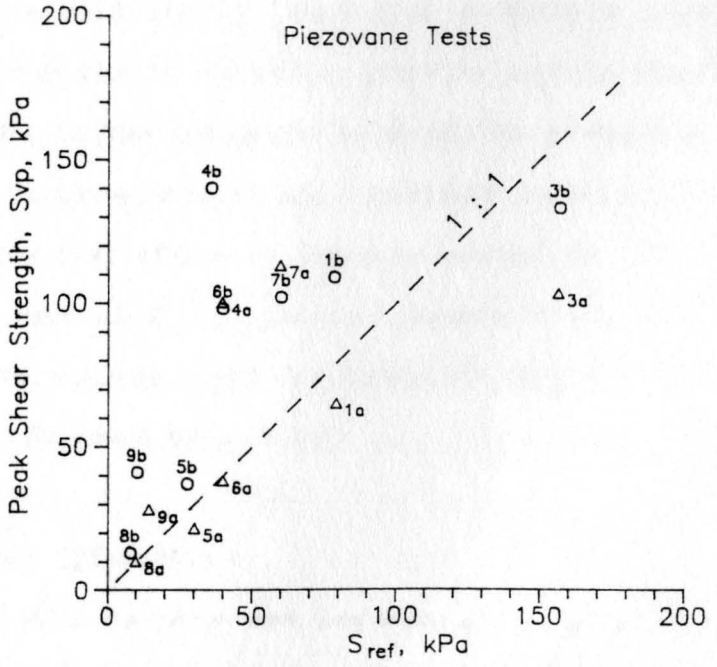

Figure 6.4 Measured Peak Shear Strength Versus Reference Shear Strength

below the steady state line. According to Castro, dilation in the shear zone causes an increase in effective normal stress during drained vane shear.

In Figure 6.4, tests PV3a and PV3b exhibit peak strengths significantly less than the reference value, implying a decrease in normal stress resulting from contractive behavior during shear. Based on observed pore pressure response and initial states from Figure 6.1, sample PV3 is the most contractive of all piezovane samples.

Although qualitative, analysis of measured peak shear strength tends to verify observed pore pressure response and associated void ratio changes. Dilative tests indicate an increase in effective stress normal to the shear plane while strongly contractive tests indicate a decrease in effective normal stress.

Piezovane steady state shear strength, especially in dilative samples, is significantly lower than undrained steady state shear strength from the CU triaxial tests as seen in Figure 6.2. This is primarily due to the drained nature of the piezovane tests. Other mechanisms at large strains may contribute to this difference. Figure 6.3 indicates that effective stresses normal to the shear plane are lower at initial K_o σ'_{vc} values. Castro et al. (1982b) encountered similar low values, and suggests it may be due to inelastic compression followed by arching.

2. Other influences

Positive pore pressure response is observed for initial states below the triaxial steady state line. This discrepancy may be due to a nonconservative triaxial steady state line, or a conservative estimate of effective stresses normal to the vane shear plane.

Strain-controlled CU triaxial tests have produced non-conservative steady state lines in past studies (Casagrande, 1971, 1976). Four consolidated drained direct shear tests were run to investigate effects of test type on position of the steady state line. Vane shear has similarities to direct shear that include unidirectional strain and forced location of the failure plane. As shown in Figure 6.1, the limited number of direct shear tests exhibited contractive behavior at states well below the triaxial steady state line. This indicates that type of loading (strain-controlled versus stress-controlled), mode of failure (unidirectional versus bidirectional), and forcing of failure planes may affect position of steady state lines.

Besides dilation, other mechanisms may cause a redistribution of stresses which result in an increase in lateral effective stress. If the coefficient of lateral stress, K, approaches 1 instead of ($1-\sin\phi'$), the piezovane tests are in closer agreement with the triaxial steady state line. Figure 6.5 shows the relationship between the triaxial steady states and piezovane tests, assuming $K = 1$.

C. Factors Affecting Experimental Results

Vane insertion affected shear strength and pore pressure response. This interpretation is made by comparing shearing results from upper (A) positions, where the sample was consolidated around the vane, with results from the lower (B) tests where the vane was advanced before shearing. The lower position tests show consistently greater shear strength, higher positive pore pressure response in contractive samples, and lower magnitudes of negative pore pressure response in dilative samples. Both phenomena are probably

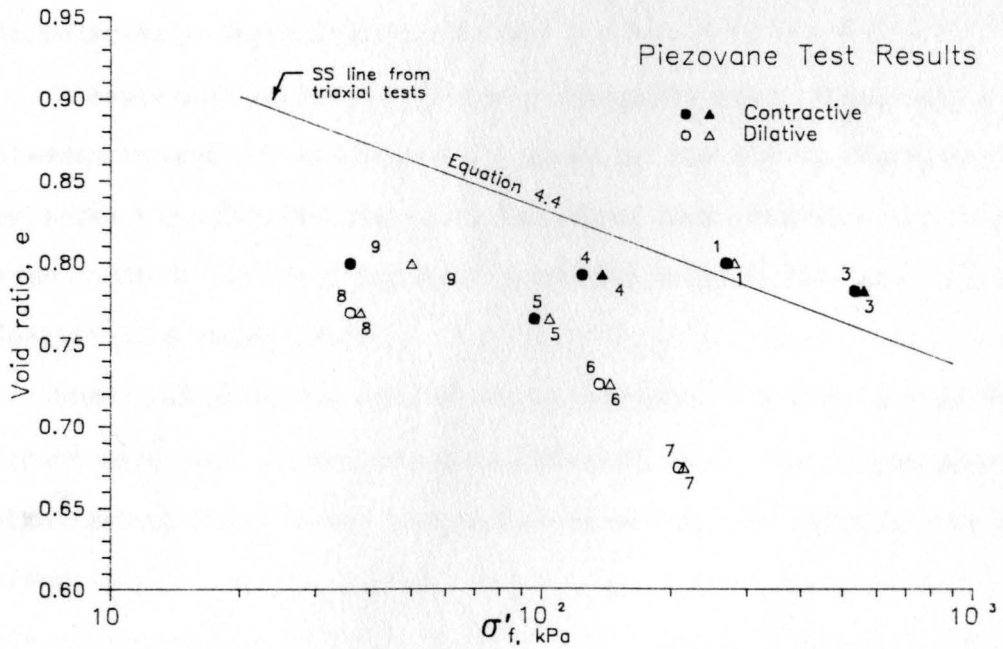

Figure 6.5 Comparison of Effective Normal Stress, Assuming K = 1

attributable to an an increased σ'_f caused by volumetric displacement of the vane.

Chamber size may have influenced radial stresses during consolidation and shearing. Referring to Figure 5.8, the consolidation curves for the piezovane tests indicate a lower compressibility than results from 1-D consolidation tests. If this is due to arching, void ratios would be higher than estimated in the upper part and lower than estimated in the lower part of the chamber. This is inconclusive, however. Other factors influence stress-strain behavior such as sample placement (Mulilis, et al, 1977) and time effects (Mitchell and Solymar, 1984). During shear, interpreted behavior such as increasing normal effective stress and arching due to inelastic deformation may have been magnified by boundary effects from the relatively rigid chamber walls.

Measurement error was probably insignificant. Cumulative error in measurement of average void ratio at the end of consolidation is approximately .009 for the piezovane tests and .012 for the triaxial tests. Other errors may have been introduced but are not easily identified or quantified.

Inertial effects appear to be minimal. Based on time rate of displacement data, the maximum acceleration at the blade edges was approximately 0.1g in the tangential direction and .008g in the normal direction.

VII. SUMMARY, CONCLUSIONS AND RECOMMENDATIONS

A. Summary

This laboratory study investigates the ability of the piezovane to directly determine soil properties associated with liquefaction potential. The soil tested is a fine grained, subrounded quartz sand. The soil's contractive/dilative tendencies and undrained steady state shear strength are established using CU triaxial tests. Steady state lines express these parameters in terms of void ratio and stress.

Piezovane shear tests in a calibration chamber show pore pressure response on the shear plane that is sufficient to display small but distinct positive and negative peaks, implying contractive and dilative behavior respectively. The piezovane induces positive pore pressure response at states of void ratio and stress that are lower than the steady states determined by CU triaxial tests. However, direct shear test results and measured peak vane shear strength indicate that pore pressure induced by the piezovane is reasonably representative of the samples' density-stress states.

Piezovane steady state shear strengths show a great deal of scatter and are significantly lower than CU triaxial steady state shear strengths. This is largely attributable to drained conditions in the shear zone.

Shear tests after vane advancement show consistently higher shear strength than tests where the sample is consolidated with the vane in

place. Pore pressure response is changed by a positive amount after vane advancement.

B. Conclusions

Trends in volumetric strain during shear can be identified by nearly drained piezovane tests in sand. Small, but distinct, pore pressure peaks are observed at the vane blade edges during shear. Piezovane shear tests in strongly dilative samples exhibit negative pore pressure peaks, while tests of samples in relatively loose states of void ratio and stress show positive pore pressure peaks. Provided this pore pressure response is verified as reflecting actual dilative and contractive states of sands, the piezovane test shows promise as an index of liquefaction potential. Positive pore pressure response would indicate potentially liquefiable soils, and negative response non-liquefiable soils.

Based on this study, the piezovane is inappropriate for measuring undrained steady state shear strength of saturated sands. Due to significant drainage, quantitative determination of shear strength is unreliable at large shear strains.

Vane insertion increases shear strength and adds an incremental amount of positive excess pore pressure to overall pore pressure response. These effects should be considered in field application of the piezovane.

C. Recommendations

Further research is needed to determine the reliability of the piezovane under field conditions and understand the complex mechanisms

of vane shear in cohesionless soil. Based on results of this study, the following recommendations are made.

Undrained piezovane shear tests are preferred over partially drained tests. Undrained shear would give pore pressure response of greater magnitude and eliminate uncertainties associated with unmeasured volume changes in the shear zone. Higher strain rates than used in this research should be investigated using Blight's equation, theoretical modelling, and laboratory testing to determine the possibility of achieving undrained conditions in sands, silty sands, and silts.

Research into the factors affecting position of the steady state line would be helpful in qualifying comparative studies such as this one. Research might include stress controlled CU triaxial tests to determine the effect of loading rate and type. Consolidated, drained direct shear and simple shear tests would determine the effects of failure mode and forced failure planes on position of the steady state line.

Pore pressure response during piezovane shear should be verified in the field. A study is recommended utilizing the piezovane at sites that have liquefied in the past. This type of study might also indicate the piezovane's value in field correlation methods.

VIII. References

Al-Mukhtar, M., Robinet, J. C., and Shahrour, I., 1988, "Monotonic and Cyclic Penetration Tests in Calibrated Chamber." Proceedings, First International Symposium on Penetration Testing, Orlando, Fl, March, A. A. Balkema, Rotterdam, Vol. 2, 621-633.

American Society of Testing and Materials, 1987, Annual Book of ASTM Standards, Designation D, Philadelphia, Pa.

Been, K., Crooks, J. H. A., and Rothenburg, L., 1988, "A Critical Appraisal of CPT Calibration Chamber Tests." Proceedings, First International Symposium on Penetration Testing, Orlando, Fl, March, A. A. Balkema, Rotterdam, Vol. 2, 651-660.

Bellotti, R., Bizzi, G., and Ghionna, V. N., 1982, "Design, Construction and Use of a Calibration Chamber." Proceedings, Second European Symposium on Penetration Testing, Amsterdam, May, A. A. Balkema, Rotterdam, Vol. 2, 439-446.

Bellotti, R., Crippa, V., Ghionna, V. N., and Pedroni, S., 1988, "Saturation of Sand Specimen for Calibration Chamber Tests." Proceedings, First International Symposium on Penetration Testing, Orlando, Fl, March, A. A. Balkema, Rotterdam, Vol. 2, 661-679.

Blatt, H., Middleton, G. V., and Murry, R. C., 1972, Origin of Sedimentary Rocks, Prentice-Hall, Englewood Cliffs, New Jersey, 634p.

Blight, G. E., 1968, "A Note on Field Vane Testing of Silty Soils." Canadian Geotechnical Journal, Vol 5, 142-149.

Cadling, L., and Odenstad, S., 1950, "The Vane Borer." Proceedings No. 2, Royal Swedish Geotechnical Institute, Stockholm, 87p.

Campanella, R. G., and Robertson, P. K., 1988, " Current Status of the piezocone Test." Proceedings, First International Symposium on Penetration Testing, Orlando, Fl, March, A. A. Balkema, Rotterdam, Vol. 1, 93-116.

Campanella, R. G., Robertson, P. K., Gillespie, D. G., 1983, "Cone Penetration Testing in Deltaic Soils." Canadian Geotechnical Testing Journal, Vol. 20, 23-35.

Canou, J., El Hachem, M., Kattan, A., and Juran, I., 1988, "Mini Piezocone Investigation Related to Sand Liquefaction Analysis." Proceedings, First International Symposium on Penetration Testing, Orlando, Fl, March, A. A. Balkema, Rotterdam, Vol. 2, 699-706.

Casagrande, A., 1940, "Characteristics of Cohesionless Soils Affecting the Stability of Slopes and Earth Fills." Boston Society of Civil Engineers, January, 257-276.

Casagrande, A., 1971, "On Liquefaction Phenomena." Geotechnique, Vol. 21, No. 3, 197-202.

Casagrande, A., 1976, "Liquefaction and Cyclic Deformation of Sands, a Critical Review." Harvard Soil Mechanics Series No. 88, Pierce Hall, Cambridge, Ma., 27p.

Castro, G., 1975, "Liquefaction and Cyclic Mobility of Saturated Sands.", Journal of Geotechnical Engineering Division, ASCE, Vol. 101, No. 6, 551-569.

Castro, G., and Poulos, S. J., 1977, "Factors Affecting Liquefaction and Cyclic Mobility." Journal of Geotechnical Engineering Division, ASCE, Vol. 103, No. 6, 501-515.

Castro, G., Enos, J. L., France, J. W., and Poulos, S. J., 1982a, "Liquefaction Induced by Cyclic Loading." Final Report, NSF/CEE-82018, National Science Foundation, March, 325p.

Castro, G., France, J. W., and Shields D. R., 1982b, "Field Index Test for Estimating Liquefaction Potential." Final Report, Award No. CEE-8114111, SBIR Phase I, National Science Foundation, March, 23p.

Chandler, R. J., 1988, "The In-Situ Measurement of the Undrained Shear Strength of Clays Using the Field Vane." Vane Shear Strength Testing in Soils: Field and Laboratory Studies, ASTM STP 1014, 13-44.

Charlie, W. A., Shinn, J., Meltzer, L. S., Martin, J. P. and Blouin, S. E., 1980, "Blast-Induced Liquefaction Phenomenon and Evaluation," Proceedings, International Symposium on Soils Under Cyclic and Transient Loading, Swansea, United Kingdom, January, 533-542.

Charlie, W. A., Veyera, G. E., and Abt, S. R., 1985a, "Predicting Blast-Induced Porewater Pressure and Increases in Soils." Journal of Civil Engineering for Practicing and Design Engineers, Vol. 4, No. 4, April, 311-328.

Charlie, W. A., Veyera, G. E., Doehring, D. O., and Abt, S.R., 1985b, "Blast Induced Liquefaction Potential and Transient Porewater Pressure Response of Saturated Sands." Final Report, Grant No. AFOSR-80-0260, Air Force Office of Scientific Research, 198p.

Committee on Earthquake Engineering, 1985, Liquefaction of Soils During Earthquakes, Commission on Engineering and Technical Systems, National Research Council, National Academy Press, Washington, D.C., 240p.

Dobry, R., Stokoe, K. H., Ladd, R. S., and Youd, T. L., 1981, "Liquefaction Susceptibility from S-Wave Velocity." In Situ Testing to Evaluate Liquefaction Susceptibility, Proceedings, Session 24, ASCE National Convention, St. Louis, 55-64.

Donald, I. B., Jordan, D. O., Parker, R. J., and Toh, C. T., 1977, "The Vane Test - a Critical Appraisal." Proceedings, Ninth International Conference on Soil Mechanics and Foundation Engineering, ISSMFE, Tokyo, Vol. 1, 81-88.

Dolson, J., 1981, "Depositional Environments and Petrography of the Dakota Group (Lower Cretaceous), Western Cheyenne Basin, Colorado." Masters Thesis, Department of Earth Resources, Colorado State University, Fort Collins, Co., 304p.

East, D. R., Hughes, J. M. O., Cincilla, W. A., and Benoit, J., 1988, "The Use of the Electric Piezocone for Mine Tailings Deposits." Proceedings, First International Symposium on Penetration Testing, Orlando, Fl, March, A. A. Balkema, Rotterdam, Vol. 2, 745-750.

Finn, W. D., Pickering, D. J., and Bransby, P. L., 1971, "Sand Liquefaction in Triaxial and Simple Shear Tests." Journal of the Soil Mechanics and Foundations Division, ASCE, Vol. 97, No. 4, 639-659.

Gilbert, P. A., 1976, "Case Histories of Liquefaction Failures," Miscellaneous Paper S-76-4, U.S Army Corps of Engineers Waterways Experiment Station, Vicksburg, Mississippi, April, 41p.

Ishihara, K., 1985, "Stability of Natural Deposits during Earthquakes." Proceedings, Eleventh International Conference on Soil Mechanics and Foundation Engineering, ISSMFE, Vol. 1, 321-376.

Kimura, T., and Saitor, K., 1983, "Effect of Disturbance Due to Insertion on Vane Shear Strength of Normally Consolidated Cohesive Soils." Soils and Foundations, Vol. 23, No. 2, 113-124.

Ladd, R., S., 1978, "Preparing Test Specimens using Undercompaction." Geotechnical Testing Journal, ASTM, GTJODJ, Vol. 1, No. 1, 16-23.

Lambe, W. T., and Whitman, R. V., 1969, Soil Mechanics, John Wiley and Sons, New York, 553p.

Long, H., Ries, E. R., and Michalapoulos, A. P., 1981, "Potential for Liquefaction Due to Construction Blasting," Proceedings, International Conference on Recent Advances in Geotechnical Engineering and Soil Dynamics, University of Missouri-Rolla, St. Louis, 191-194.

Marcuson, W. F., Franklin, A. G., Hadala, P. F., 1980, "Liquefaction Potential of Dams and Foundations." Research Report S-76-2, U. S. Army Engineer Waterways Experiment Station, Vicksburg, Miss., 28p.

Marchetti, S., 1982, "Detection of Liquefiable Sand Layers by means of Quasi-static Penetration Tests." Proceedings, Second European Symposium on Penetration Testing, Amsterdam, May, A. A. Balkema, Rotterdam, Vol. 2, 689-695.

Mahmoud, M., 1988, "Vane Testing in Soft Clays." Report of discussion, British Geotechnical Society, in Ground Engineering, October, 36-40.

Matsui, T., and Abe, N., 1981, "Shear Mechanisms of Vane Test in Soft Clays." Soils and Foundations, Vol. 21, No. 4, 69-80.

Mitchell, J. K., and Solymar, Z. V., 1984, "Time-dependent Strength Gain in Freshly Deposited or Densified Sand." Journal of Geotechnical Engineering Division, ASCE, Vol.110, No. 11, 1559-1576.

Monell, S. A., 1989, Dry and Wet system flow diagrams (unpublished), Colorado Lien Company, Fort Collins, Colorado.

Mulilis, J. P., Seed, H. B., and Chan, C. K., 1977, "Effects of Sample Preparation on Sand Liquefaction." Journal of Geotechnical Engineering Division, ASCE, Vol.103, No. 2, 91-108.

Peacock, W. H., and Seed, H. B., 1968, "Sand Liquefaction under Cyclic Loading Simple Shear Conditions." Journal of the Soil Mechanics and Foundations Division, ASCE, Vol. 94, No. 3, 689-708.

Peck, R. B., 1979, "Liquefaction Potential: Science Versus Practice." Journal of Geotechnical Engineering Division, ASCE, Vol.105, No. 3, 393-398.

Poulos, S. J., 1981, "The Steady State of Deformation." Journal of Geotechnical Engineering Division, ASCE, Vol. 107, No. 5., 553-561.

Poulos, S. J., 1988, "Strength for Static and Dynamic Stability Analysis." Hydraulic Fill Structures, Specialty Conference, Geotechnical Division, ASCE, Fort Collins, CO., 452-474.

Poulos, S. J., Castro, G., and France, J. W., 1985, "Liquefaction Evaluation Procedure." Journal of the Geotechnical Engineering Division, ASCE, Vol. 111, No. 6, 772-792.

Rad, N. S., and Tumay, M. T., 1987, "Factors Affecting Sand Specimen Preparation by Raining." Geotechnical Testing Journal, ASTM, Vol. 10, No. 1, 31-37.

Robertson, P. K., 1986, "In Situ Testing and its Application to Foundation Engineering." Canadian Geotechnical Journal, Vol 5, 573-594.

Robertson, P. K., and Campanella, R. G., 1985, "Liquefaction Potential of Sands using the CPT." Journal of the Geotechnical Engineering Division, ASCE, Vol. 111 No. 3, 384-403.

Robertson, P. K., and Campanella, R. G., 1986, "Estimating Liquefaction Potential of Sands using the Flat Plate Dilatometer." Geotechnical Testing Journal, ASTM, Vol. 9, No. 1., 38-40.

Roscoe, K. H., Schofield, A. N., and Wroth, C. P., 1958, "On Yielding of Soils." Geotechnique, Vol. 8, 22-53.

Schmertmann, J. H., 1978, "Study of Feasibility of using Wissa-type Piezometer Probe to Identify Liquefaction Potential of Saturated Fine Sands." Technical Report S-78-2, U. S. Army Engineer Waterways Experiment Station, 73p.

Schofield, A. N., and Wroth, C. P., 1968, Critical State Soil Mechanics, McGraw-Hill, London. pp 19-21, 226.

Seed, H. B., 1968, "Landslides During Earthquakes due to Soil Liquefaction." Journal of the Soil Mechanics and Foundations Division, ASCE, Vol. 94, No. 5, 1055-1122.

Seed, H. B., 1985, "Influence of SPT Procedures in Soil Liquefaction Resistance Evaluations." Journal of the Soil Mechanics and Foundations Division, ASCE, Vol. 111, No. 12, 1425-1445.

Seed, H. B., and Lee, K. L., 1966, "Liquefaction of Saturated Sands during Cyclic Loading." Journal of the Soil Mechanics and Foundations Division, ASCE, Vol. 92, No. 6, 105-134.

Seed, H. B., and Idriss, I., M., 1967, "Analysis of Liquefaction: Niigata Earthquake." Journal of the Soil Mechanics and Foundations Division, ASCE, Vol. 93, No. 3, 83-108.

Seed, H. B., and De Alba, P., 1986, "Use of SPT and CPT Tests for Evaluating the Liquefaction Resistance of Sands." Proceedings, Use of In Situ Tests in Geotechnical Engineering, Specialty Conference, Geotechnical Engineering Division, ASCE, Blacksburg, Va., June, 281-302.

Silver, M. L., 1977, "Laboratory Triaxial Testing Procedures to Determine the Cyclic Strength of Soils." Report NUREG-0031, United States Nuclear Regulatory Commission, 129p.

Subcommittee on Soil Testing, 1987, "Test methods for Consolidated Triaxial Tests." (draft), ISSMFE, Norwegian Geotechnical Institute. 65p.

Taylor, D. W., 1939, "A Comparison of Results of Direct Shear and Cylindrical Compression Tests." Proceedings, 42nd Annual Meeting, American Society for Testing Materials, Technical Papers, Volume 39, 1058-1070.

Terzaghi, K., 1946, Theoretical Soil Mechanics, John Wiley and Sons, New York, 510p.

Tokimatsu, K., 1988, "Penetration Tests for Dynamic Problems." Proceedings, First Intl. Symposium on Penetration Testing, Orlando, Fl., March, Balkema, Rotterdam, Vol. 1., 117-136.

Wilson, N. E., 1963, "Laboratory Vane Shear Tests and the Influence of Pore-water Stresses." Symposium on Laboratory Testing of Soils, ASTM STP No. 361, 377-385.

Woods, R., and Henke, R., 1981, "Seismic Techniques in the Laboratory." Journal of Geotechnical Engineering Division, ASCE, Vol. 107, No. 10, 1309-1325.

Youd, T. L., and Hoose, S., N., 1976, "Liquefaction during 1906 San Francisco Earthquake." Journal of Geotechnical Engineering Division, ASCE, Vol. 102, No. 5, 425-439.

Appendix A

TRIAXIAL TEST RESULTS

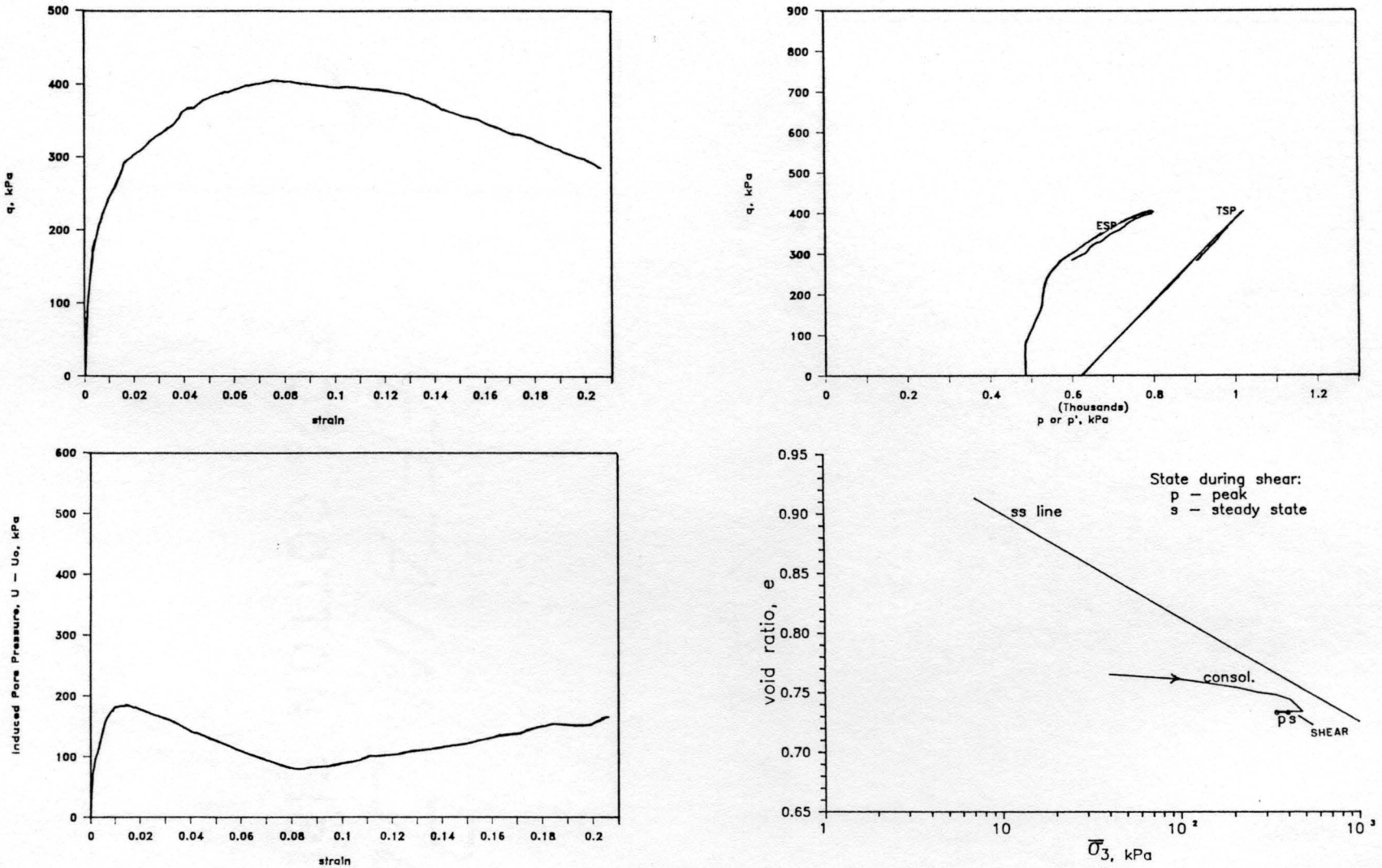

Figure A.1.1. CU Triaxial Test Data. Test R1, e_c=.734, σ'_{3c}=487 kPa.

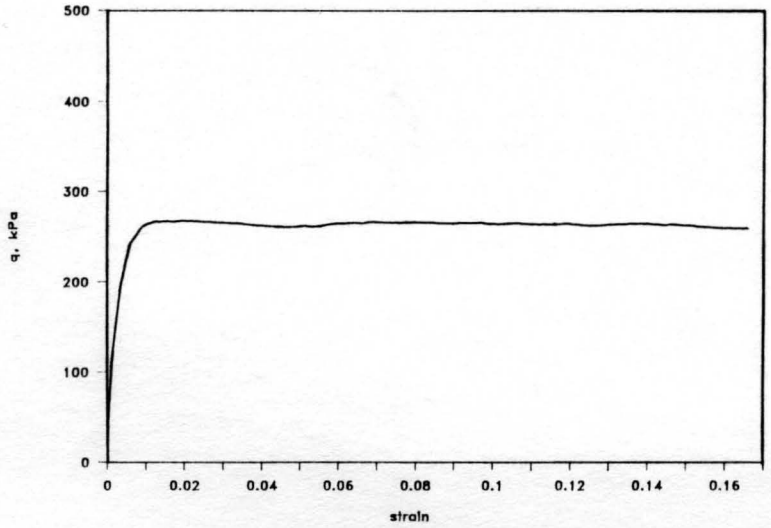

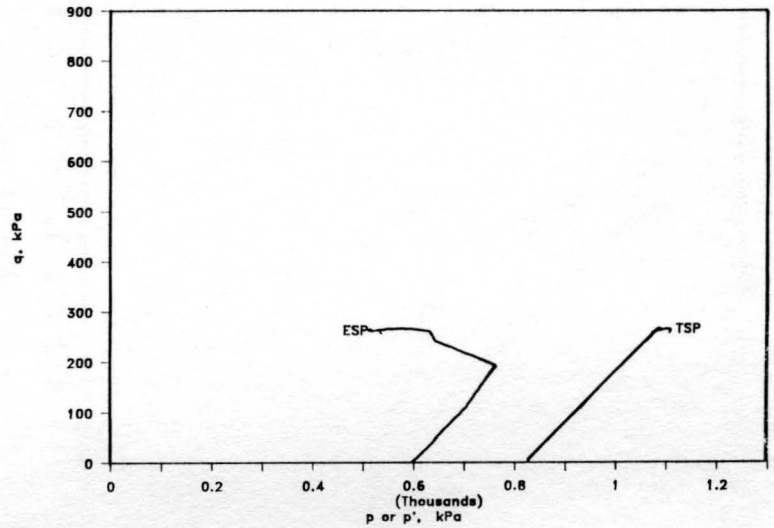

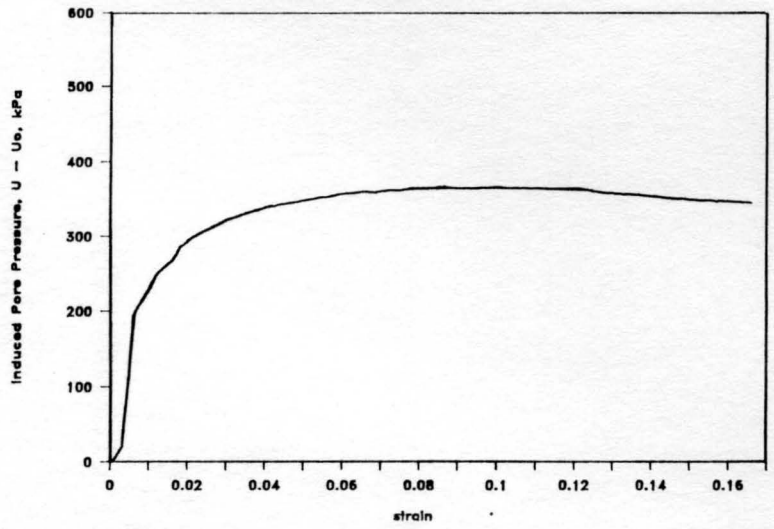

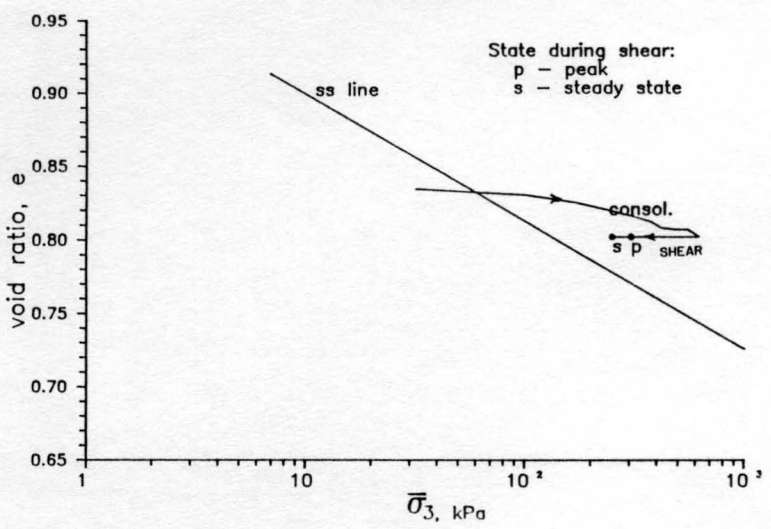

Figure A.1.2. CU Triaxial Test Data. Test R2, e_c=.802, σ'_{3c}=616 kPa.

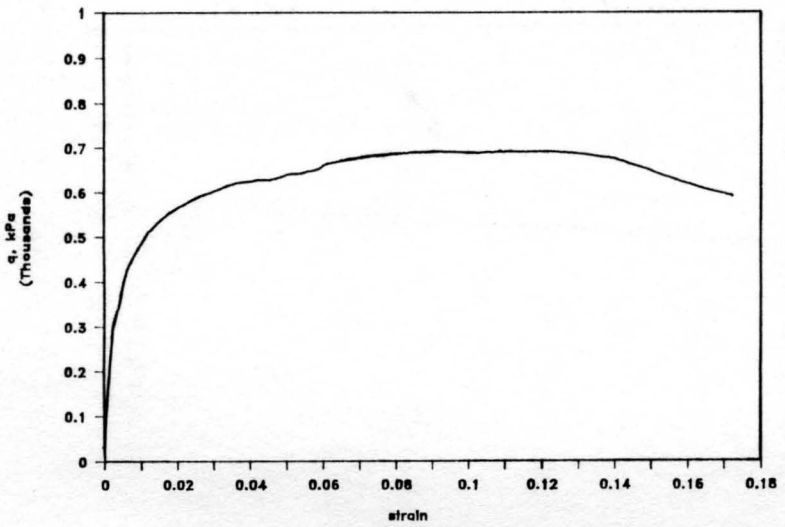

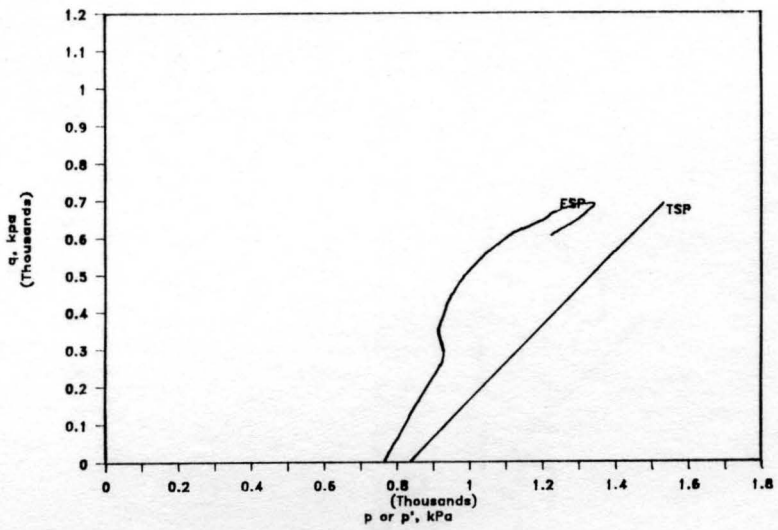

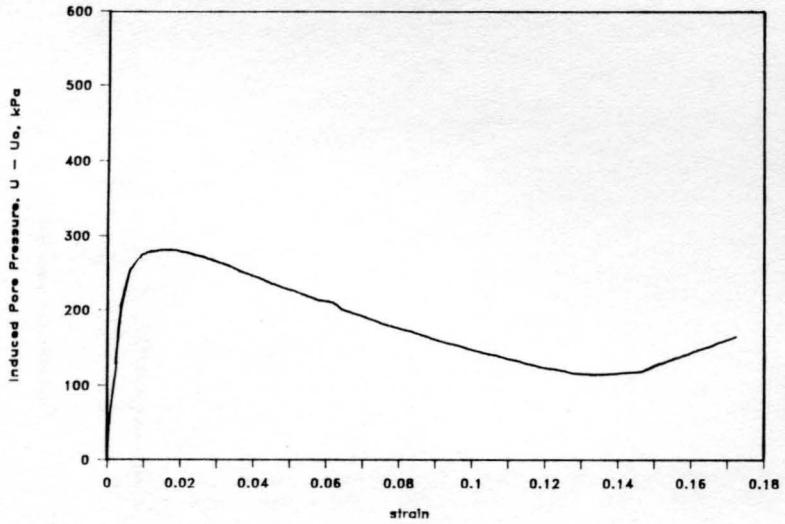

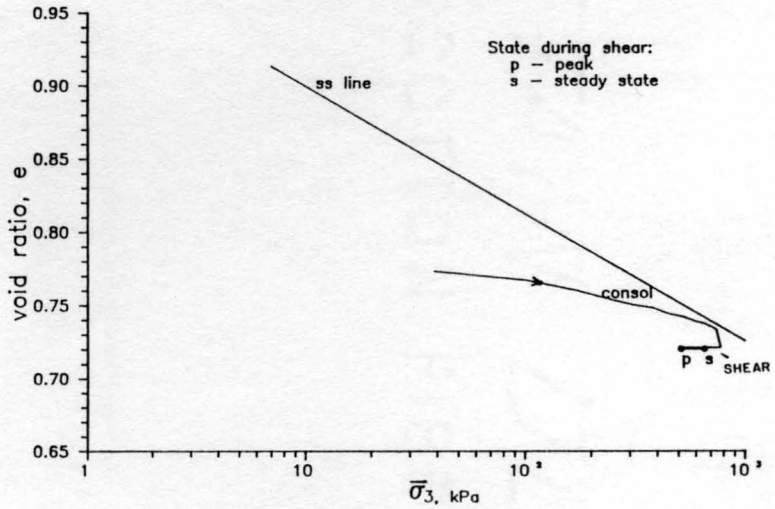

Figure A.1.3. CU Triaxial Test Data. Test R3, e_c=.721, σ'_{3c}=772 kPa.

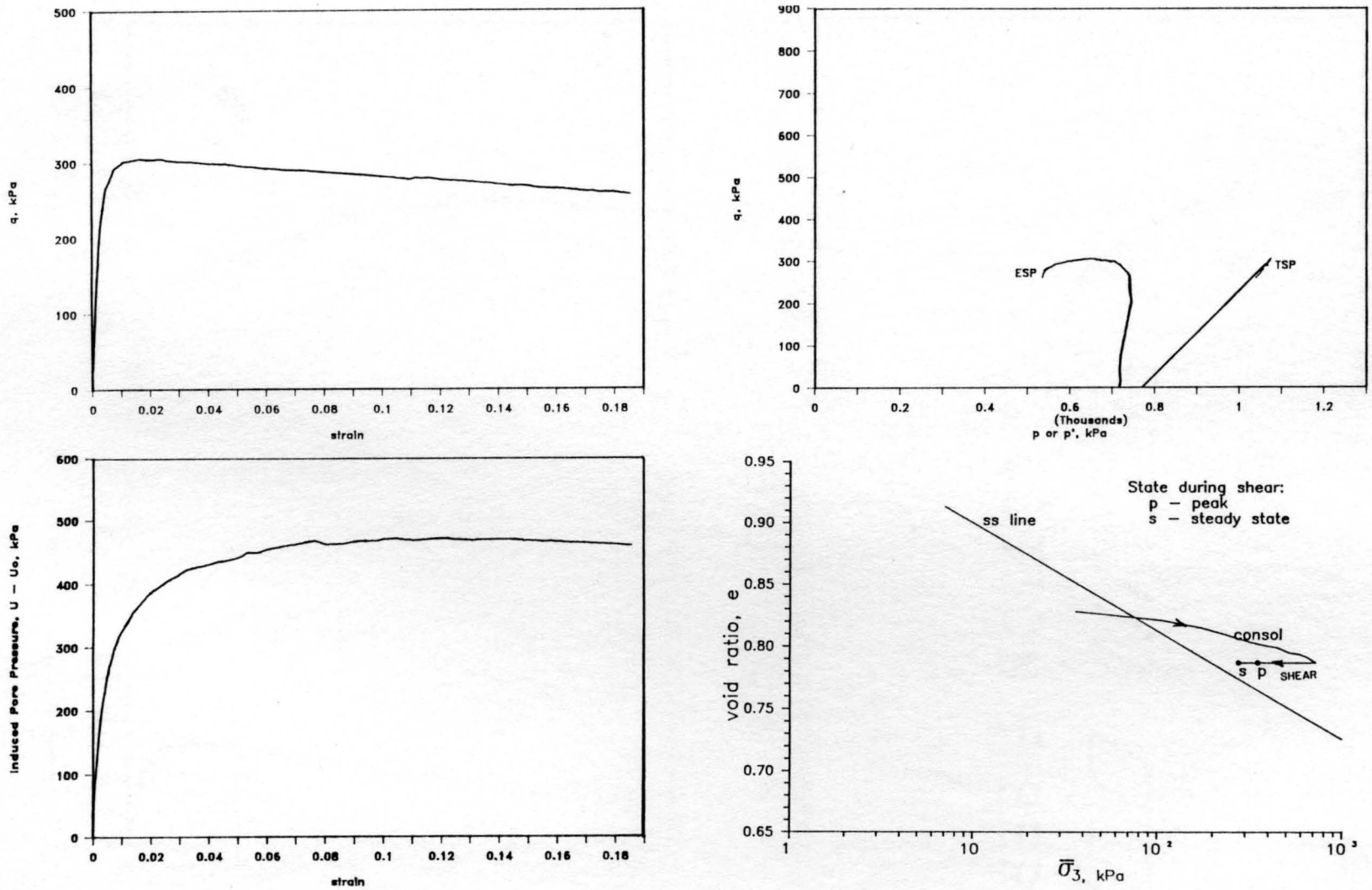

Figure A.1.4. CU Triaxial Test Data. Test R4, e_c=.787, σ'_{3c}=723 kPa.

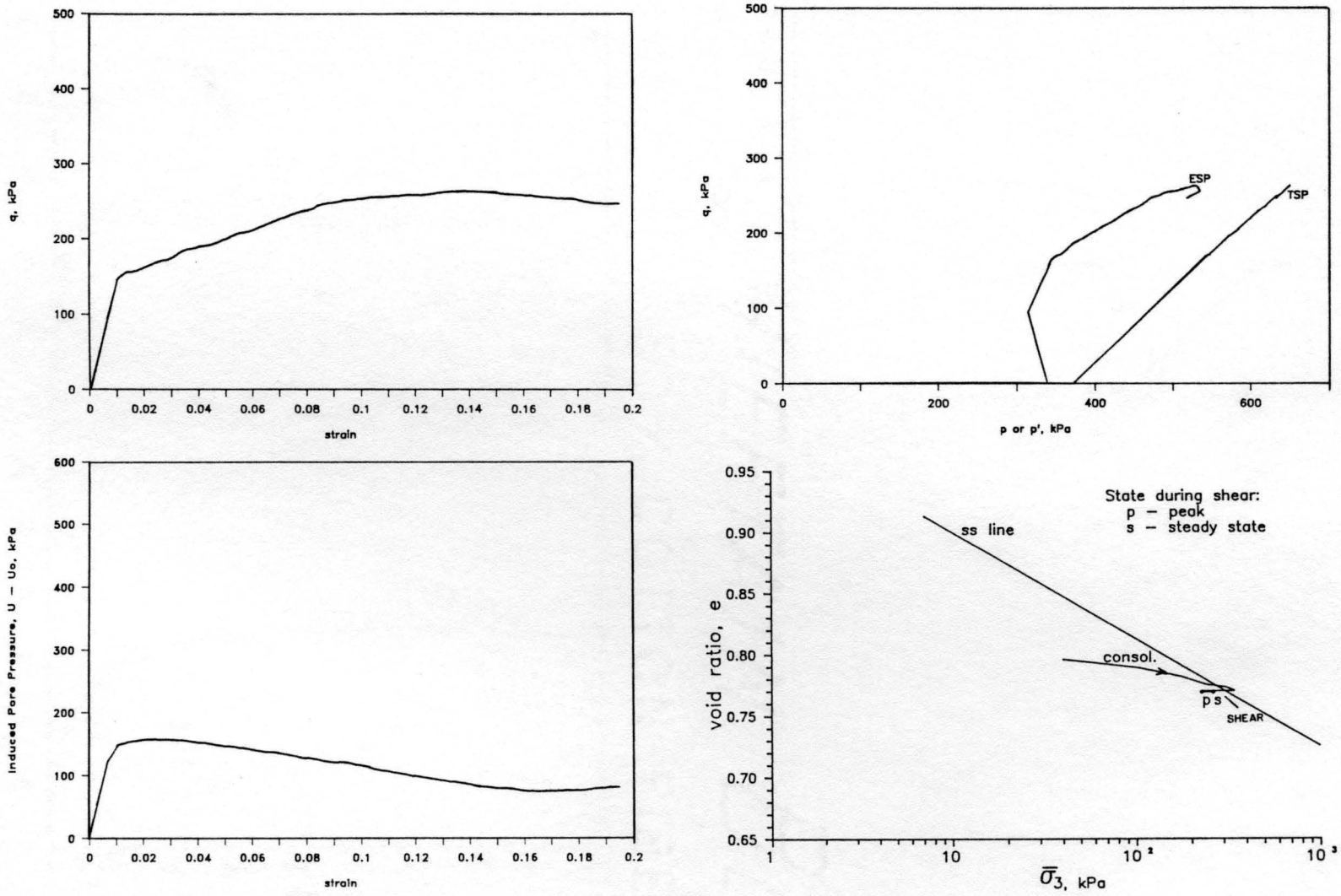

Figure A.1.5. CU Triaxial Test Data. Test R5, e_c=.770, σ'_{3c}=344 kPa.

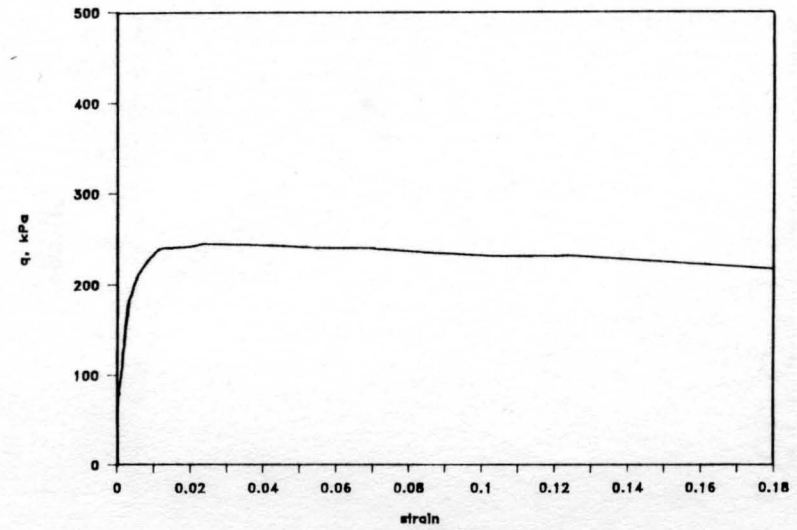

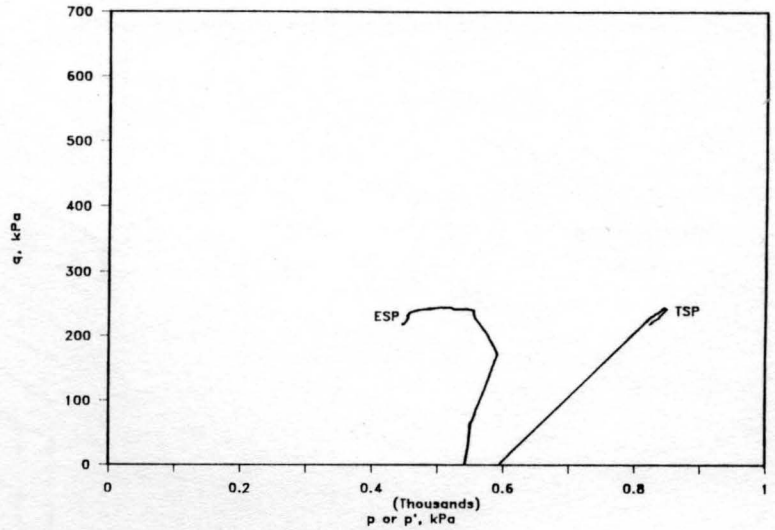

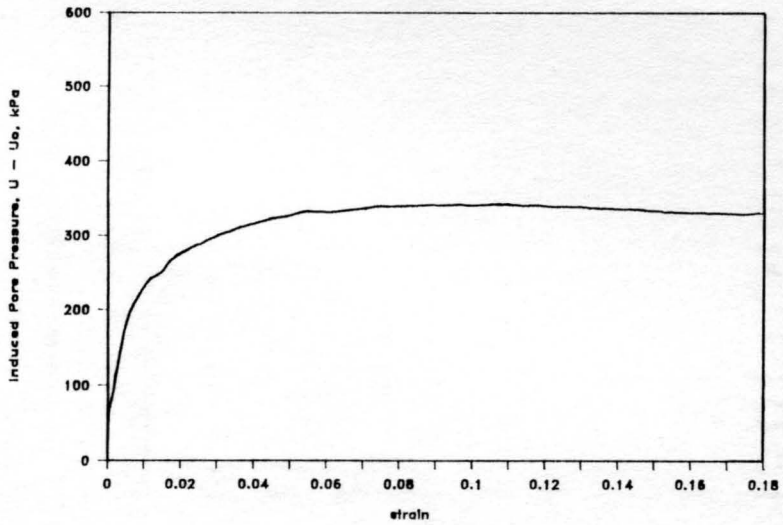

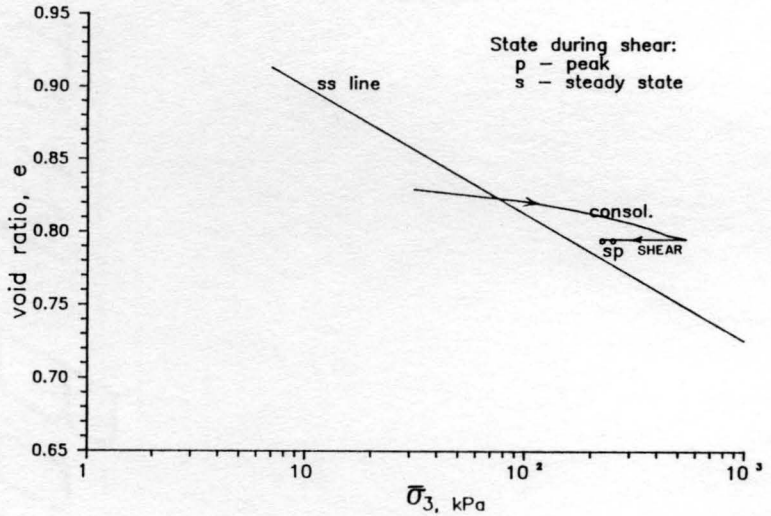

Figure A.1.6. CU Triaxial Test Data. Test R6, e_c=.794, σ'_{3c}=550 kPa.

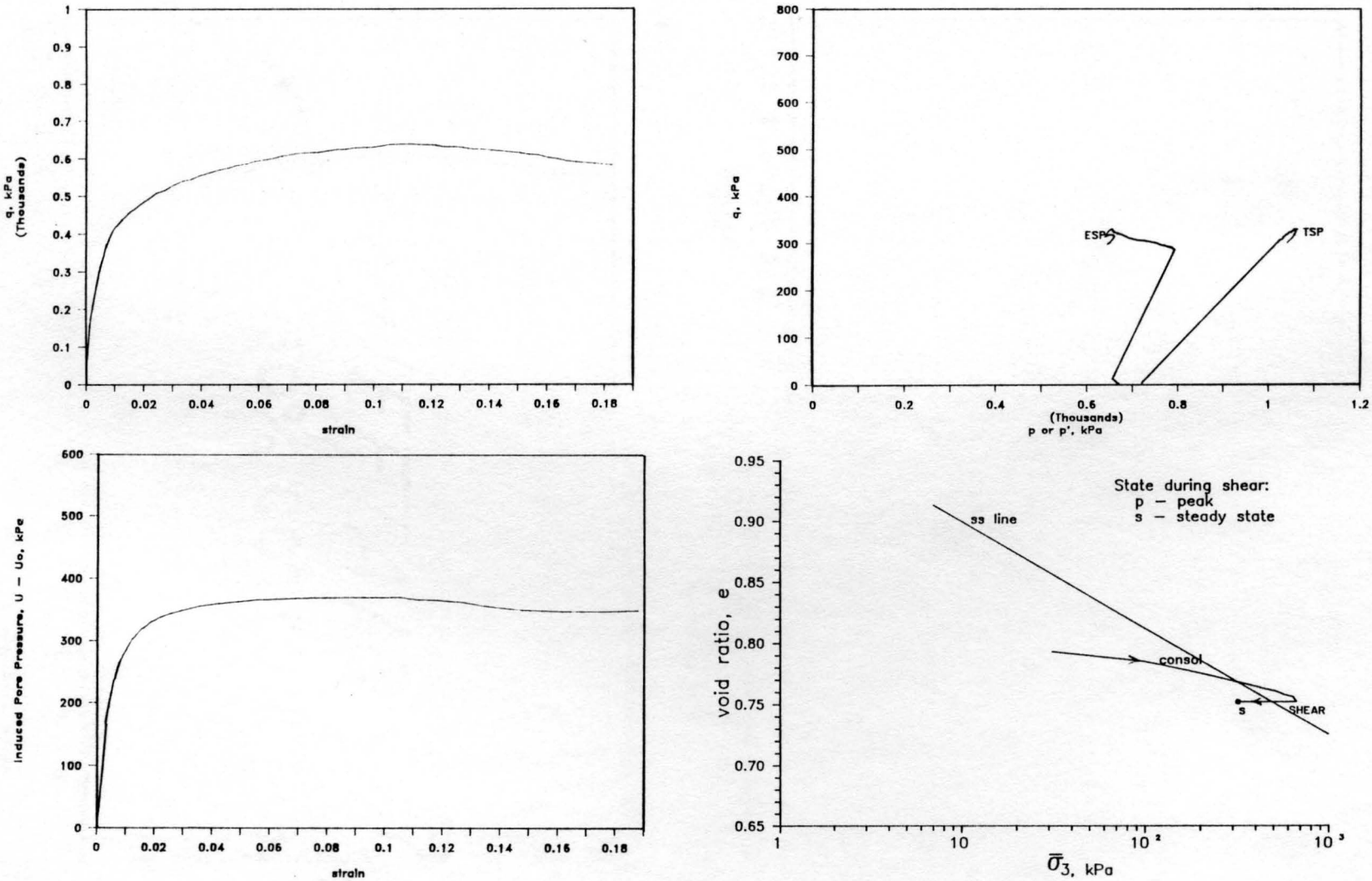

Figure A.1.7. CU Triaxial Test Data. Test R8, e_c=.752, σ'_{3c}=676 kPa.

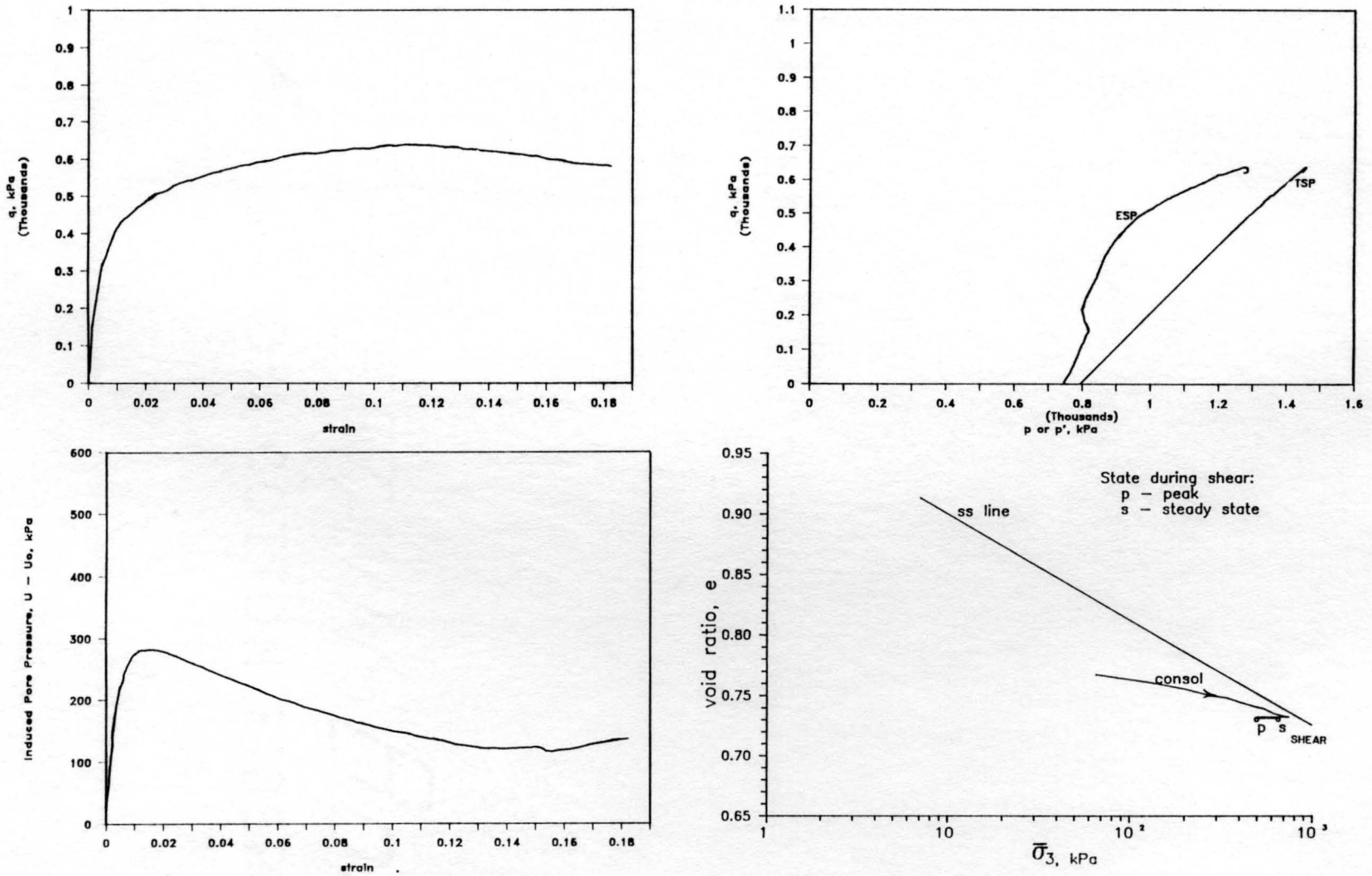

Figure A.1.8. CU Triaxial Test Data. Test R9, e_c=.731, σ'_{3c}=751 kPa.

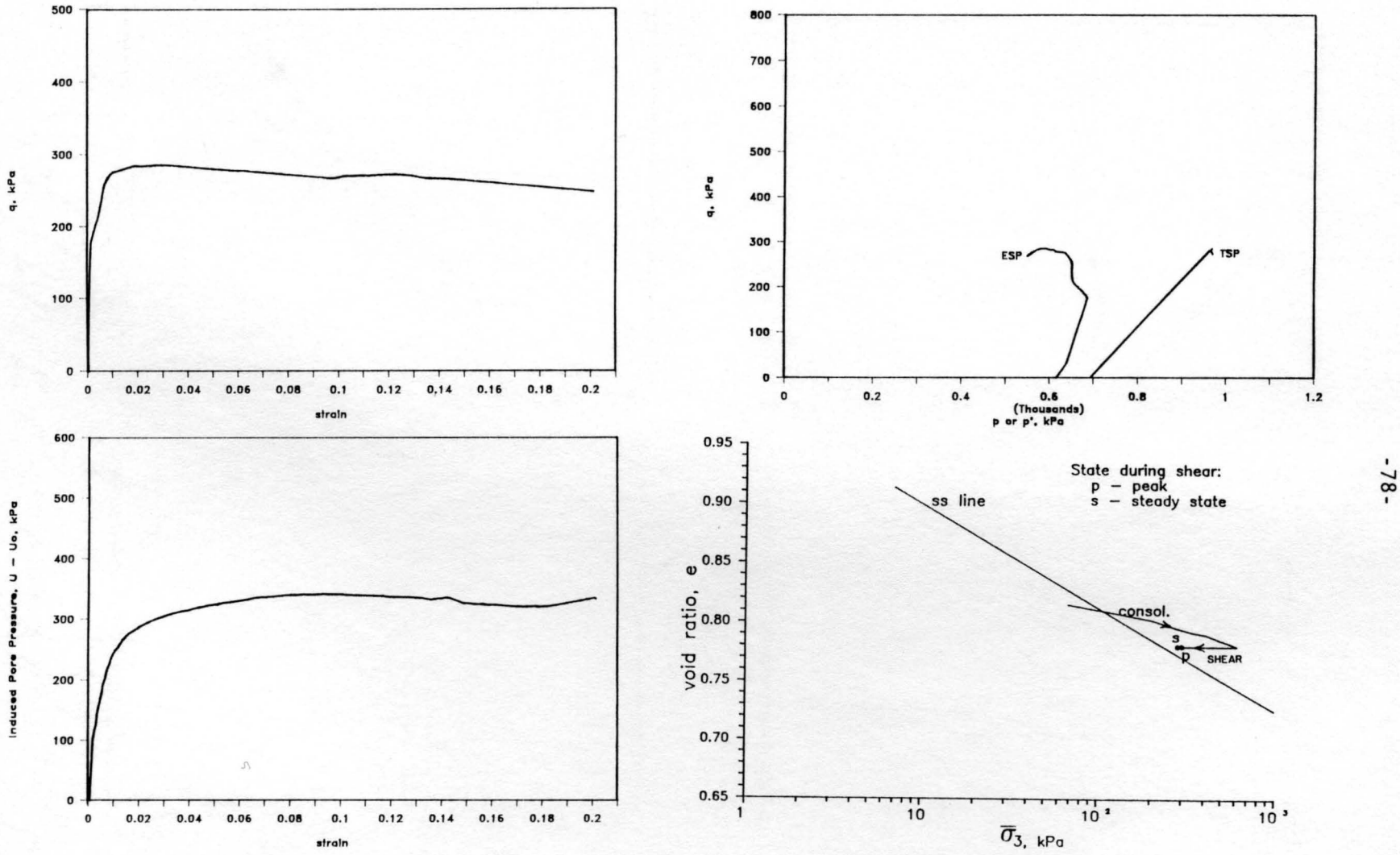

Figure A.1.9. CU Triaxial Test Data. Test R10, e_c=.780, σ'_{3c}=618 kPa.

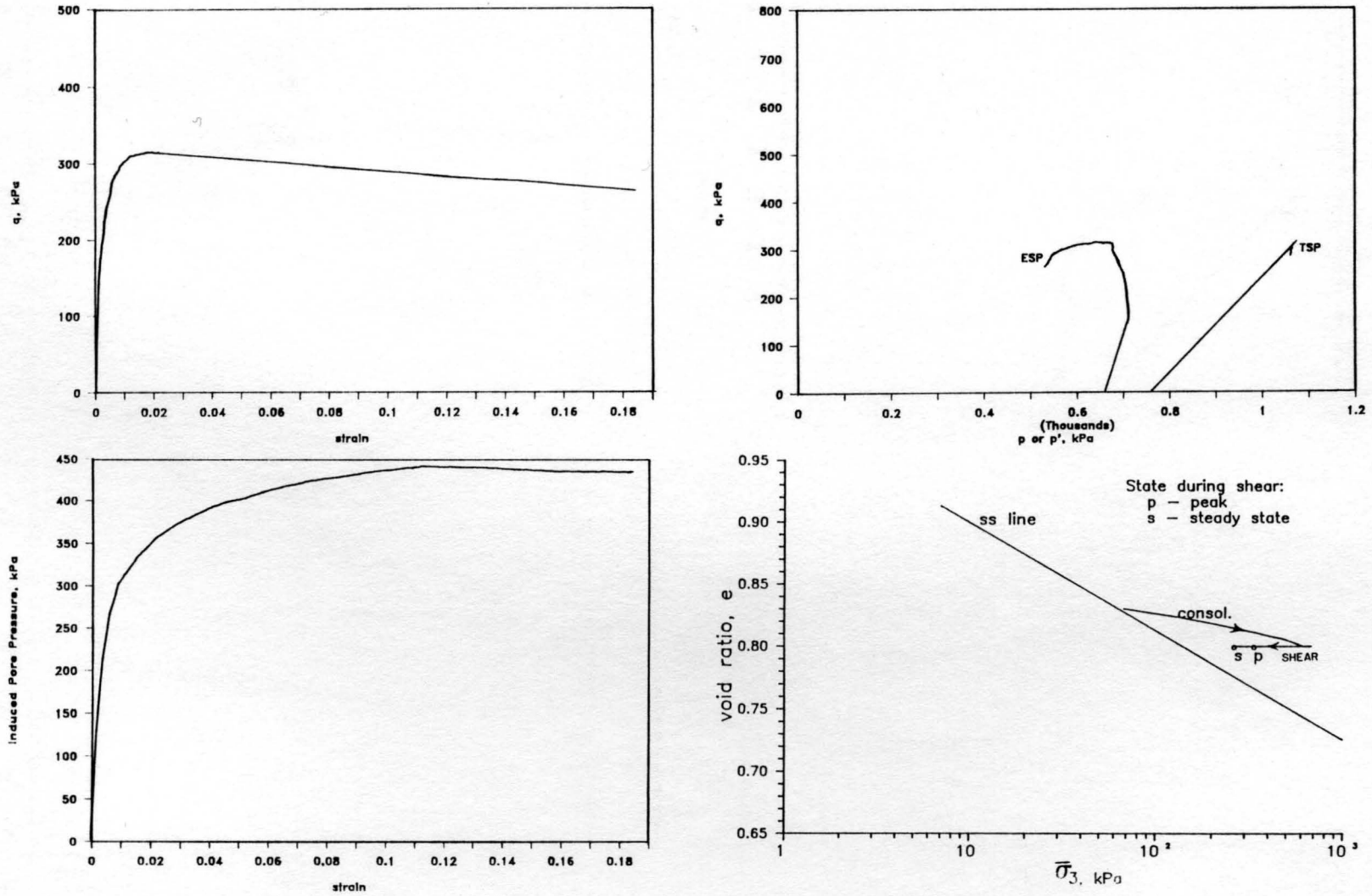

Figure A.1.10. CU Triaxial Test Data. Test R11, e_c=.799, σ_{3c}'=688 kPa.

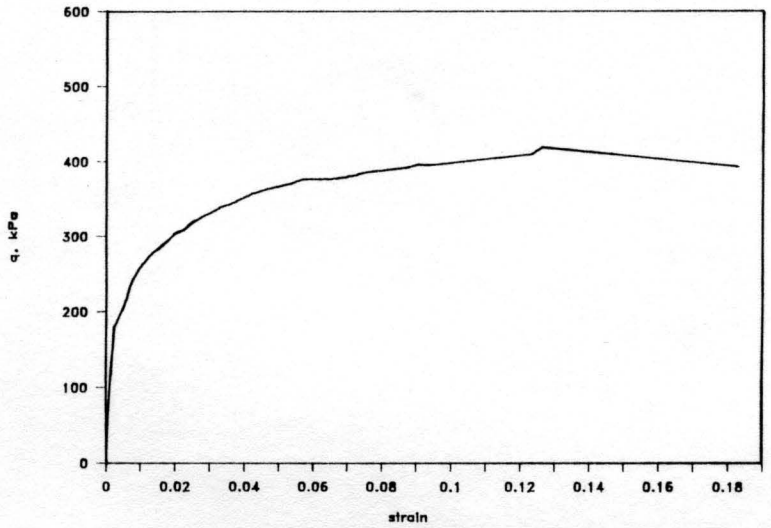

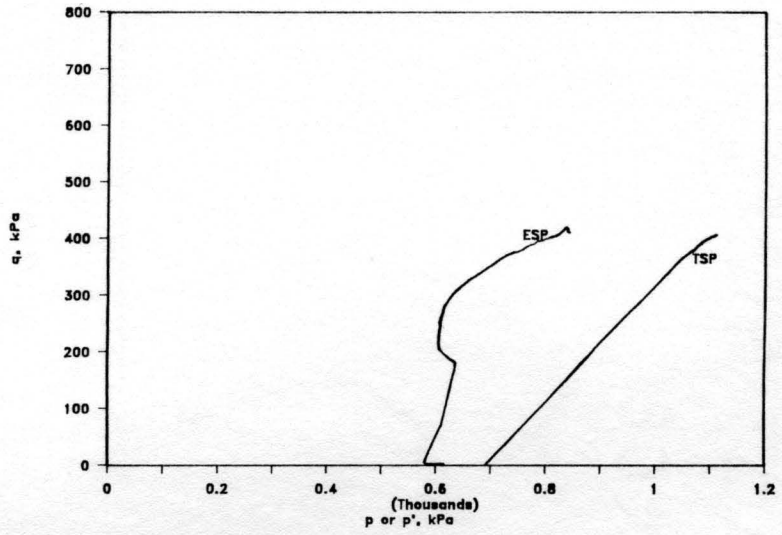

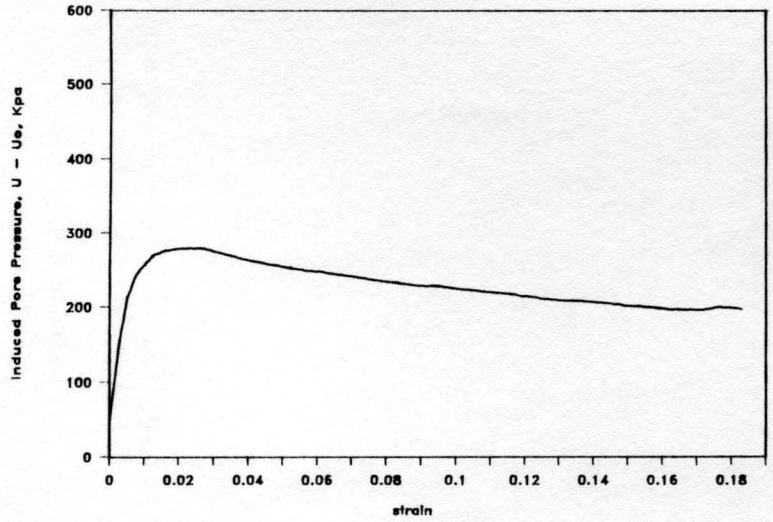

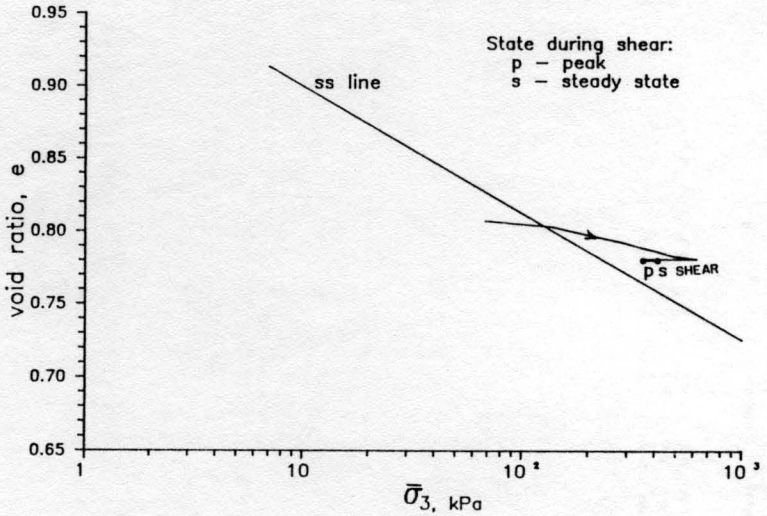

Figure A.1.11. CU Triaxial Test Data. Test R12, e_c=.781, σ'_{3c}=619 kPa.

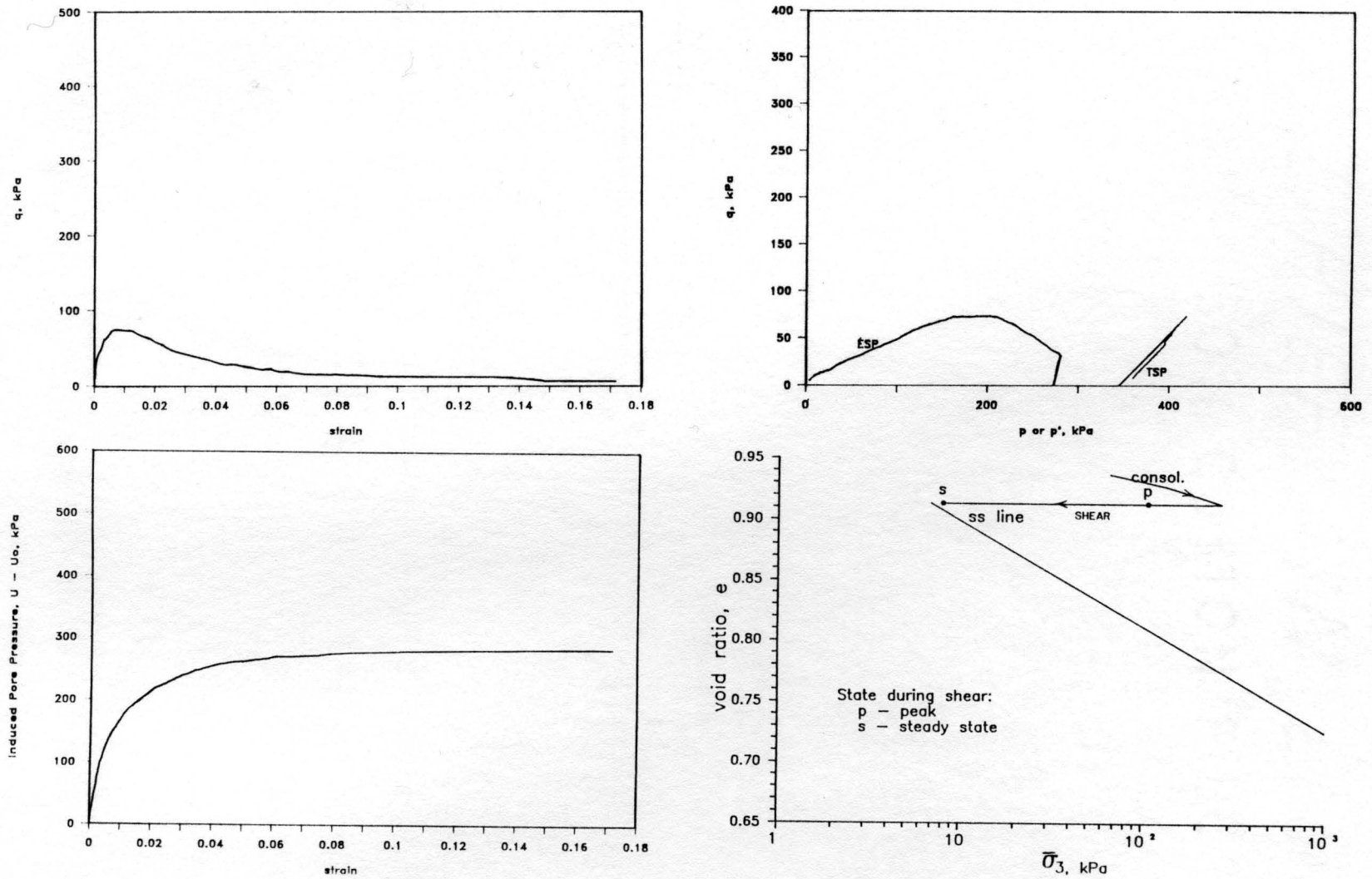

Figure A.1.12. CU Triaxial Test Data. Test R13, e_c=.913, σ'_{3c}=274 kPa.

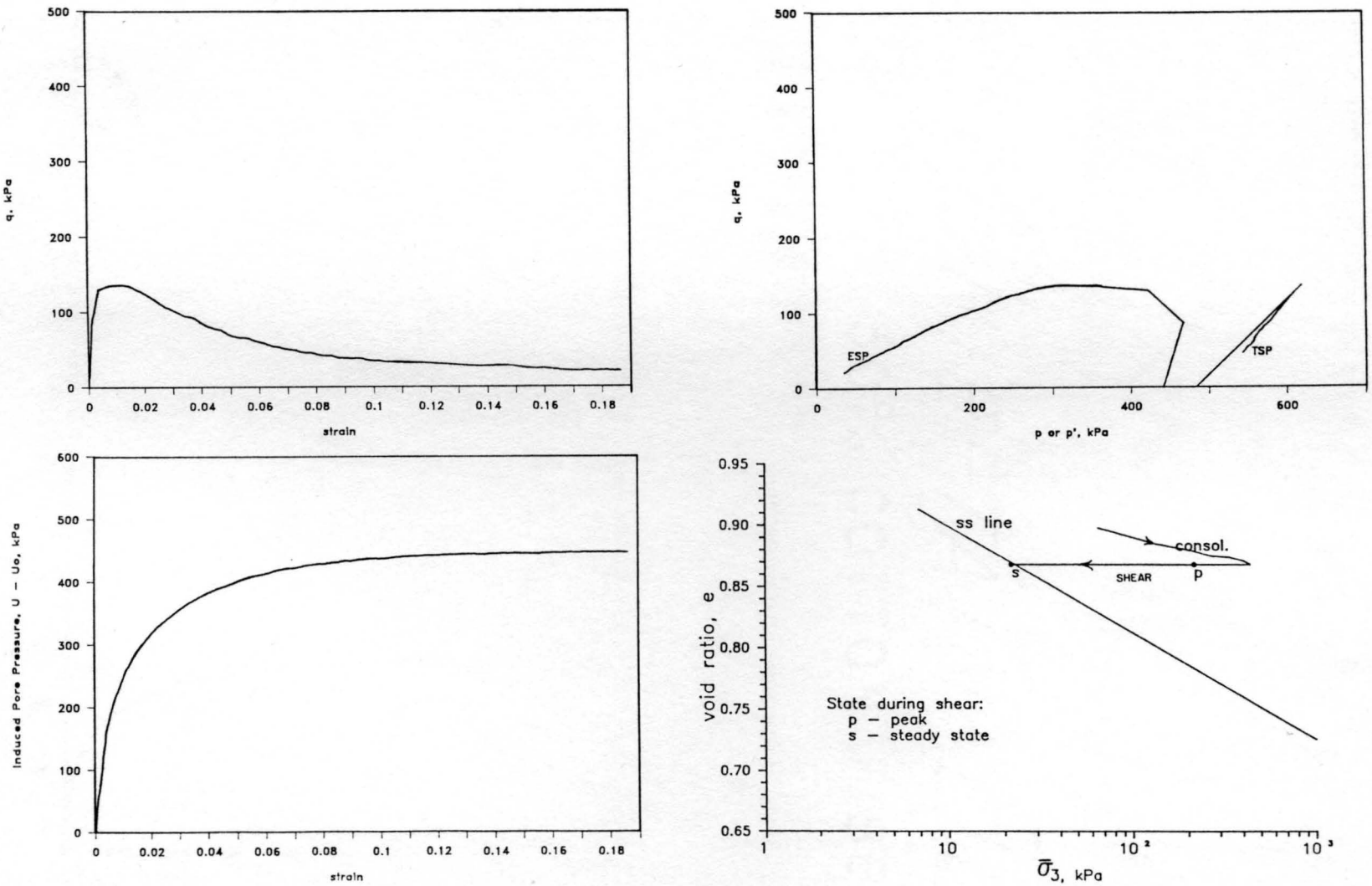

Figure A.1.13. CU Triaxial Test Data. Test R14, e_c=.868, σ'_{3c}=445 kPa.

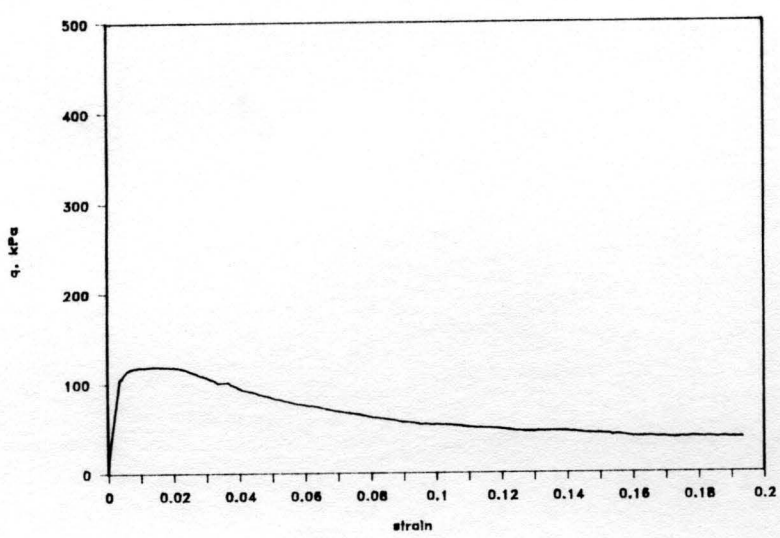

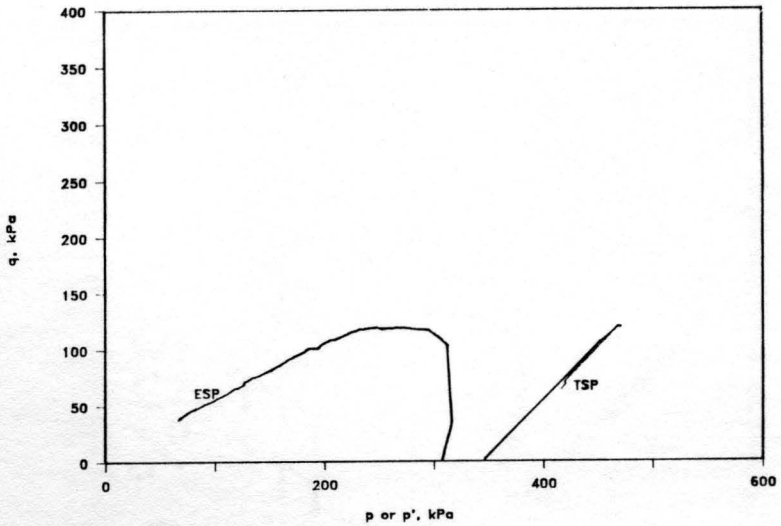

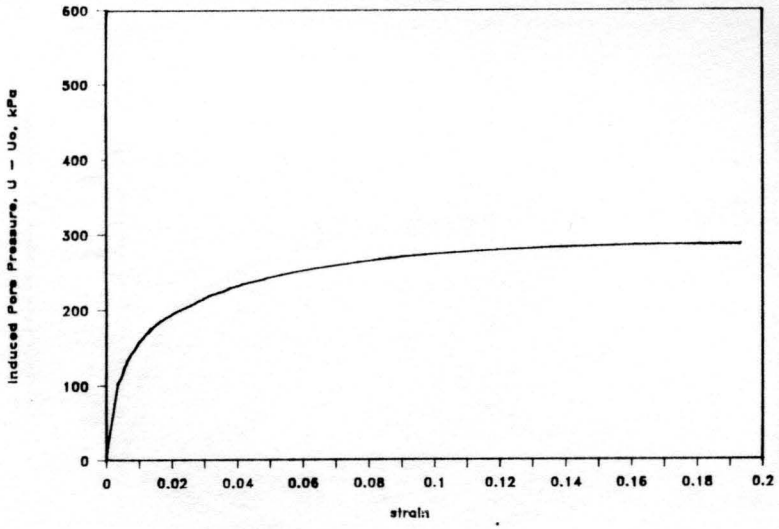

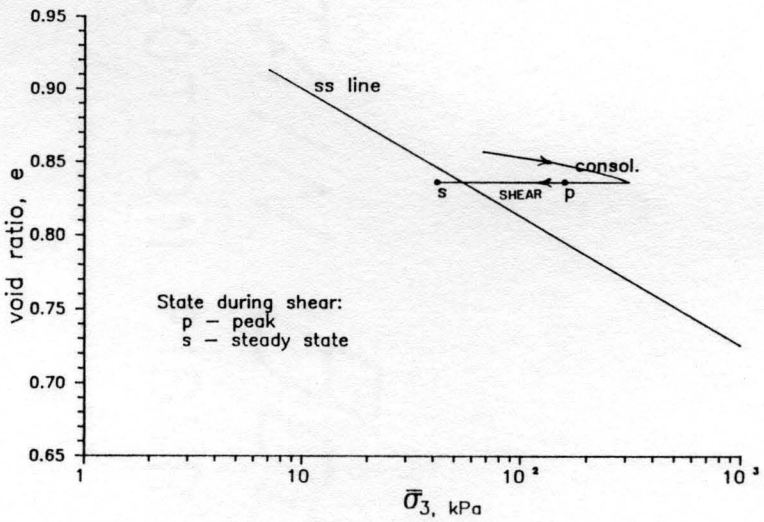

Figure A.1.14. CU Triaxial Test Data. Test R15, e_c=.836, σ'_{3c}=308 kPa.

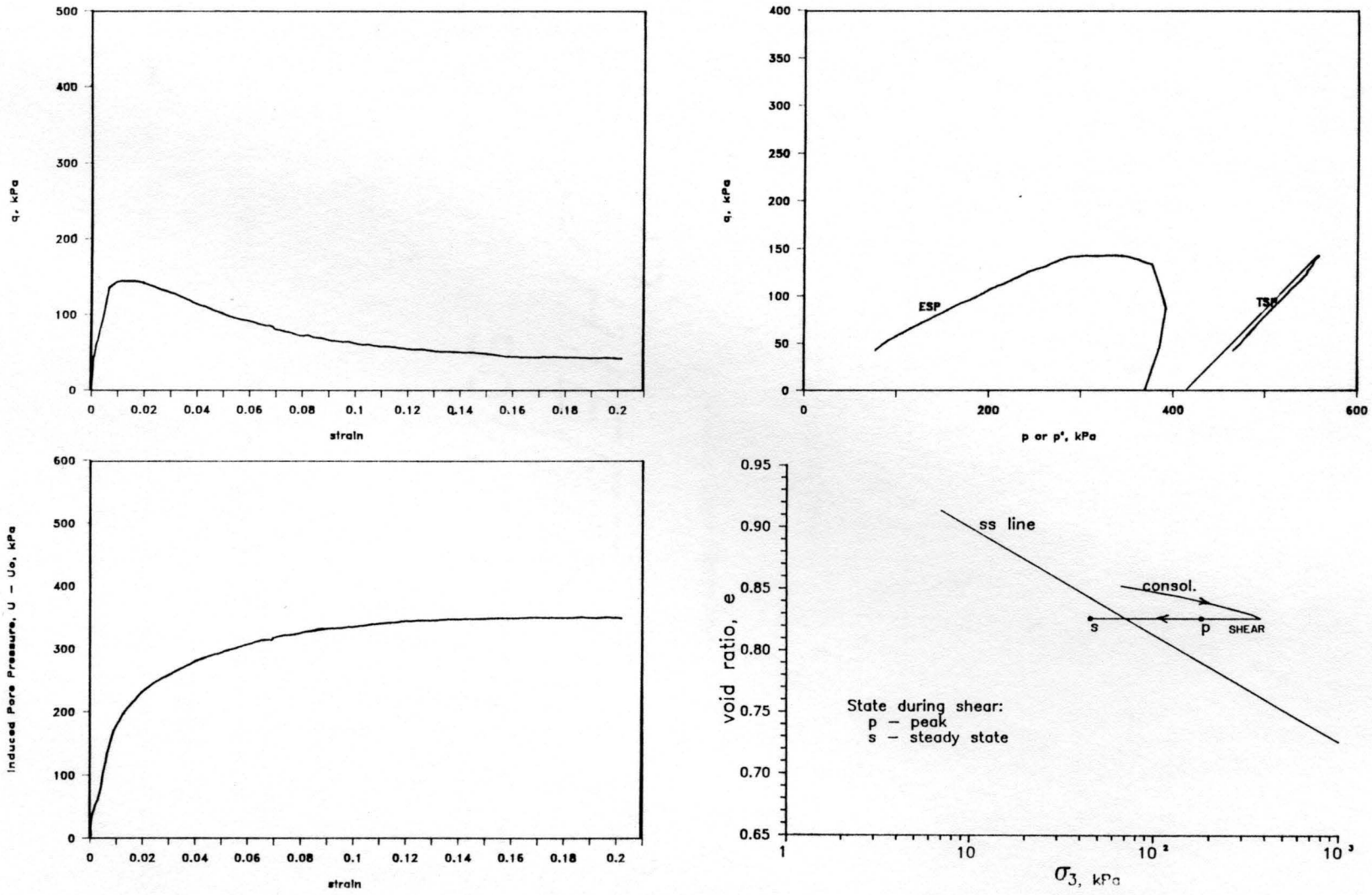

Figure A.1.15. CU Triaxial Test Data. Test R16, e_c=.826, σ'_{3c}=376 kPa.

APPENDIX B

Piezovane Test Results

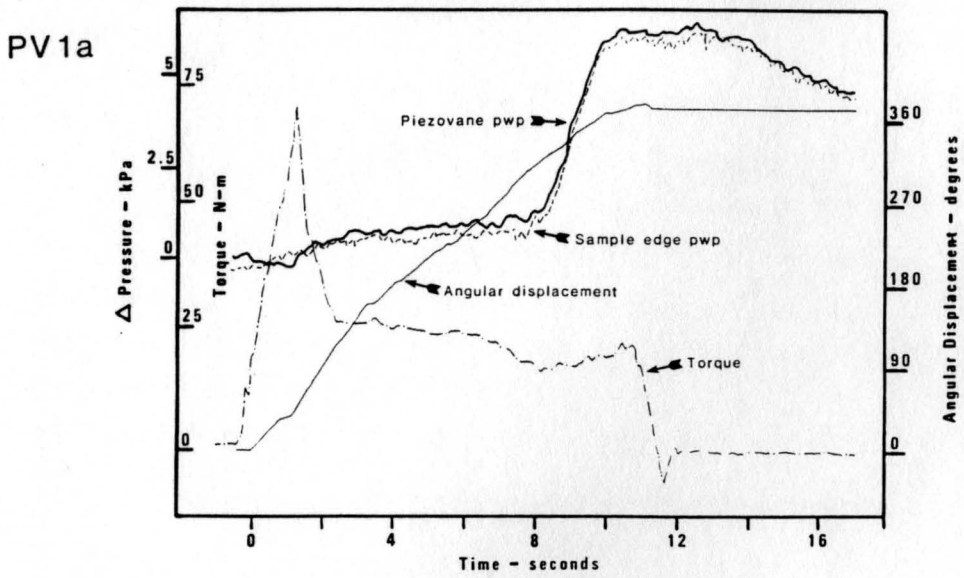

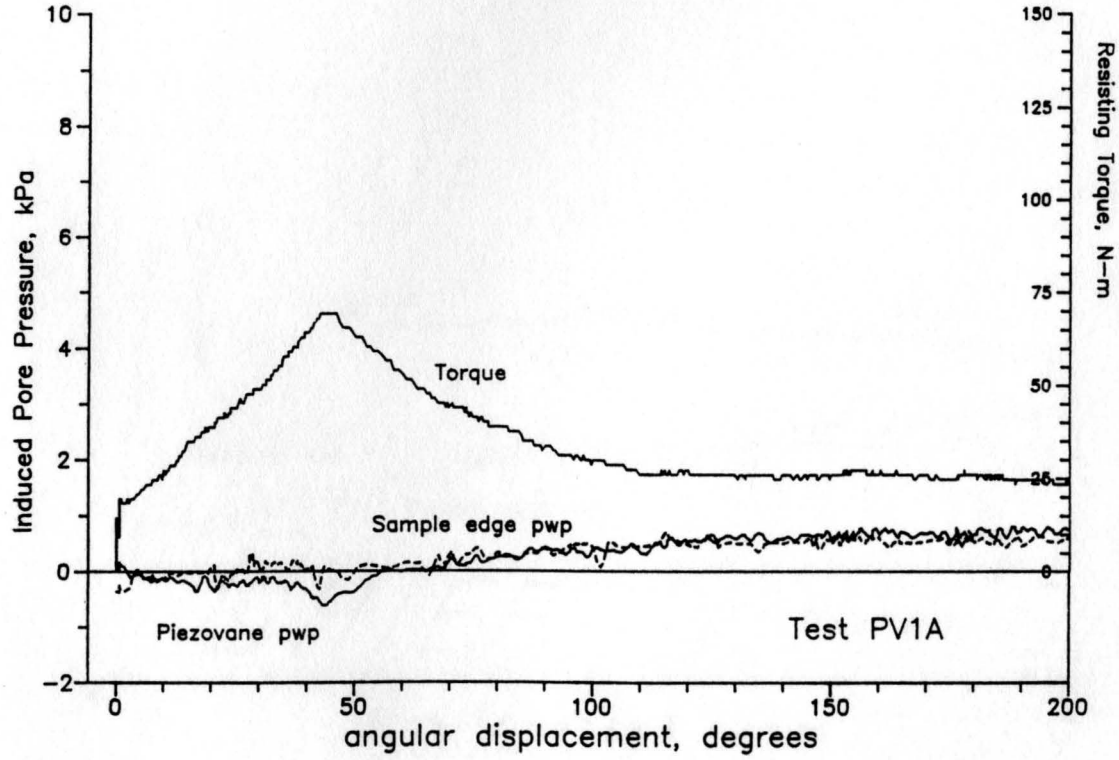

Figure B.1.1a Piezovane test PV1A, e_c = .799, σ'_{vc} = 276 kPa.

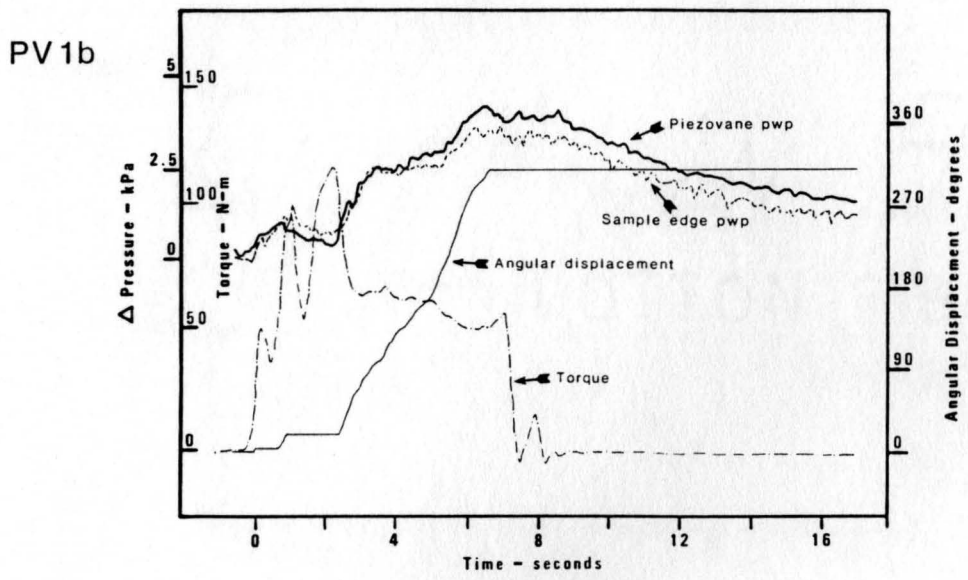

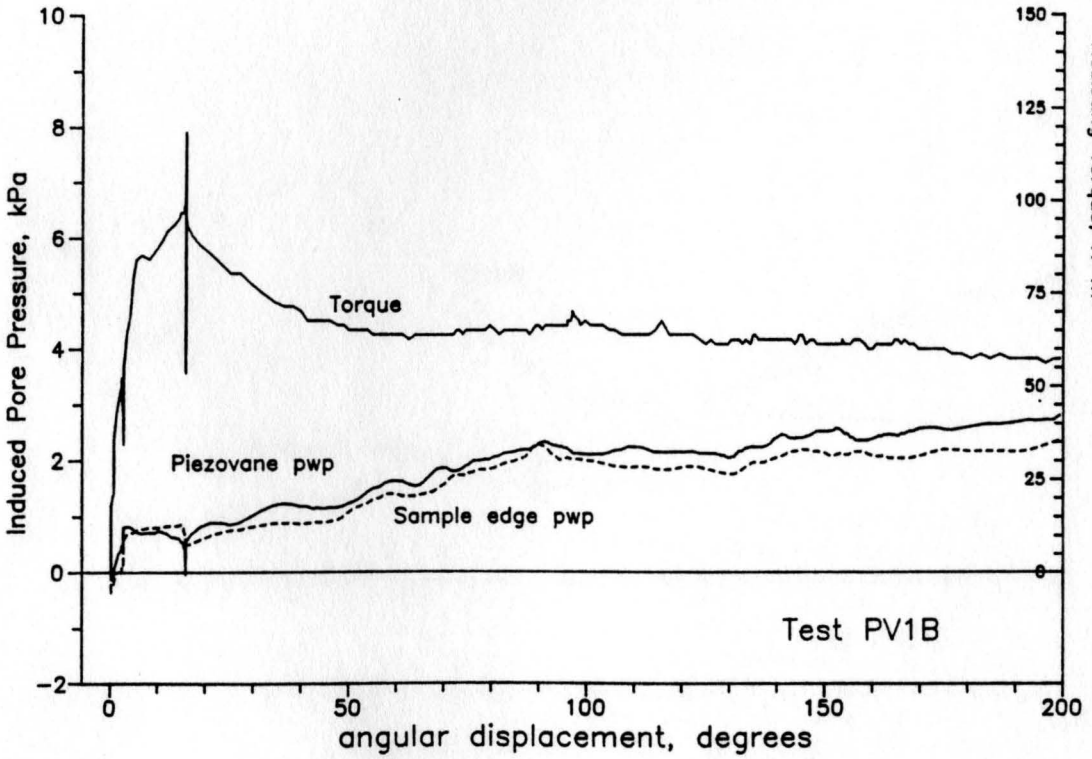

Figure B.1.1b Piezovane Test PV1B, e_c = .799, σ'_{vc} = 276 kPa.

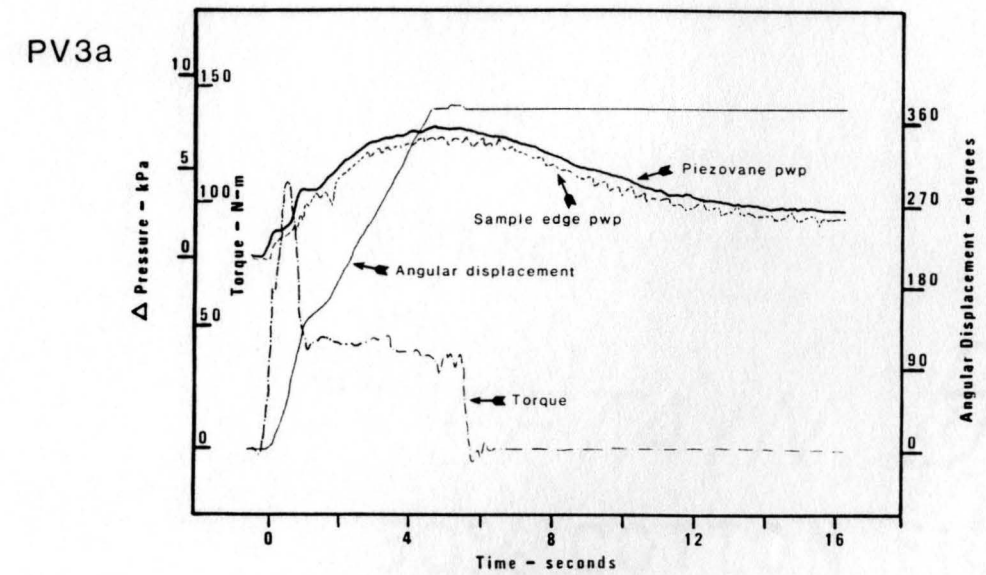

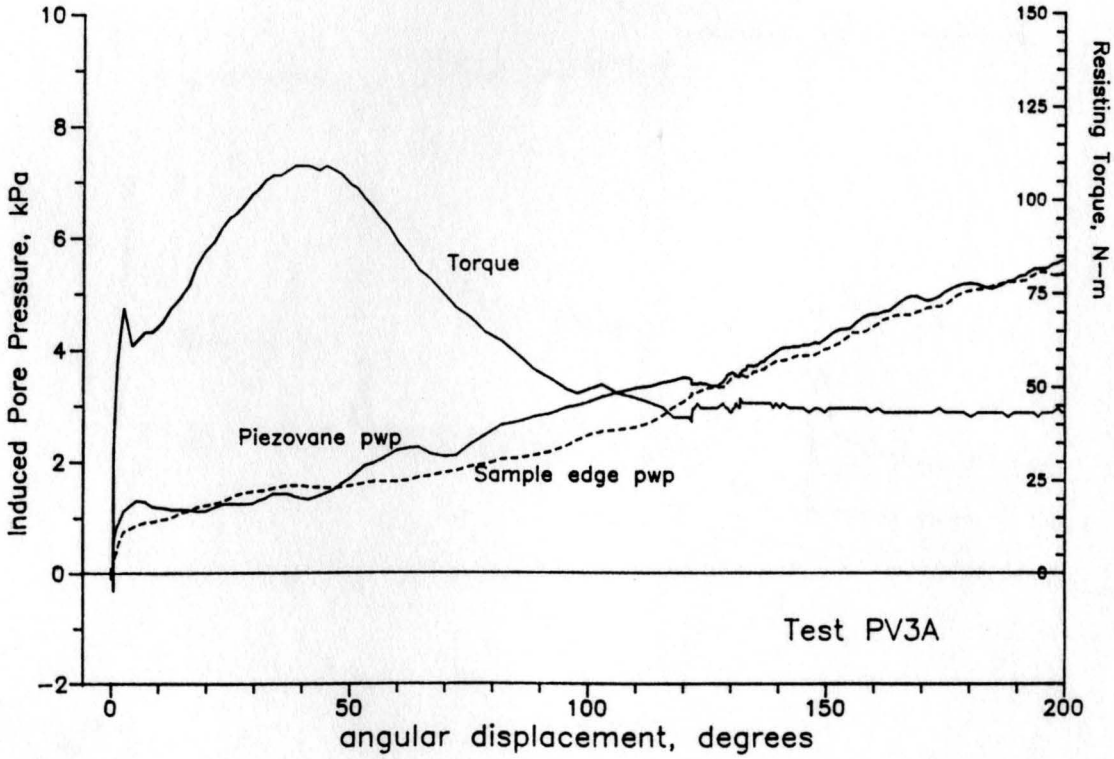

Figure B.1.2a. Piezovane test PV3A, e_c = .782, σ'_{vc} = 552 kPa.

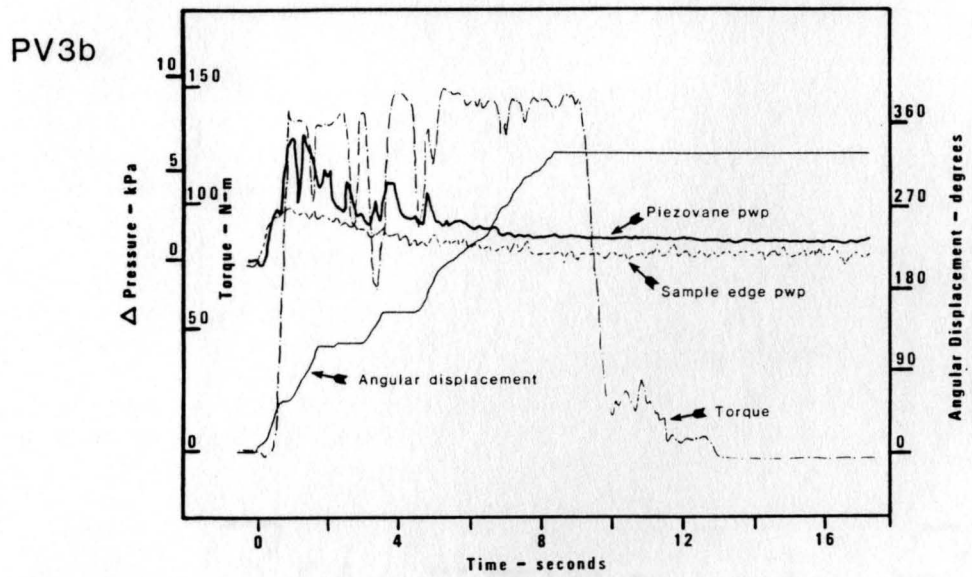

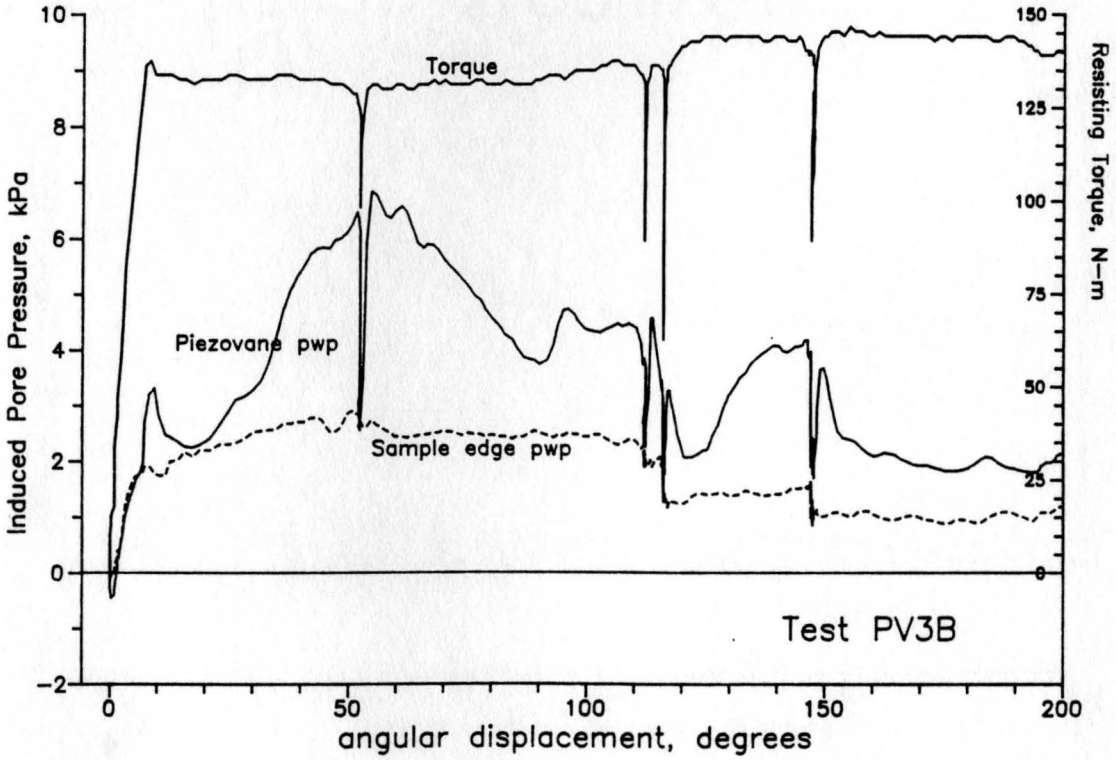

Figure B.1.2b. Piezovane Test PV3B, e_c = .782, σ'_{vc} = 552 kPa.

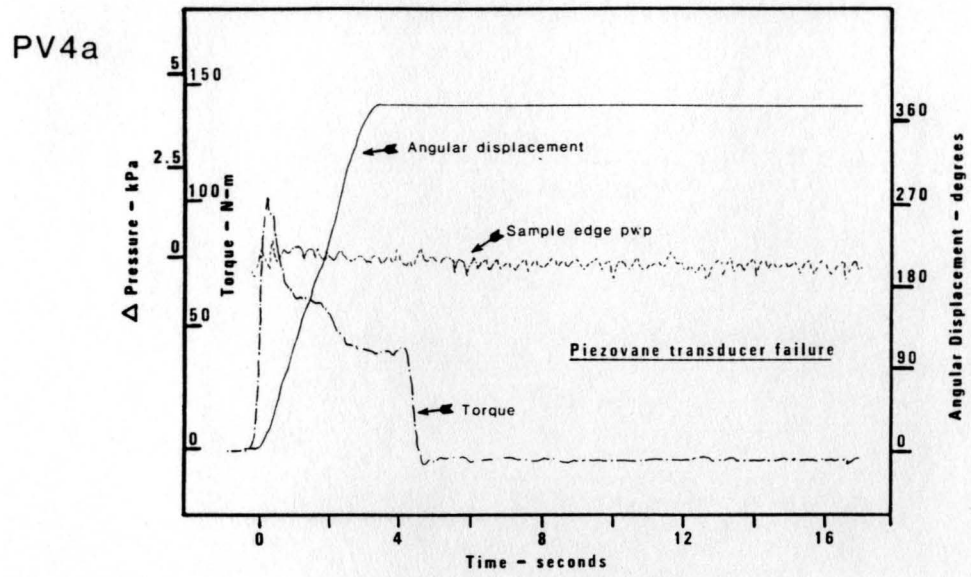

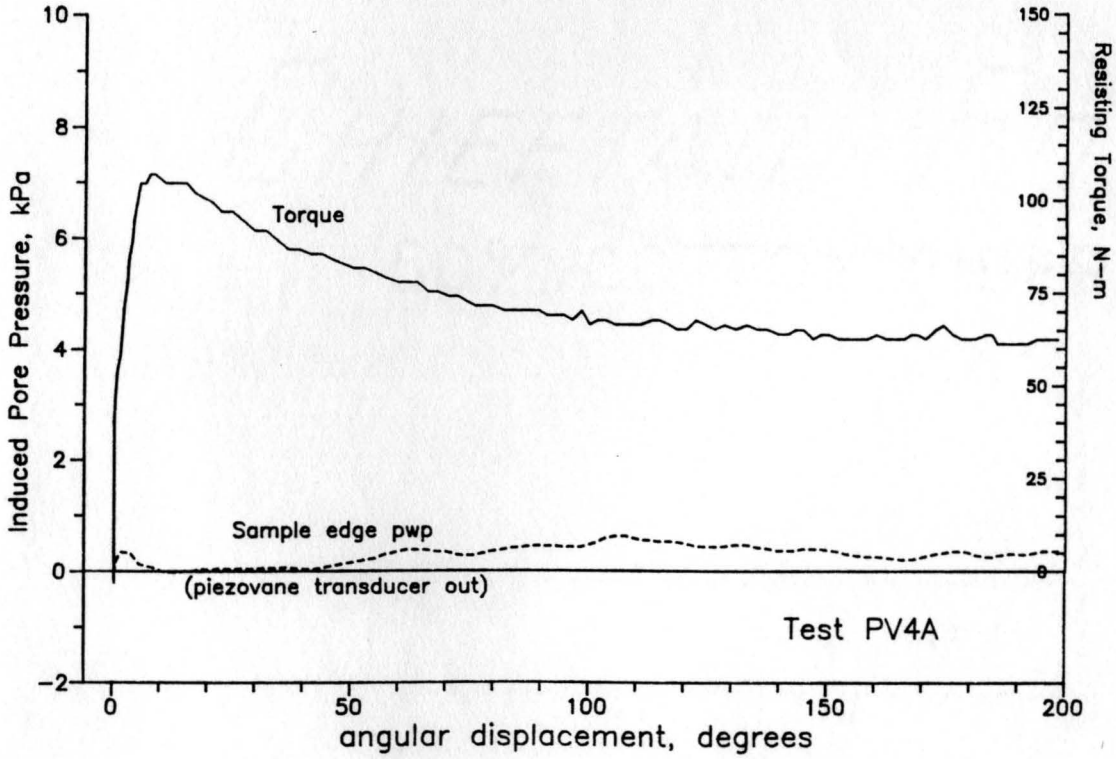

Figure B.1.3a. Piezovane test PV4A, e_c = .792, σ'_{vc} = 138 kPa.

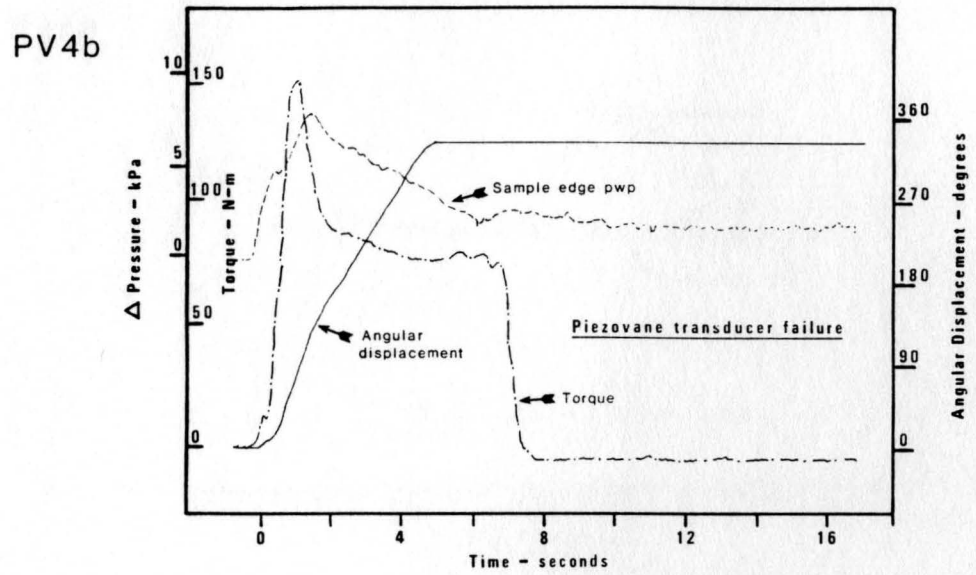

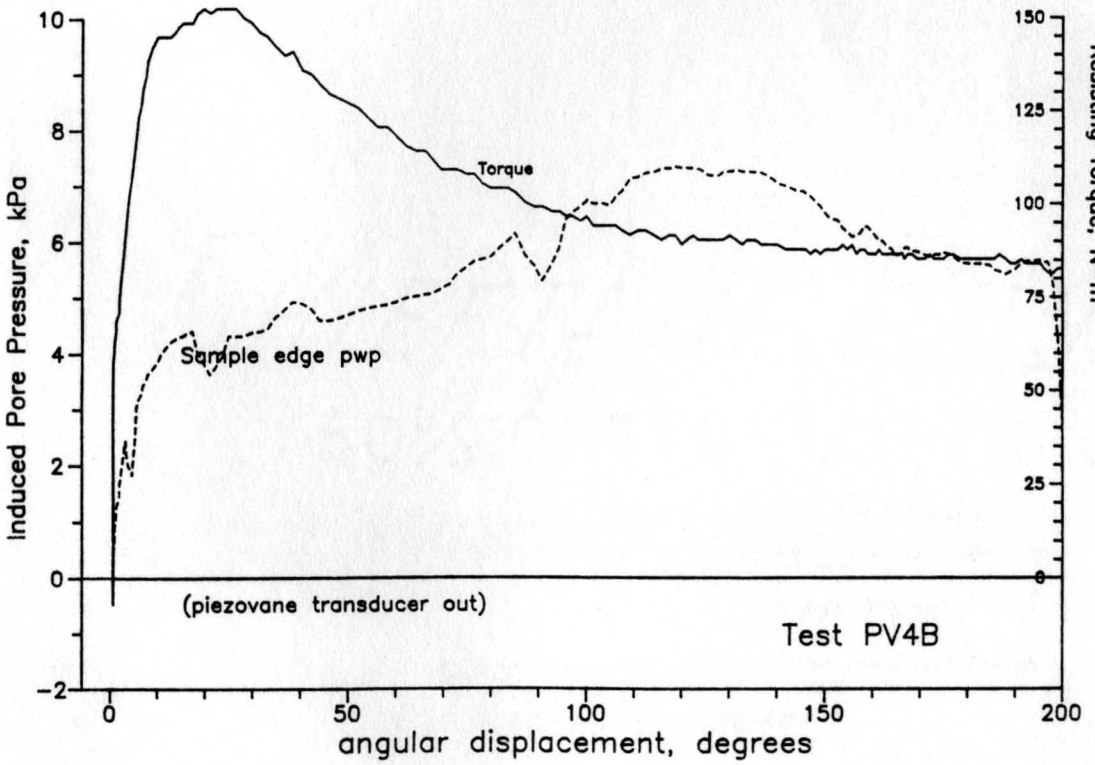

Figure B.1.3b. Piezovane Test PV4B, e_c = .792, σ'_{vc} = 138 kPa.

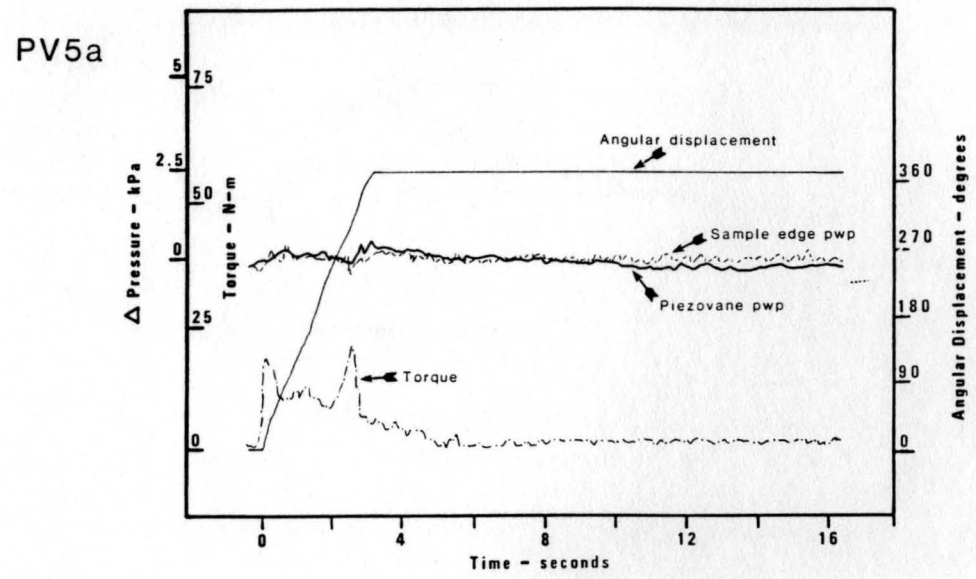

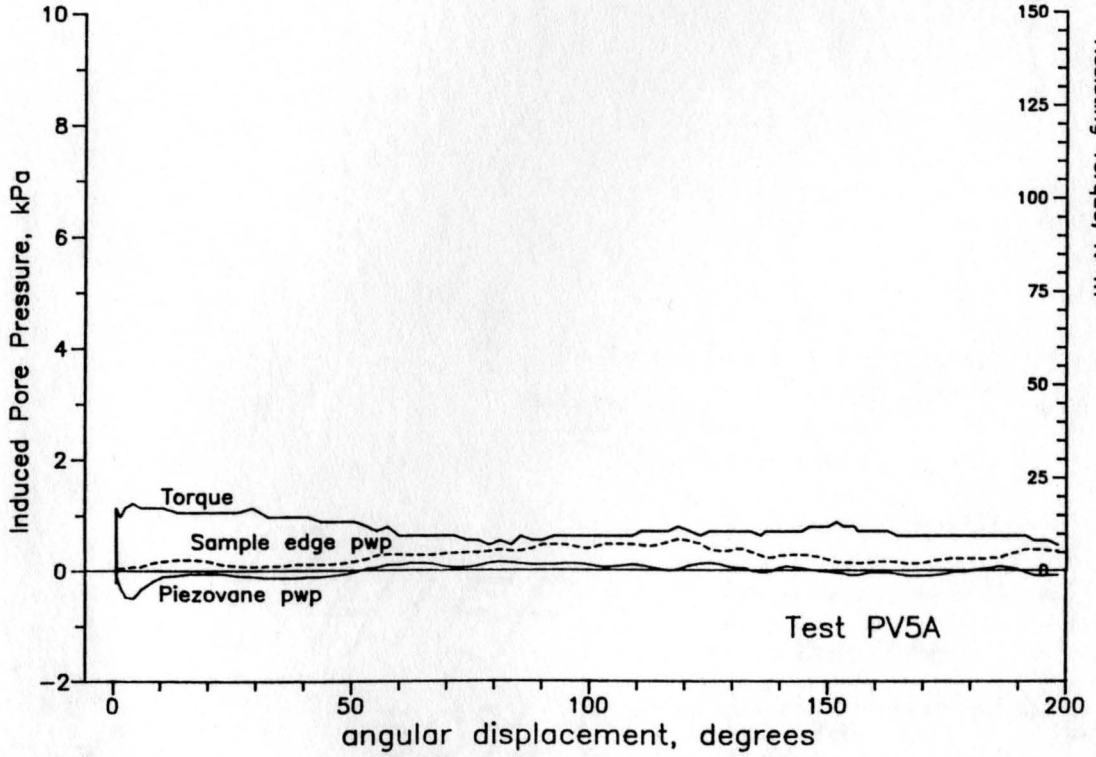

Figure B.1.4a. Piezovane test PV5A, e_c = .765, σ'_{vc} = 104 kPa.

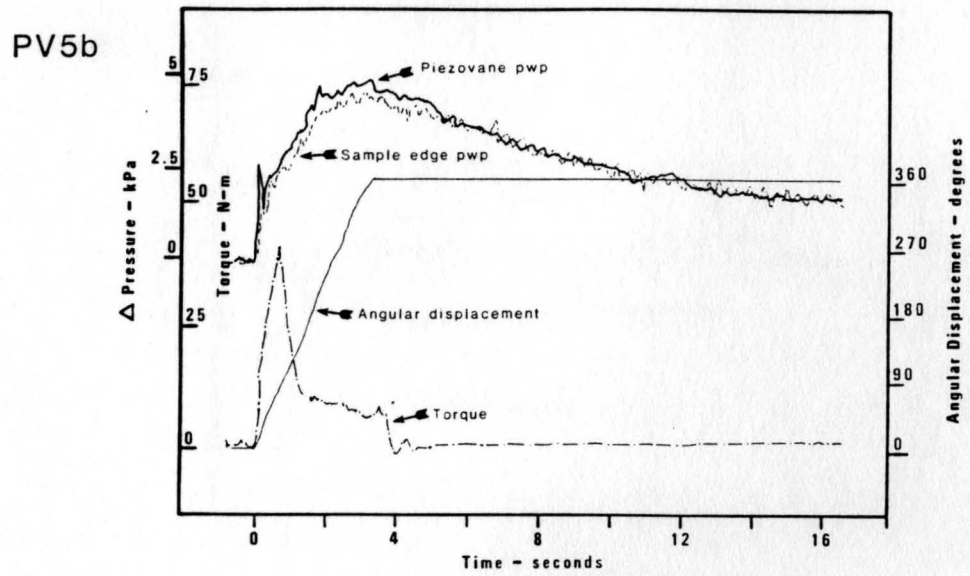

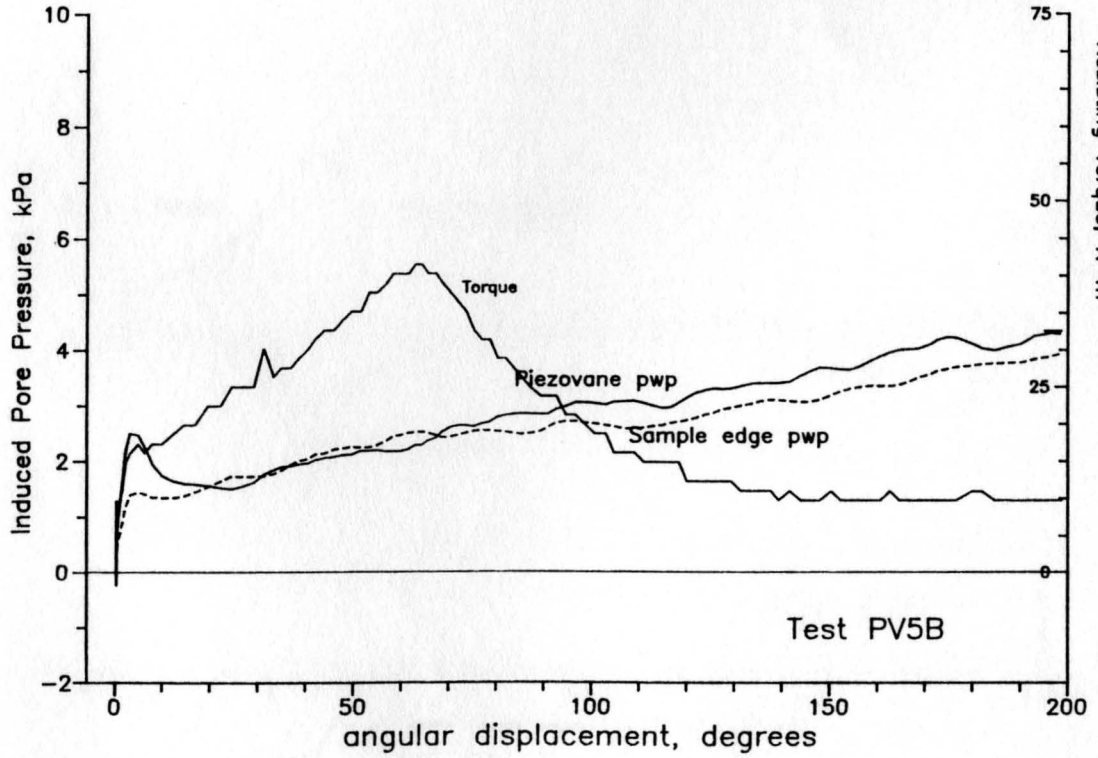

Figure B.1.4b. Piezovane Test PV5B, e_c = .765, σ'_{vc} = 104 kPa.

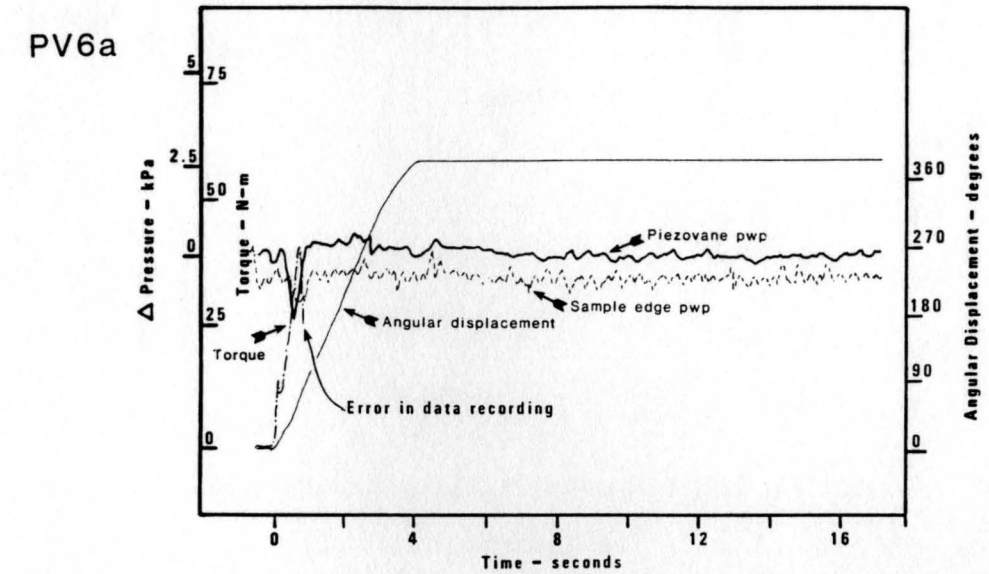

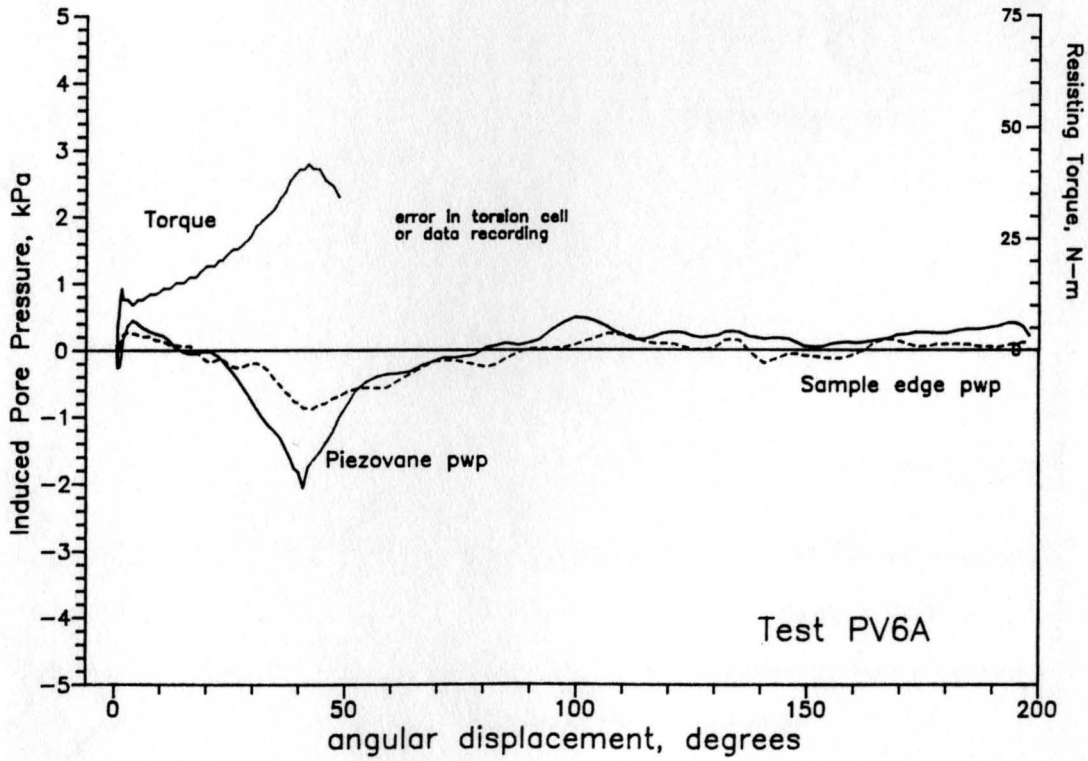

Figure B.1.5a. Piezovane test PV6A, e_c = .725, σ'_{vc} = 138 kPa.

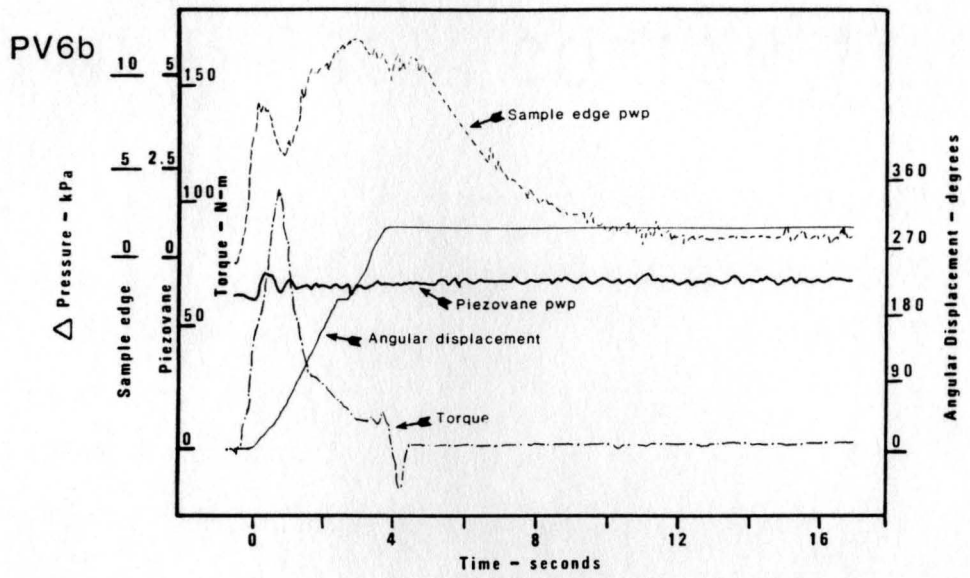

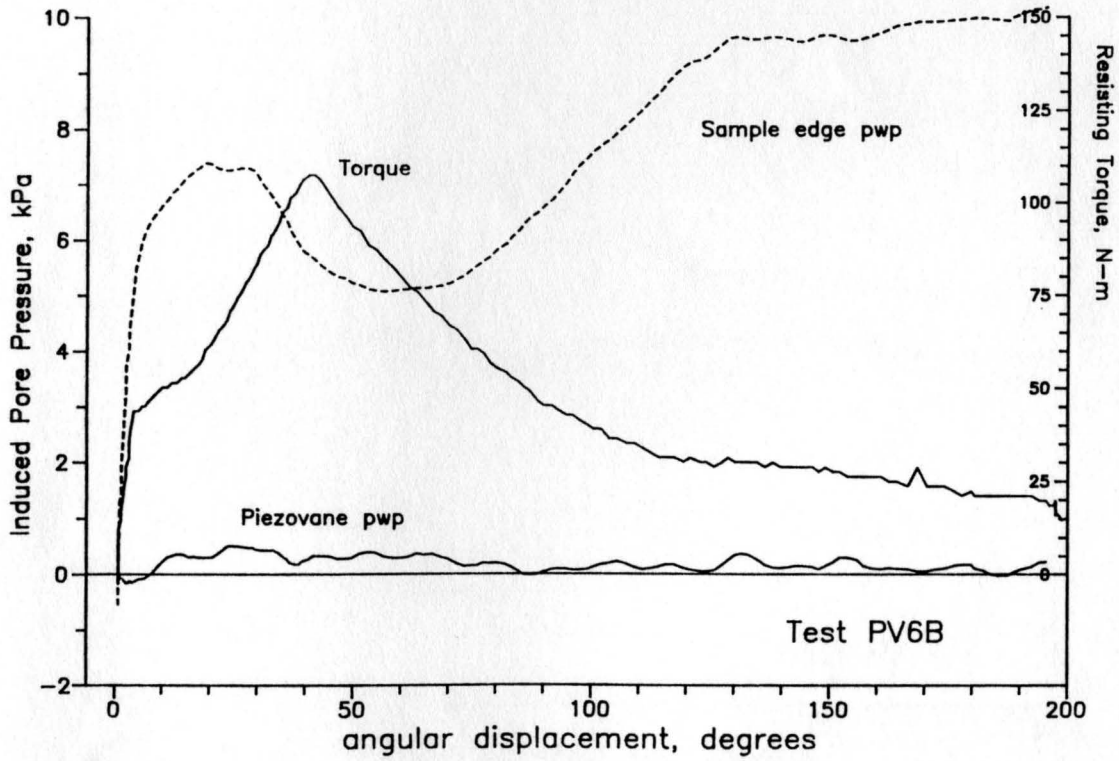

Figure B.1.5b. Piezovane Test PV6B, e_c = .725, σ'_{vc} = 138 kPa.

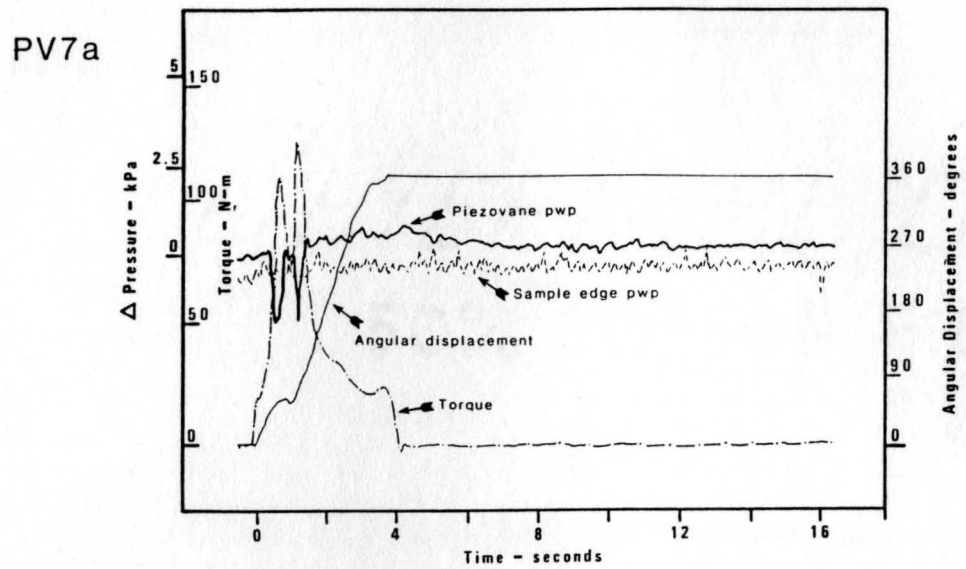

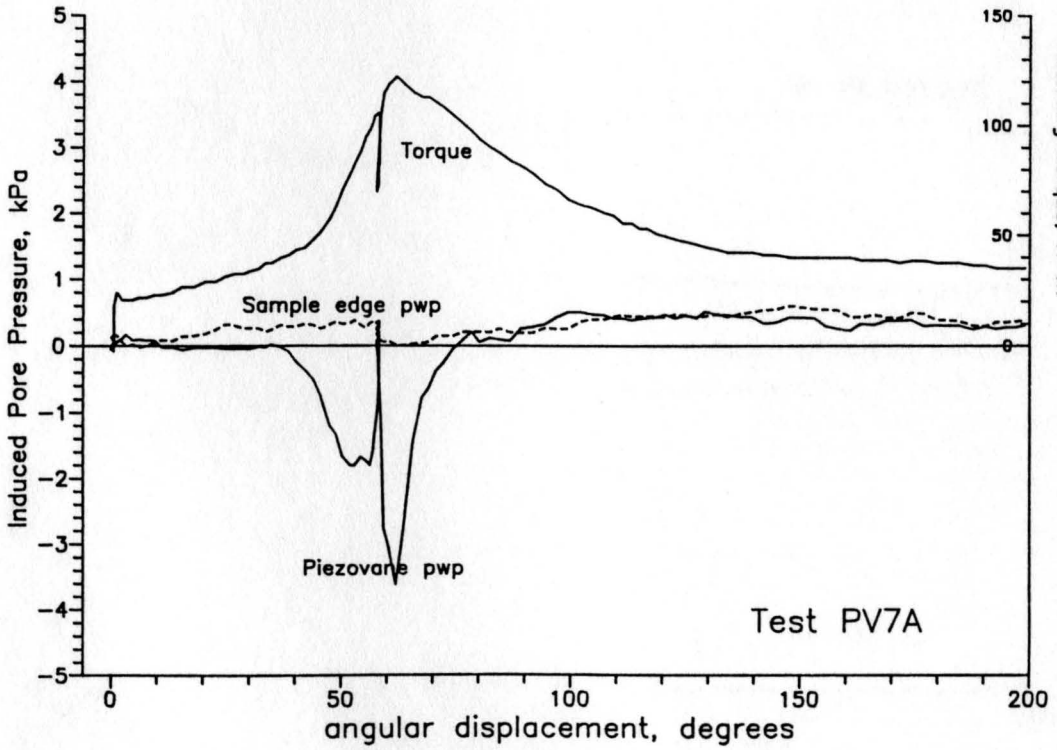

Figure B.1.6a. Piezovane test PV7A, e_c = .674, σ'_{vc} = 206 kPa.

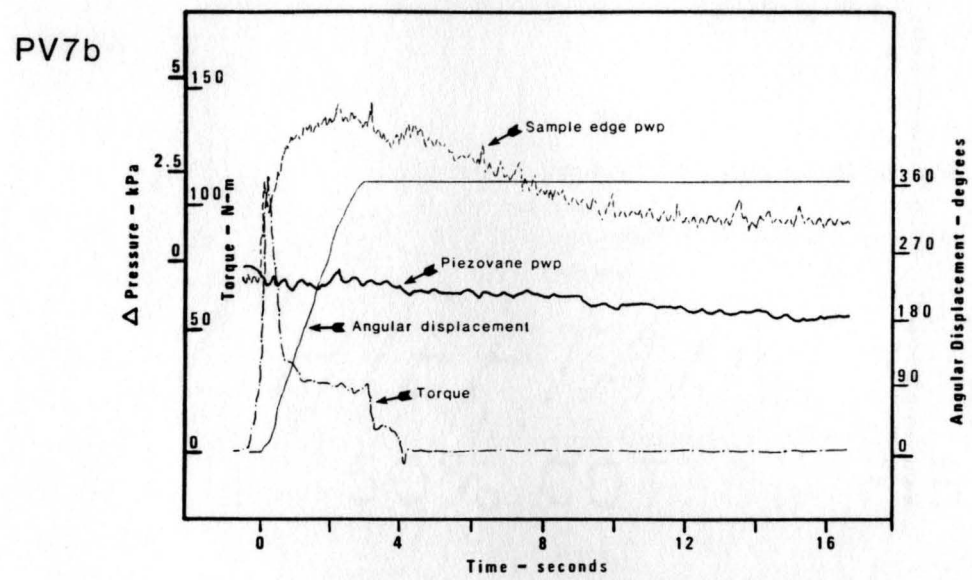

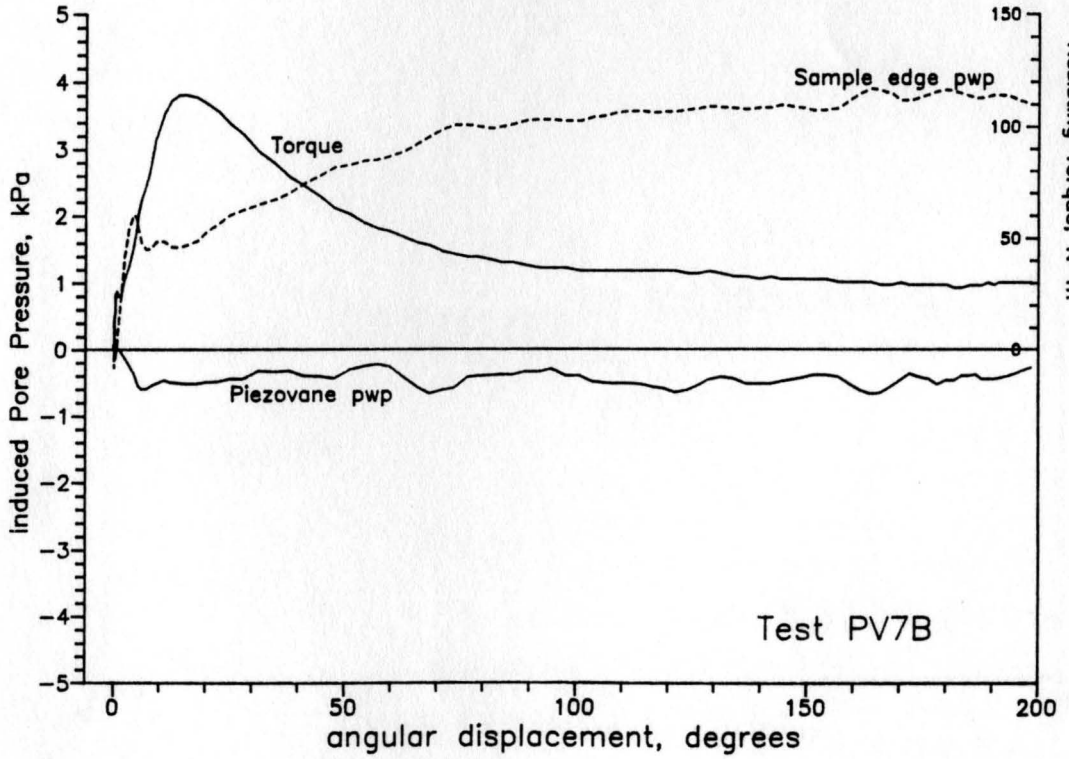

Figure B.1.6b. Piezovane Test PV7B, e_c = .674, σ'_{vc} = 206 kPa.

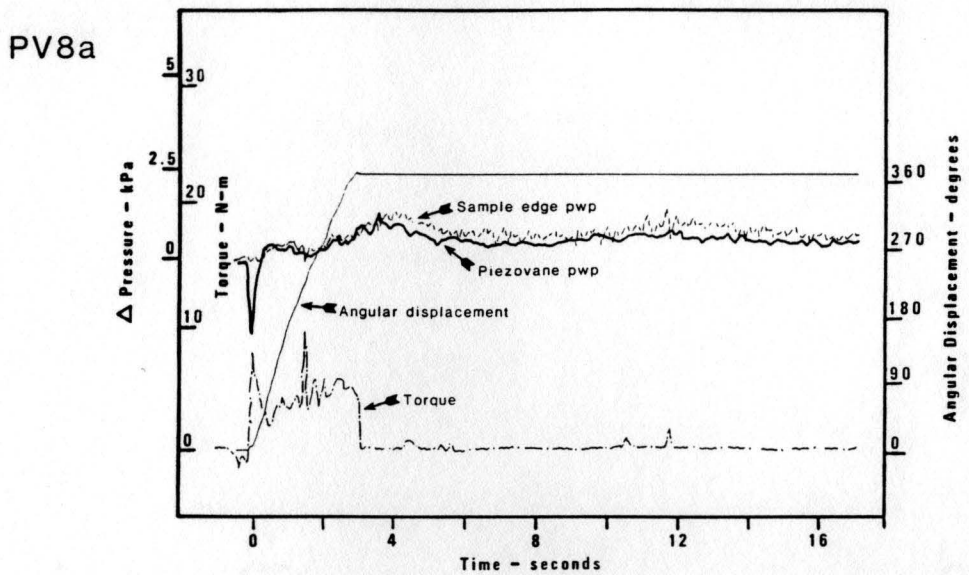

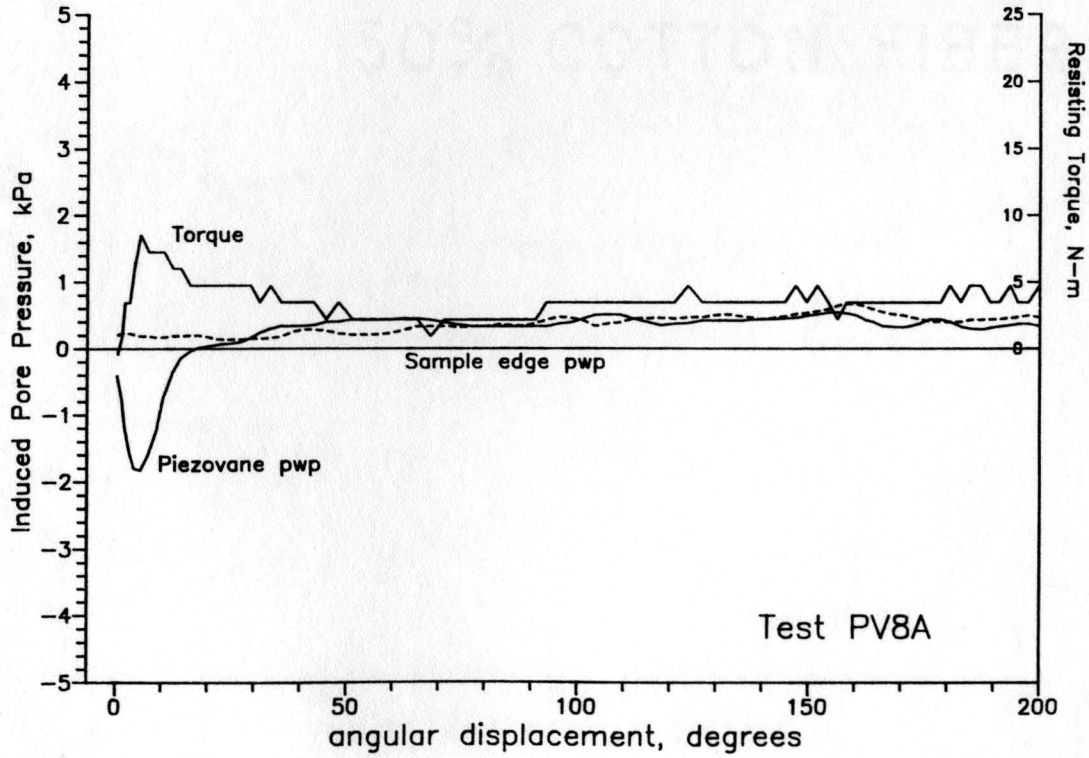

Figure B.1.7a. Piezovane test PV8A, e_c = .769, σ'_{vc} = 34 kPa.

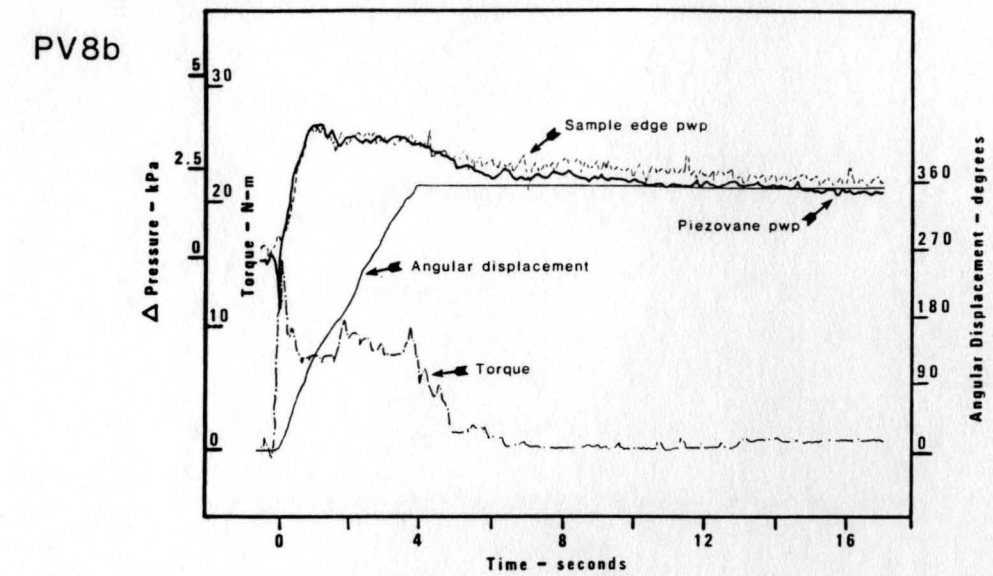

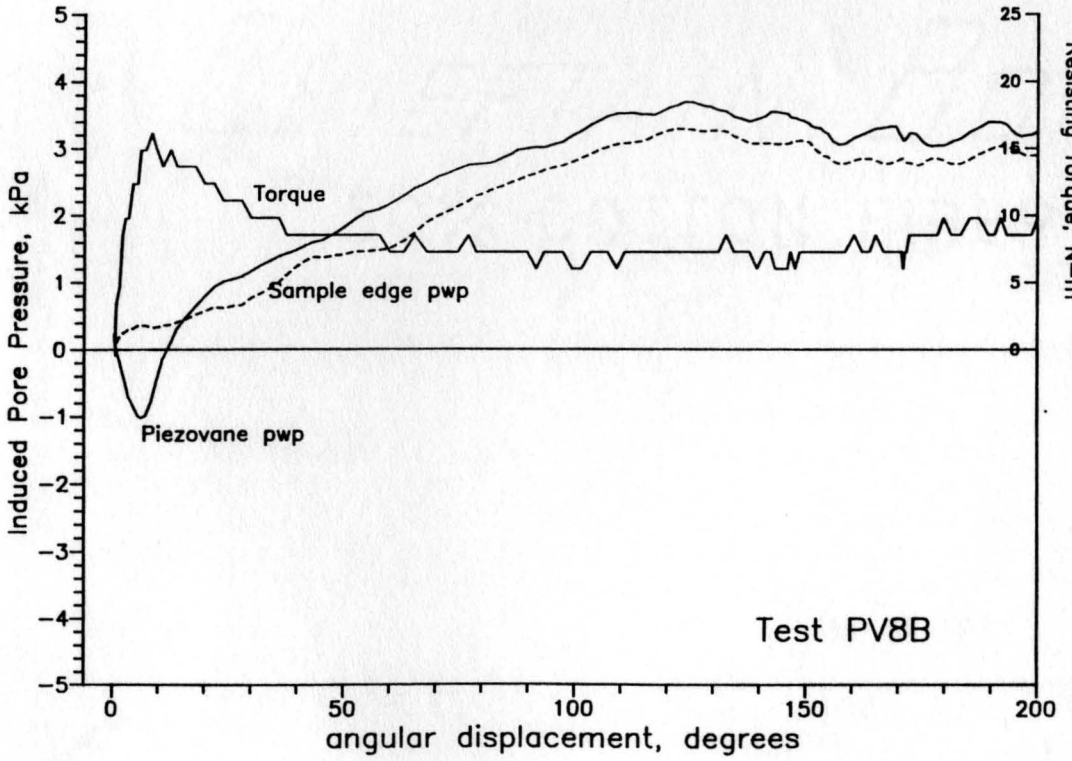

Figure B.1.7b. Piezovane Test PV8B, e_c = .769, σ'_{vc} = 34 kPa.

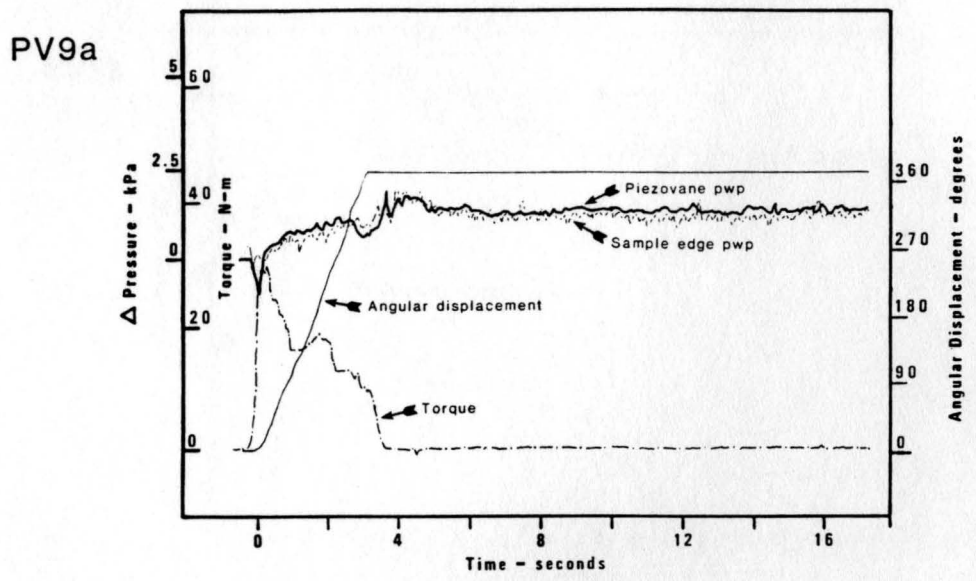

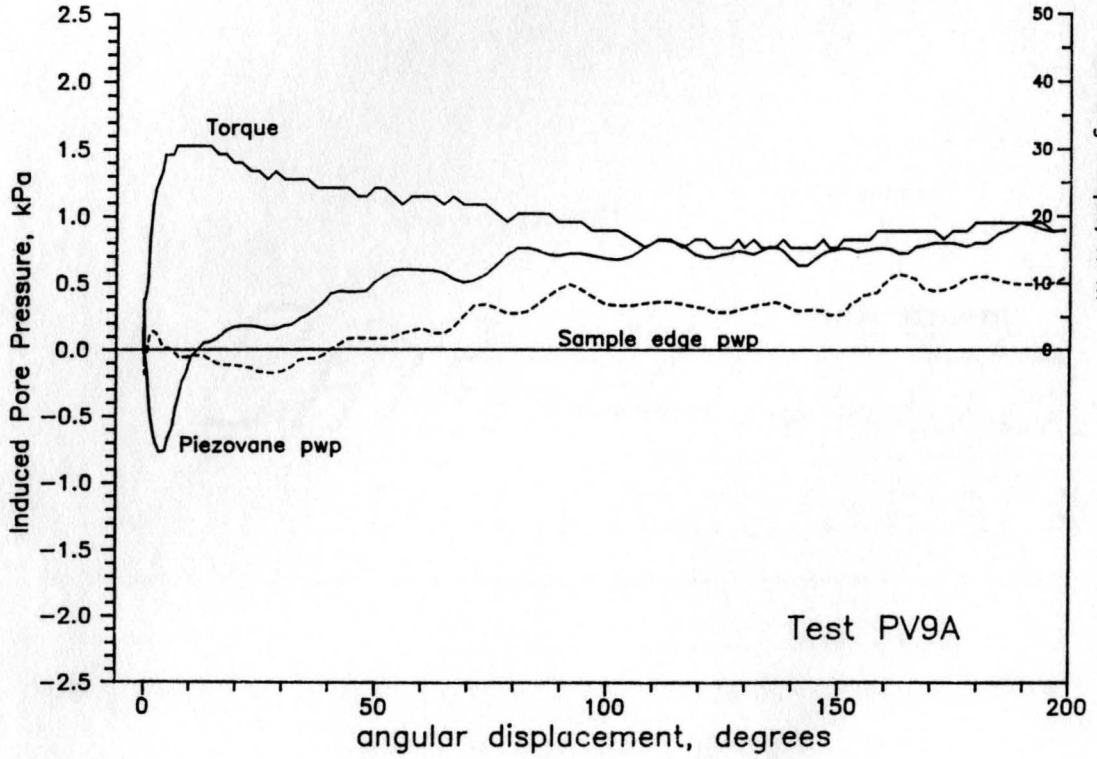

Figure B.1.8a. Piezovane test PV9A, e_c = .799, σ'_{vc} = 52 kPa.

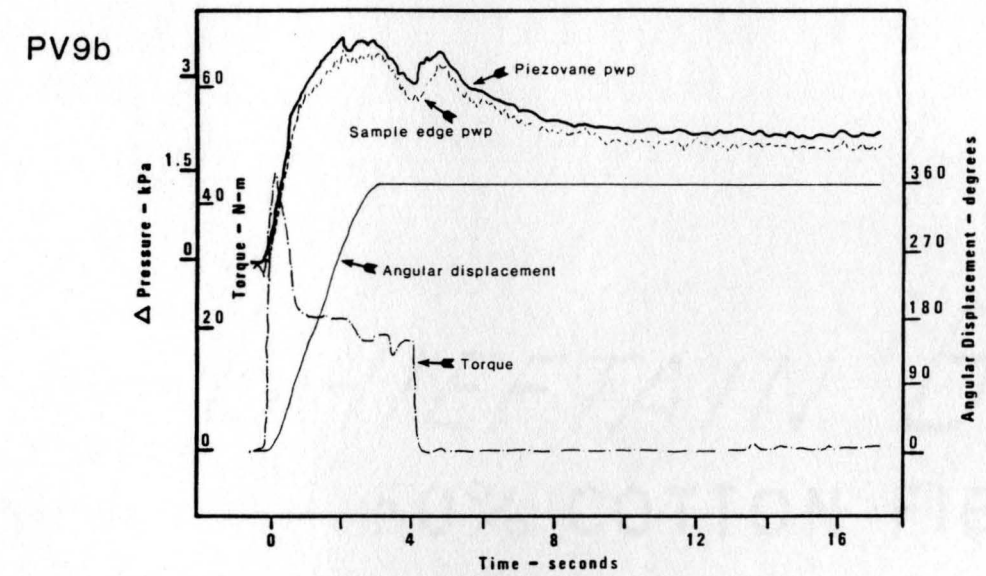

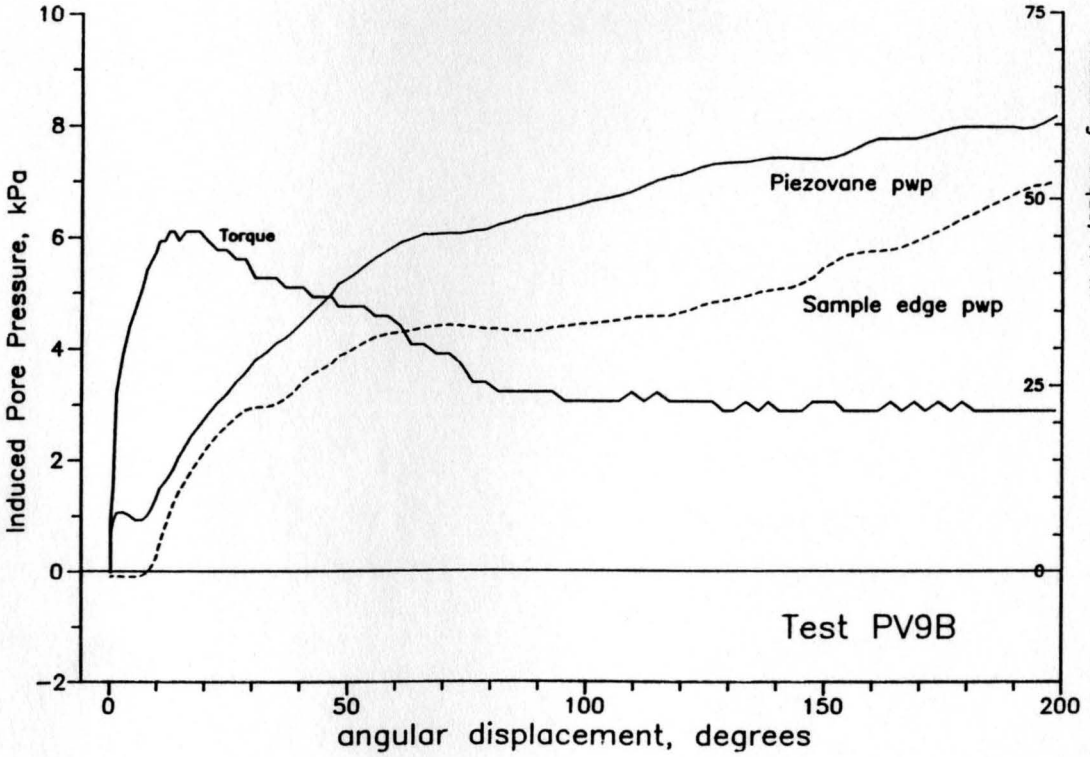

Figure B.1.8b. Piezovane test PV9B, e_c = .799, σ'_{vc} = 52 kPa.

APPENDIX C

Piezovane Testing Procedure

1. Sample placement

Moist tamping methods were used to place 8 of the 9 samples tested. Test PV7 was placed by pluviation methods to obtain a high relative density (e = .66). This was done to avoid probable "locked in" stresses resulting from the high compactive effort it would have taken to place the sand moist at this density.

A. Preparation

Before placement, if the bulk sample was wet it was allowed to dry to a water content optimum for loose compaction (usually 2-5%). The sample was then thoroughly mixed on four large tarps using the cone-and-quarter method. Microwave water contents from each of the four bulk piles were adequate to determine uniformity of moisture content (ASTM water contents were subsequently determined from samples taken during placement).

B. Moist tamping method

Materials: 1. Tamper, 2.8kg, 18 cm diameter
2. Ohaus Solution Balance, 20kg cap.
3. Engineer's tape measure

1. Lift heights were calculated based on Ladd's (1978) under compaction method. The number of lifts totalled 20 so the piezovane shear zone intersected at least 3 layers. An undercompaction value of 5% for the bottom lift was used as in the triaxial testing.

2. The balance was set (allowing for tare) at the individual lift weight using standard masses. The dry weights were used for samples initially dry.

3. The datum for the tamping rod collar was a straight section of 2X4 placed across the top flange of the chamber. The reference height was measured in the empty chamber. Tamping rod collar heights were predetermined by subtracting cumulative sample thicknesses from step 1.

4. The tamping rod collar was set for the appropriate lift.

5. The individual lift was weighed out. If the sample was dry, an appropriate amount of water was added after weighing and mixed thoroughly by rolling on a small tarp. Care was taken to prevent any sample loss.

6. The lift was gently placed in the chamber, spreading by hand to a uniform thickness. The layer was tamped into place using the method described in the ISSMFE (1987) test method. This usually required little more than flattening out the sample (3 or 4 cm drop).

7. Steps 4 through 6 were repeated until the sample is completed to the underside of the flange.

8. The sample was completed by filling in the flange volume at the appropriate density. Water contents were taken at a minimum frequency of every other lift. All samples showed very uniform moisture contents with a standard deviations of 0.08 to 0.14 percent.

C. Pluviation

Pluviation or "raining" of dry sand into position is thought to provide the best method of duplicating natural structure in a dense state. An excellent discussion of this approach along with guidelines in application are provided by Rad and Tumay (1985).

The device used in this study used 2 U.S. gallon plastic bucket as a sand column and shutter. Shutter hole pattern was type C with a

shutter hole porosity of 5 percent. The diffuser consisted of number 10 and 14 standard sieves attached to the bottom of the bucket.

The sample was weighed as in step 5 above and placed in the device. Sand was released by quickly removing a plastic sheet covering the shutter holes. A constant, slow, circular motion was used, maintaining a 4 cm drop height. Interference by the top flange restricted coverage by this method in the top 1/3 of the chamber. This top portion had to be filled by carefully raining sand through the sieves with a small hand scoop.

2. Saturation

Procedure hereafter refers to Figure C.1 for valve locations.

A. CO2 Preflushing and wetting

1. Preflushing. After connecting lines to the CO_2 bottle, CO_2 was allowed to flow through the disconnected line opposite valve 1. Flow rate was adjusted by valve 2 until audible from about 3 inches away. This usually required about 2.5 psi shut in pressure from the bottle. Valve 1 was then closed, directing CO_2 through the sample. CO_2 flushing was stopped (usually after 20-30 minutes) once a match could be extinguished when held 1/2 to one inch from the surface of the sample.

2. Wetting. Deaired water was allowed to enter the sample controlling the rate with valve 1. One quarter turn gave a sufficiently slow filling time (2-4 hours). Any collapse after filling was noted.

A section of rubber membrane material was placed over the sample surface after sample placement. This was done to 1) create a slight

PIEZOVANE TESTING APPARATUS

FLUID SYSTEM

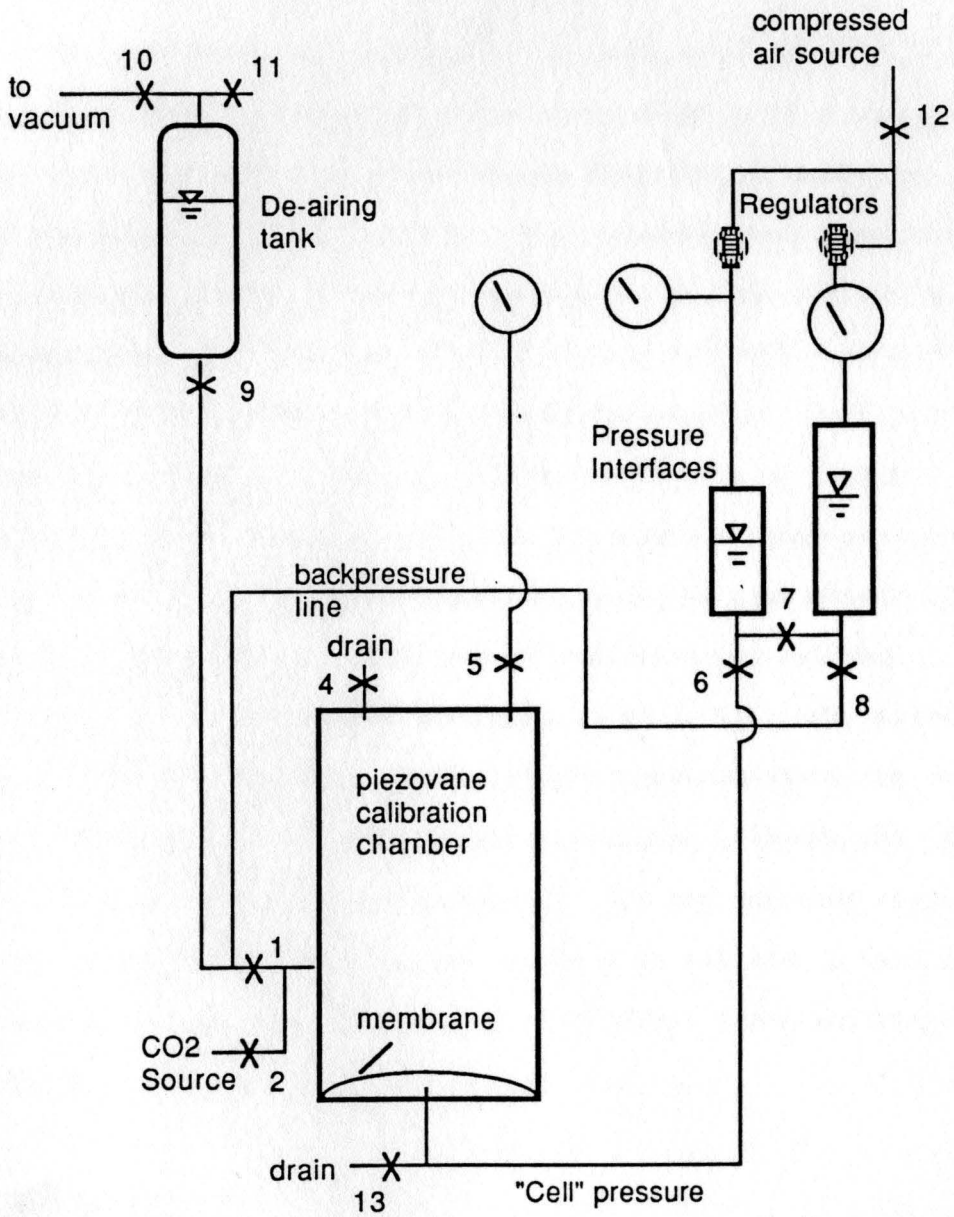

Figure C.1 Fluid System Showing Valve Locations

positive pressure or crude nonreturn valve during CO_2 flushing and 2) prevent general contamination. The rubber sheet was kept in place until vane insertion.

C. Piezovane insertion and sealing

The piezovane was saturated by submergence in a large aluminum vat filled with deaired water. Air was purged with a syringe. The piezovane was attached to the torque shaft while remaining submerged and a plastic bag placed over it. The assembly was then hoisted up and over the sample, carefully holding the plastic bag containing the deaired water and piezovane. The piezovane was then inserted in the sample. The bag usually burst and emptied after the top ports were below the free water surface. The bag could then be removed. If the bag prematurely burst or there was any other remote suspicion of air entry, this entire step was repeated. Once the transducer was below the free water surface, the rate of insertion was relaxed. Keeping the shaft as centered and vertical as possible, the assembly was lowered until 19 inches shaft height remained above the top of the sample (This allowed >2 vane heights clearance between the bottom of the cap and top of the piezovane). The cap was then seated on the flange. The flange "O" ring was coated with silicon grease prior to insertion. Cap bolts were sealed with Teflon paste and torqued 50 to 60 ft-lbs.

D. Saturation

1. Flushing

After attaching drain line and opening valve 4, deaired tap water was flushed through the sample. Height of the drain outlet was

adjusted to minimize seepage forces (gradients could be approximated using the deairing tank head, piezovane transducer and top bourdon gage). Flushing was stopped at 1.5 to 3 pore volumes.

2. Backpressure

Backpressure was set in increments of 34.5 kPa followed by a corresponding application of cell pressure. This pressure equalization was necessary to prevent punching the membrane through the bottom opening. Care was taken not to consolidate the sample when applying cell pressure. The sample was then allowed to "saturate" for 8 - 10 hours.

3. "C" parameter check

The piezovane and side transducers were balanced immediately after closing valves 1, 4 and 5 (valve 5 leads to a high displacement gage). A pressure increment of 69 kPa was applied to the cell and transducer response was recorded. During application, possible transient response due to unsaturated conditions was monitored on the oscilloscope. This was necessary in the collapsed samples where very high "C" values could result with only partial saturation.

E. Consolidation

Consolidation was accomplished by applying cell pressures and recording the corresponding displacement indicated by the sight tube on the backpressure interface. Increments of pressure were initially 17 or 35 kPa. Times for volume stabilization were 10 minutes to 2 hours per increment. Once sufficiently low volume changes occurred in a short time, pressure increments were increased to 69 kPa.

The full length of the sight tube was used to minimize draining steps and reduce cumulative reading error in restarting. The tests usually required 1 to 2 draining steps giving a maximum cumulative measurement error of 60 cc.

F. Shearing

Bridge conditioners were allowed sufficient time to warm up (at least 30 minutes). Data acquisition was set to an 8 msec sampling interval using a menu driven software program. the last step before shearing was to balance the bridges and set the potentiometer voltage to 10.00 volts. The sample was sheared immediately after balancing to minimize drift at the start of recording. Shearing was accomplished by hand with the use of a torque wrench attached directly to the square drive on the torsion cell. Rotation rates varied from about 70 to 90 degrees per second for most samples.

After shearing, the jacking frame was attached to the threaded rods above the top flange. The piezovane was advanced slowly with a hydraulic jack until 8.5 inches of the shaft were exposed above the top of the cap. (This advanced the vane approximately 2 vane lengths.) The shearing steps were then repeated for the lower position.

APPENDIX D

Modified Cadling's Equation

Derivation of Modified Cadling's Equation

On vertical plane:

$$\text{Torque, } M_v = \pi D^2 H S_v/2$$

On horizontal plane:

$$M_H = 2 \int_0^{D/2} S_H \, 2\pi r^2 \, dr = \frac{S_h \pi D^3}{6}$$

$$\text{Total torque, } M = M_v + M_H = \frac{\pi D^2 H}{2} S_v + \frac{\pi D^2}{6} S_H$$

Assuming: $S_H = \sigma_v \tan\phi'_{avg}$, $K = K_o$

$$S_H = \frac{\sigma_H}{K_o} \tan\phi'$$

Substituting for S_H gives

$$M = S_v \pi D^3 \left(\frac{H}{2D} + \frac{1}{6K_o}\right)$$

if $K_o = 1 - \sin\phi'_{avg}$, $K_o = 0.5$.

And if $H/D = 2$, $S_v = \frac{3M}{4 \pi D^3}$